UNIVERSITY OF JYVÄSKYLÄ
DEPARTMENT OF PHYSICS

MASTER'S THESIS IN NATURAL SCIENCES
&
RESEARCH TRAINING THESIS

COMPUTATIONAL MODELLING OF BORON NITRIDE NANOSTRUCTURES BASED ON DENSITY-FUNCTIONAL TIGHT-BINDING

Johannes Samuli Nokelainen

2014

Instructor: Academy Research Fellow Pekka Koskinen

Acknowledgements

I am grateful to my instructor Pekka Koskinen for the computer code used in this work as well as all the help involved and Department of Physics for financial support. I also acknowledge my girlfriend Tiina for all the support with this project. Moreover, I want to express my gratitude to Markku and Sameli for help with orthography of these theses.

Abstract

Boron nitride (BN) nanostructures are both structurally and elastically very similar to the corresponding carbon structures. The major difference is that BN is a wide bandgap insulator whereas carbon structures are either conductors or semiconductors. Therefore BN is a highly promising nanomaterial and it is expected to have applications in nanotechnology e.g. as encapsulating nanomaterials and nanofillers in composite materials.

Properties of BN nanostructures are usually computationally researched either with the density-functional theory (DFT) or tight-binding (TB) models. The former is accurate but computationally demanding whereas the latter is computationally light but inaccurate. In this work I shall present combinination of these two theories into tight-binding density-functional theory (DFTB). I also take into account the energy term that is in the second order in density fluctuations. The resultant theory is significantly more accurate than TB and computationally faster than DFT. However, it includes parameters that have to be determined in advance. Firstly, it is needed to compute the TB-inherited S- and H^0-matrix elements related to overlaps and eigenenergies of atomic orbitals of the system. Secondly, the repulsion potentials V_{rep} between the nuclei must be determined. The idea behind them is to fine tune them in such a way that DFT and DFTB results are in correspondence in as many relevant situations as possible.

I also shall present the BN parametrization determined by me and the computational results obtained with it for properties of both perfect and defected BN layers and nanotubes. In the case of BN layers the studied defects are B-, N- and BN-vacancies and in the case of nanotubes Stone-Wales defects. The obtained electron structures for undefected structures as well as the formation energies of defects are in relatively good accordance with the corresponding DFT results. The Young's moduli of perfect structures and agree well with the reference results. However, the elastic Poisson's ratios contradict strongly with the DFT references. All in all my parametrization is capable of producing sufficiently good results. However, there are room for improvement, as results of an earlier BN parametrization are notably closer to the DFT results at least in the case of nanotubes. I most likely should have used more reference structures where I ensured the consistence of DFTB and DFT.

Tiivistelmä

Boorinitridin (BN) nanorakenteet ovat sekä rakenteellisesti että lujuusominaisuuksiensa puolesta hyvin samankaltaisia vastaavien hiilirakenteiden kanssa. Suurimpana erona on BN:n sähköinen eristävyys kun taas hiilirakenteet ovat johteita tai puolijohteita. BN onkin hyvin lupaava nanomateriaali ja sille on odotettavissa sovelluksia muun muassa muiden nanorakenteiden suojaajana ja komposiittimateriaalien nanokudosaineena.

BN:n nanorakenteiden ominaisuuksia tutkitaan laskennallisesti yleensä joko tiheysfunktionaaliteorialla (DFT) tai tiukan sidoksen (TB) malleilla. Ensin mainittu on tarkka mutta laskennallisesti vaativa, kun taas jälkimmäinen on laskennallisesti kevyt mutta epätarkka. Tässä työssä esittelen näiden teorioiden yhdistämisen tiukan sidoksen tiheysfunktionaaliteoriaksi (DFTB) ottaen huomioon myös tiheysfluktuaatioissa toista kertalukua olevan energiatermin. Seurauksena on huomattavasti DFT:tä nopeampi ja TB:tä laskennallisesti tarkempi teoria. Se kuitenkin vaatii ennalta määritettäviä parametreja. Ensinnäkin on laskettava tiukan sidoksen mallista periytyvät S- ja H^0-matriisielementit, jotka liittyvät systeemin atomiorbitaalien keskinäiseen limittäytyneisyyteen ja ominaisenergioihin. Lisäksi atomiydinten väliset repulsiopotentiaalit V_{rep} on määritettävä. Niiden kohdalla johtava ajatus on pyrkiä hienosäätämään ne sellaisiksi, että DFT:n ja DFTB:n tulokset vastaisivat toisiaan mahdollisimman hyvin mahdollisimman monessa relevantissa tilanteessa.

Esittelen myös määrittämäni parametrisaation BN:lle ja sitä käyttäen laskemani tulokset sekä virheettömien että vaurioituneiden BN-tasojen ja -nanoputkien ominaisuuksille. BN-tasojen kohdalla tutkimani vauriot ovat B-, N- ja BN-vakansseja ja nanoputkien kohdalla Stone-Wales -virheitä. Saamani virheettömien rakenteiden elektronirakenteet ovat suhteellisen lähellä vastaavia DFT-tuloksia, samoin kuin vaurioituneiden rakenteiden muodostumisenergiat. Vaurioitumattomien rakenteiden kimmokertoimet ja kaikkien tutkittujen systeemien rakenteelliset ominaisuudet vastaavat viitetuloksia pääosin hyvin. Sen sijaan elastiset Poissonin suhteet eroavat merkittävästi DFT-viitearvoista. Kaiken kaikkiaan parametrisaationi on siis kykeneväinen suhteellisen hyviin tuloksiin. Parantamisen varaa kuitenkin on, sillä aikaisemman BN-parametrisoinnin tulokset ovat huomattavasti lähempänä DFT:n tuloksia ainakin nanoputkien tapauksessa. Minun olisi luultavasti erityisesti tullut käyttää useampia rakenteita, joissa varmistin DFTB:n ja DFT:n yhteensopivuuden.

Contents

List of Figures

List of Tables

1 Introduction

Boron nitride (BN) is an isoelectric analog of carbon (C): in B–N bonding the average number of electrons per atom is 2 in the $2p$ layer, as in carbon (carbon is $2p^2$, boron is $2p^1$ and nitrogen is $2p^3$). Thus they are mostly found in the same phases, produce similar structures and have many shared extraordinary properties. Even their bond lengths are nearly equal [1]. For example, hardness of the cubic boron nitride (discovered in 1986 [2]) is second only to diamond, whose structural equivalent it is.

However, in recent years the research on these materials has focused on their nanostructures due to their wide range of applications. These structures are based on hexagonal sp^2-hybridized honeycomb lattice forms of BN and C (*h-BN* and *h-C*, respectively). In the case of boron nitride the atoms alternate in the lattice hexagons and a B atom is bonded to three N atoms (and vice versa) adjacent to it. Every neighbouring pair of N and B atoms is in this case bonded to each other by a covalent bond so that there exists only B-N bonds. In these bonds the partial displacement of the electron density is to an N atom making them slightly ionic contrary to the carbon case.

The intensive research on nanostructures of BN and C began from the discovery of carbon nanotubes (CNTs) in 1991 [3]. After this *boron-nitride nanotubes* (BNNTs) were theoretically predicted in 1994 [4, 5] and then successfully synthesized in 1995 [6]. Subsequently other 1D BN nanomaterials such as nanowires, nanoribbons, nanofibers and nanorods were synthesized [7–10]. Furthermore, inspired by the carbon fullerenes, corresponding 1D BN nanostructures were produced in 1998 [11]. But the greatest discovery was yet to come—in 2004 graphene was sensationally discovered [12]. After that it did not take long before also free-standing 2D BN flakes were peeled off from a BN crystal in 2005 [13].

Primarily, the interest in BN nanostructures has been due to the fact that in contrast to their metallic or semiconducting structural carbon analogs, they are wide bandgap ($5.0\,\mathrm{eV}$–$6.0\,\mathrm{eV}$) insulators. Other notable properties include outstanding thermal conductivity and high specific heat. Also they can resist oxidation well even in very high temperatures. Mechanically they are nearly as tough as the corresponding carbon structures. These properties encourage their applications e.g. as protective shields encapsulating nanomaterials, nanofillers in composite materials, nanoscale calorimeters, microelectronic processors, macroscopic refrigerators and energy-saving buildings [14]. Unfortunately implementing these in practice has been hindered by very challenging synthesization processes. This is also one of the most important reasons why h-BN research has lagged behind h-C research. Research of these two fields largely goes hand in hand though, since actually at present day the most extensive study is on BN structures that also involve carbon.

The standard way to study these nanostructures computationally is with the density-functional theory (DFT) when accuracy is desired or with tight-binding (TB) if performance is required for example due to large size of the system in study. But also a less employed intermediate point between these two extremes—density-functional tight-binding (DFTB)—does exist. Similarly to the BN nanostructure research, this theory is quite young, derived in 1989 [15] and improved in 1998 [16]. It is derived from full DFT with TB approximations, so it is not ab initio and requires a pre-made parametrization instead. Now, the goal of this thesis is to construct such parametrization for boron nitride as well as possible and then study the most important basic (electric and mechanical) properties of both perfect and defective nanotubes and layers. Also the DFTB theory will be reviewed in detail. I will focus on pure BN structures, even though usually in practice hydrogen and carbon are involved.

2 The tight-binding density-functional (DFTB) theory

In this section I will review the derivation of the theory of density-functional tight-binding (DFTB), and it is the research training part of this work. The used units are as follows:

$$\begin{aligned}
\text{Energy } E\text{:} &\qquad 1\,\text{Ha} = 27.2114\,\text{eV}. && (2.1)\\
\text{Length } r\text{:} &\qquad 1\,\text{Bohr} = 0.5292\,\text{Å}. && (2.2)\\
\text{Mass } m\text{:} &\qquad 1\text{ atomic mass unit} = 1.6605 \times 10^{-27}\,\text{kg}. && (2.3)\\
\text{Time } t\text{:} &\qquad 1.0327\,\text{fs}. && (2.4)
\end{aligned}$$

With these units the fundamental constants can be chosen to be

$$\begin{aligned}
e &= 1, && (2.5)\\
\epsilon_0 &= \frac{1}{4\pi}, && (2.6)\\
\hbar &= 0.0234 \quad \text{and} && (2.7)\\
k_\mathrm{B} &= 3.1668 \times 10^{-6}. && (2.8)
\end{aligned}$$

2.1 The foundations of density-functional theory (DFT)

2.1.1 The many-body problem

The solid state and nanophysics as well as chemistry are essentially quantum mechanics of systems consisting of nuclei and electrons. In general, the wave function of such a system is a function of position and spin of each electron and each nucleus. However, due to the three orders of magnitude larger mass of the nuclei, they are practically frozen compared to the quick electrons. Also their charge density is very strongly confined. For these reasons it is usually sufficient to approximate them semiclassically as point-like classical particles. Therefore in practice the problem of interest for an N-electron system is usually for the electronic wave function $\Psi(\mathbf{x}_1, \ldots, \mathbf{x}_N)$, where $\mathbf{x}_i$ denotes the position-spin pair $\mathbf{x}_i = (\mathbf{r}_i, \sigma_i)$. The role of the ions is reduced to being a part of the external potential $V(\mathbf{r})$. It is now a sum of Coulombic contributions and e.g. external electric fields.

Also the ion-ion interaction energy E_{II}, which reads

$$E_{\text{II}} = \frac{1}{2} \sum_{I<J}^{N} \frac{Z_I Z_J}{|\mathbf{R}_I - \mathbf{R}_J|}, \tag{2.9}$$

must be added to the total energy of the system. Above Z_I and Z_J are the atomic numbers and $\mathbf{R}_I$ and $\mathbf{R}_J$ the positions of nuclei I and J, respectively. Nevertheless, Ψ must fulfil the Schrödinger equation

$$\hat{H} \left| \Psi(\mathbf{x}_1, \ldots, \mathbf{x}_N) \right\rangle = E_{\text{e}} \left| \Psi(\mathbf{x}_1, \ldots, \mathbf{x}_N) \right\rangle, \tag{2.10}$$

where E_{e} is the electronic energy and

$$\hat{H} = \hat{T} + \hat{V} + \hat{W}, \tag{2.11}$$

where

$$\hat{T} = \sum_{i=1}^{N} \frac{1}{2} \nabla_i^2 \tag{2.12}$$

$$\hat{V} = \sum_{i=1}^{N} V(\mathbf{x}_i), \tag{2.13}$$

$$\hat{W} = \sum_{i>j}^{N} W(\mathbf{x}_i, \mathbf{x}_j). \tag{2.14}$$

The total energy E of the system now reads

$$E = E_\mathrm{e} + E_\mathrm{II}, \tag{2.15}$$

but for convention let us omit E_II for a while.

2.1.2 The Hohenberg-Kohn theorem

A system may have several independent wave functions that yield the lowest energy. In this case the ground state is called *degenerate*. But from now on we assume that this is not the case, i.e., the ground state (GS) wave function $|\Psi_\mathrm{GS}\rangle$ is unique up to a trivial phase factor: $|\Psi_\mathrm{GS}\rangle \neq \mathrm{e}^{\mathrm{i}\alpha}|\Phi_\mathrm{GS}\rangle$ $(\alpha \in \mathbb{R})$. Similarly two potentials are considered different only if they differ from each other by more than a trivial constant: $V_1 \neq V_2 + C$ $(C \in \mathbb{R})$.

With this requirement of non-degenerate ground states we can derive the standard Hohenberg-Kohn theorems, that tie together the potential $V(\mathbf{r})$ of the system and its ground state density $n_\mathrm{GS}(\mathbf{r})$. They were introduced in 1964 by Pierre Hohenberg and Walter Kohn [17] and first of them is the following:

Hohenberg-Kohn Theorem 1. *The external potential $V(\mathbf{r})$ is a unique functional of the ground state wave function and vice versa.*

This is readily shown: Consider a counterexample with two different potentials that yield the same ground state $|\Psi_\mathrm{GS}\rangle$

$$\hat{H}_1 |\Psi_\mathrm{GS}\rangle = \left(\hat{T} + \hat{V}_1 + \hat{W}\right) |\Psi_\mathrm{GS}\rangle = E_1 |\Psi_\mathrm{GS}\rangle \quad \text{and} \tag{2.16}$$

$$\hat{H}_2 |\Psi_\mathrm{GS}\rangle = \left(\hat{T} + \hat{V}_2 + \hat{W}\right) |\Psi_\mathrm{GS}\rangle = E_2 |\Psi_\mathrm{GS}\rangle . \tag{2.17}$$

Subtraction of these two equations gives

$$\left(\hat{V}_1 - \hat{V}_2\right) |\Psi_\mathrm{GS}\rangle = (E_1 - E_2) |\Psi_\mathrm{GS}\rangle = C |\Psi_\mathrm{GS}\rangle . \tag{2.18}$$

This is in contradiction with our assumption, and thus there can not exist two different potentials with the same ground state density. And the correspondence is one-to-one, since by the non-degeneracy definition for each potential (and thus for each Hamiltonian) only one ground state wave function exists.

Hohenberg-Kohn Theorem 2. *The ground state wave function is a unique functional of the ground state total density* $n_{\mathrm{GS}}(\mathbf{r})$ *and vise versa.*

This is also shown straightforwardly, again by finding a contradiction from the assumption: Let there be two ground state wave functions $|\Psi_1\rangle$ and $|\Psi_2\rangle$ that produce the same ground state density $n(\mathbf{r})$. Then

$$\begin{aligned} E_1 = \langle\Psi_1|\hat{H}_1|\Psi_1\rangle &= \langle\Psi_1|\hat{H}_2 + \hat{V}_1 - \hat{V}_2|\Psi_1\rangle \\ &= \langle\Psi_1|\hat{H}_2|\Psi_1\rangle + \int \mathrm{d}^3\mathbf{r}\, n(\mathbf{r})\,(V_1(\mathbf{r}) - V_2(\mathbf{r})) \\ &> E_2 + \int \mathrm{d}^3\mathbf{r}\, n(\mathbf{r})\,(V_1(\mathbf{r}) - V_2(\mathbf{r}))\,, \end{aligned} \tag{2.19}$$

where I used the fact that $\langle\Psi_1|\hat{H}_2|\Psi_1\rangle > E_2$, since Ψ_1 is not the ground state wave function for $\hat{H}_2$. The previous is naturally true also in the index interchange $1 \leftrightarrow 2$, so we also obtain

$$E_2 > E_1 + \int \mathrm{d}^3\mathbf{r}\, n(\mathbf{r})\,(V_2(\mathbf{r}) - V_1(\mathbf{r}))\,. \tag{2.20}$$

Adding these two equations together leads us to the contradiction $E_1 + E_2 > E_1 + E_2$. Therefore there can not be two wave functions with the same ground state density, and the correspondence is again one-to-one, since by definition of the density, a ground state can have only one density.

Together the HK theorems 1 and 2 form the final Hohenberg-Kohn theorem:

Hohenberg-Kohn Theorem 3. *The external potential* $V(\mathbf{r})$ *is a unique functional of the ground state density* $n_{\mathrm{GS}}(\mathbf{r})$ *and vice versa.*

The density-functional theory boils down to this remarkable theorem. Now we can begin to apply it.

2.2 The Hohenberg-Kohn variational principle

Since the ground state wave function is a functional of $n_{\mathrm{GS}}(\mathbf{r})$, the expectation value $O = \langle\Psi[n_{\mathrm{GS}}]|\hat{O}|\Psi[n_{\mathrm{GS}}]\rangle$ of any ground state observable $\hat{O}$ is its functional as well. Particularly this applies for energy:

$$E_{\mathrm{GS}}[n_{\mathrm{GS}}(\mathbf{r})] = \langle\Psi[n_{\mathrm{GS}}(\mathbf{r})]|\hat{H}|\Psi[n_{\mathrm{GS}}(\mathbf{r})]\rangle\,. \tag{2.21}$$

But consider the functional

$$E[n(\mathbf{r})] = \langle\Psi[n(\mathbf{r})]|\hat{H}|\Psi[n(\mathbf{r})]\rangle = F_{\mathrm{HK}}[n(\mathbf{r})] + \int \mathrm{d}^3\mathbf{r}\, V(\mathbf{r})n(\mathbf{r}), \tag{2.22}$$

where $n(\mathbf{r})$ is not the ground state density for $\hat{H}$, and $F_{\mathrm{HK}}[n]$ is the *Hohenberg-Kohn functional*:

$$F_{\mathrm{HK}}[n(\mathbf{r})] = \langle\Psi[n(\mathbf{r})]|\hat{T} + \hat{W}|\Psi[n(\mathbf{r})]\rangle\,. \tag{2.23}$$

Now it is obvious that $E[n] \geq E_{\mathrm{GS}}[n_{\mathrm{GS}}]$, and the equality applies only for $n(\mathbf{r}) = n_{\mathrm{GS}}(\mathbf{r})$. This means that we can find the ground state by minimizing the functional $E[n(\mathbf{r})]$. But to be exact, it turns out that $n(\mathbf{r})$ must be V*-representable*, which means that it has to be the ground state density for some other system characterized by some potential other than $V(\mathbf{r})$ [18]. Nevertheless, let us from now on assume that this is the case. The minimum is obtained for the density that satisfies

$$\int \mathrm{d}\mathbf{r}\, \left.\frac{\delta E[n]}{\delta n(\mathbf{r})}\right|_{n_{\mathrm{GS}}} \delta n(\mathbf{r}) = 0. \tag{2.24}$$

To conserve charge, we should only allow density variations for which

$$\int \mathrm{d}\mathbf{r}\, \delta n(\mathbf{r}) = 0. \tag{2.25}$$

This implies that

$$\left.\frac{\delta E[n]}{\delta n(\mathbf{r})}\right|_{n_{\mathrm{GS}}} = \text{constant}, \quad \text{or} \tag{2.26}$$

$$E[n_{\mathrm{GS}} + \delta n] = E[n_{\mathrm{GS}}] + \mathscr{O}(\delta n^2). \tag{2.27}$$

This is known as the KS stationary principle. It is equivalent to

$$\left.\frac{\delta F_{\mathrm{HK}}[n]}{\delta n(\mathbf{r})}\right|_{n_{\mathrm{GS}}} = -V(\mathbf{r}), \tag{2.28}$$

where the constant has been embedded into $V(\mathbf{r})$ because it simply amounts to gauge of the potential and it is usually fixed in such a way that $V(\mathbf{r}) \to 0$ for $|\mathbf{r}| \to 0$.

2.3 The Kohn-Sham construction

According to the Hohenberg-Kohn theorem the GS density $n_{\mathrm{GS}}(\mathbf{r})$ is related to a fixed external potential V uniquely. Consider now the imaginary system of non-interacting (except via Pauli exclusion principle) electron gas with the *same* ground state density. In this case $\hat{W} = 0$, but since the HK theorem did not take into account the two-particle interaction at any stage, it is still possible to find a *single-particle* potential $V_{\mathrm{s}}(\mathbf{r})$ that is uniquely connected to $n_{\mathrm{GS}}(\mathbf{r})$. This is a great simplification from a many-body system into an effectively single-particle system. With this I mean that the Schrödinger equation of this system

$$\sum_{i}^{N} H_{\mathrm{s}}(\mathbf{r}_i) \left|\Psi(\mathbf{r}_1, \ldots, \mathbf{r}_N)\right\rangle = E_{\mathrm{s}} \left|\Psi(\mathbf{r}_1, \ldots, \mathbf{r}_N)\right\rangle, \tag{2.29}$$

where

$$H_{\mathrm{s}}(\mathbf{r}) = -\frac{1}{2}\nabla^2_{\mathbf{r}} + V_{\mathrm{s}}(\mathbf{r}), \tag{2.30}$$

separates into single-particle equations

$$H_{\mathrm{s}}(\mathbf{r}) \left|\psi_i(\mathbf{r})\right\rangle = \epsilon_i \left|\psi_i(\mathbf{r})\right\rangle . \tag{2.31}$$

With $\{\psi_i(\mathbf{r})\}$ and $\{\epsilon_i\}$ the solutions to the problem (2.29) read[1]

$$\Psi_{\mathrm{GS}}(\mathbf{r}_1, \ldots, \mathbf{r}_N) = \begin{vmatrix} \psi_1(\mathbf{r}_1) & \ldots & \psi_N(\mathbf{r}_1) \\ \vdots & \ddots & \vdots \\ \psi_1(\mathbf{r}_N) & \ldots & \psi_N(\mathbf{r}_N) \end{vmatrix}, \tag{2.32}$$

$$n_{\mathrm{GS}}(\mathbf{r}) = \sum_i^N \int \mathrm{d}\mathbf{r} \, \left|\psi_i(\mathbf{r})\right|^2, \quad \text{and} \tag{2.33}$$

$$E_{\mathrm{GS}} = \sum_i^N \epsilon_i. \tag{2.34}$$

Since the Pauli exclusion principle forbids any electrons to occupy the same state simultaneously, the above ground state quantities were used by using N states lowest in energy. Assuming spin degeneracy, pre-factor of 2 appears for all these quantities and summation only goes up to $N/2$.

---

[1] I do not present the derivation of this result here, but verifying that it is the desired Ψ is not difficult. Firstly, Ψ_{GS} clearly satisfies the antisymmetricity requirement $\Psi_{\mathrm{GS}}(\mathbf{r}_1, \ldots, \mathbf{r}_a, \mathbf{r}_{a+1}, \ldots) = \Psi_{\mathrm{GS}}(\mathbf{r}_1, \ldots, \mathbf{r}_{a+1}, \mathbf{r}_a, \ldots)$, which is due to the fact that electrons are fermions. Also for orbitals ψ that do normalize to unity, the total density integrates to N. Finally, by inserting (2.32) into (2.29), we can see that it indeed is an eigenstate for $\hat{H}_{\mathrm{s}}$: A general term in (2.32), is of the form $\psi_{P(1)}(\mathbf{x}_1)\cdots\psi_{P(a)}(\mathbf{x}_a)\cdots$, where P is a permutation of integers $a \in \mathbb{N}$. Now, $\sum_i \hat{H}_{\mathrm{s}}(\mathbf{r}_i)\psi_{P(1)}(\mathbf{r}_1)\cdots\psi_{P(N/2)}(\mathbf{r}_{N/2}) = \sum_i \epsilon_i \psi_{P(1)}(\mathbf{r}_1)\cdots\psi_{P(N)}(\mathbf{r}_N)$, and since this holds for every term, $\hat{H}_{\mathrm{s}}\Psi = \sum_i \epsilon_i \Psi$. Thus (2.32) indeed is an eigenstate for $\hat{H}_{\mathrm{s}}$.

2.3.1 The single-particle potential $V_\mathrm{s}(\mathbf{r})$

Eqs. (2.32–2.34) now sum up the KS construction together with Eq. (2.31). Provided $V_\mathrm{s}[n](\mathbf{r})$, the KS equations are now solvable. Its form is naturally not trivial, since it includes all the complex many-body effects. Anyhow, let us begin its analyzation by dividing the energy functional into two parts:

$$\begin{aligned} E_\mathrm{s}[n(\mathbf{r})] &= T_\mathrm{s}[n(\mathbf{r})] + F_\mathrm{s}[n(\mathbf{r})], \quad \text{where} \qquad (2.35)\\ T_\mathrm{s}[n(\mathbf{r})] &= \sum_i \langle \psi_i[n]| -\frac{1}{2}\nabla^2 |\psi_i[n]\rangle = \sum_i -\frac{1}{2}\int \mathrm{d}^3\mathbf{r}\, \psi_i^*(\mathbf{r})\nabla^2\psi_i(\mathbf{r})\\ &= \frac{1}{2}\sum_i \int \mathrm{d}^3\mathbf{r}\, |\nabla\psi_i(\mathbf{r})| \quad \text{and} \qquad (2.36)\\ F_\mathrm{s}[n(\mathbf{r})] &= \sum_i \langle \psi_i[n]|\hat{V}_\mathrm{s}[n(\mathbf{r})]|\psi_i[n]\rangle = \sum_i \int \mathrm{d}^3\mathbf{r}\, \psi_i^*(\mathbf{r})V_\mathrm{s}(\mathbf{r})\psi_i(\mathbf{r})\\ &= \int \mathrm{d}^3\mathbf{r}\, V_\mathrm{s}[n(\mathbf{r})]n(\mathbf{r}). \qquad (2.37) \end{aligned}$$

So $T_\mathrm{s}[n(\mathbf{r})]$ is the kinetic energy of the free electron gas. It is not the same as the kinetic energy of the real interacting system, but the hope is that it is roughly similar in magnitude. Now the form of $F[n(\mathbf{r})]$ must be deduced. It is not, of course, trivial at all. It is sensible to divide it to different terms arising from different sources. Firstly, $F[n(\mathbf{r})]$ must contain

$$\int \mathrm{d}\mathbf{r}\, V[n(\mathbf{r})]n(\mathbf{r}), \qquad (2.38)$$

i.e., the energy yielded by the potential of the original Hamiltonian. Secondly, it must contain the *Hartree energy*

$$E_\mathrm{H}[n(\mathbf{r})] = \frac{1}{2}\iint \mathrm{d}\mathbf{r}\mathrm{d}\mathbf{r}'\, \frac{n(\mathbf{r})n(\mathbf{r}')}{|\mathbf{r}-\mathbf{r}'|}. \qquad (2.39)$$

This term approximates the many-particle interaction in the most simple and naive possible way—it describes how the charge cloud with given density $n(\mathbf{r})$ repels itself. The factor of $1/2$ is to void the effect of double-counting in E_{H}.

The rest of $F[n(\mathbf{r})]$ is defined as the *exchange-correlation* energy $E_{\mathrm{xc}}[n(\mathbf{r})]$. It is the term that hides the complexity of the many-body physics and takes care that for each density the functional $E[n(\mathbf{r})]$ is equal in both interacting and non-interacting case. So

$$F[n(\mathbf{r})] = \int \mathrm{d}\mathbf{r}\, V[n(\mathbf{r})]n(\mathbf{r}) + E_{\mathrm{H}}[n(\mathbf{r})] + E_{\mathrm{xc}}[n(\mathbf{r})]. \tag{2.40}$$

It can also be written as

$$E_{\mathrm{xc}}[n(\mathbf{r})] = \langle\Psi[n]|\hat{T}|\Psi[n]\rangle - T_{\mathrm{s}}[n(\mathbf{r})] + \langle\Psi[n]|\hat{W}|\Psi[n]\rangle - E_{\mathrm{H}}[n(\mathbf{r})]. \tag{2.41}$$

Its interpretation is clear from this: it contains the difference of many-particle and single-particle kinetic energy and difference of many-particle and single-particle electron-electron interaction energy.

Now, just as in the interacting case, we can see that around the ground state density we must have

$$\left.\frac{\delta T_{\mathrm{s}}[n(\mathbf{r})]}{\delta n(\mathbf{r})}\right|_{n_{\mathrm{GS}}} = -\left.\frac{\delta F_{\mathrm{s}}[n(\mathbf{r})]}{\delta n(\mathbf{r})}\right|_{n_{\mathrm{GS}}} = -V_{\mathrm{s}}[n](\mathbf{r}). \tag{2.42}$$

The functional derivative of $F[n(\mathbf{r})]$ reads

$$\frac{\delta F_{\mathrm{s}}[n(\mathbf{r})]}{\delta n(\mathbf{r})} = V_{\mathrm{s}}[n](\mathbf{r}) = V(\mathbf{r}) + V_{\mathrm{H}}[n(\mathbf{r})] + \frac{\delta V_{\mathrm{xc}}[n(\mathbf{r})]}{\delta n(\mathbf{r})}, \tag{2.43}$$

where $V_{\mathrm{H}}[n(\mathbf{r})]$ is the *Hartree potential* and $V_{\mathrm{xc}}[n(\mathbf{r})]$ is the *exchange-correlation potential*:

$$V_{\mathrm{H}}[n(\mathbf{r})] = \int \mathrm{d}\mathbf{r}' \, \frac{n(\mathbf{r}')}{|\mathbf{r}-\mathbf{r}'|} \quad \text{and} \tag{2.44}$$

$$V_{\mathrm{xc}}[n(\mathbf{r})] = \frac{\delta E_{\mathrm{xc}}[n(\mathbf{r})]}{\delta n(\mathbf{r})}. \tag{2.45}$$

2.3.2 Solving the Kohn-Sham construction

Eqs. (2.32–2.34) now sum up the KS construction together with Eqs. (2.31) and (2.43). Solution of this problem is obtained in *self-consistent* manner. The procedure is as follows:

1. Begin with an input density $n_{\mathrm{in}}(\mathbf{r})$.
2. Construct with it a guess for $V_{\mathrm{s}}[n_{\mathrm{GS}}](\mathbf{r})$ with the functional (2.43), i.e.,

   $$V_{\mathrm{s}}[n_{\mathrm{in}}](\mathbf{r}) = V(\mathbf{r}) + V_{\mathrm{H}}[n_{\mathrm{in}}(\mathbf{r})] + \frac{\delta V_{\mathrm{xc}}[n_{\mathrm{in}}(\mathbf{r})]}{\delta n_{\mathrm{in}}(\mathbf{r})}. \tag{2.46}$$

   This way, the V-representability is ensured.
3. Solve with it the single-particle KS Schrodinger equation (2.31):

   $$\left(-\frac{1}{2}\nabla^2 + V_{\mathrm{s}}[n_{\mathrm{in}}](\mathbf{r})\right)\psi_i[n_{\mathrm{in}}](\mathbf{r}) = \epsilon_i[n_{\mathrm{in}}]\psi_i(\mathbf{r}). \tag{2.47}$$

4. Now let us denote the density produced by it as $n_{\mathrm{out}}(\mathbf{r})$:

   $$n_{\mathrm{out}}[n_{\mathrm{in}}](\mathbf{r}) = \sum_{i=1}^{N} |\psi_i[n_{\mathrm{in}}](\mathbf{r})|^2 \, . \tag{2.48}$$

   If $n_{\mathrm{out}}(\mathbf{r})$ is sufficiently close to $n_{\mathrm{in}}(\mathbf{r})$, convergence has been achieved and the process has been finished. Otherwise n_{out} becomes the new n_{in} and a new cycle starts from the first step.

Unfortunately, there do exist certain convergence problems in this process. Firstly, as discussed, the initial guess must be good enough. Secondly, with bad luck the system might still converge to wrong density. Thirdly, consider a situation where during the self-consistent solving cycle at some point ψ_N and ψ_{N+1} are very close in energy but very different in density (the indices have been ordered by energy so that $\epsilon_i < \epsilon_{i+1}\,\forall i$). Now, according to Eq. (2.33), ψ_{N+1} will be cut out from $n(\mathbf{r})$. But if during the next cycle the energy of ψ_{N+1} becomes smaller than that of ψ_N, ψ_N will be cut out instead of ψ_{N+1}. This situation might then reverse in the next cycle. Now, even if each and every ψ_i was close to the correct solution all along, this behavior results in a major transition in the density, and convergence is not achieved. But this can be avoided by introducing a smooth way of cutting the orbital contributions from $n(\mathbf{r})$. The standard way to achieve this is by using thermal broadening via Fermi-Dirac statistics so that the occupation number $\sqrt{f_i}$ of state ψ_i with energy ϵ_i is (remember that $k_\mathrm{B} = 1$ in our units)

$$f(\epsilon_i) = \frac{1}{\exp\left((\epsilon_i - \mu)/T\right) + 1}, \tag{2.49}$$

with such chemical potential μ that $\sum_i f_i = N$. Now $n = \sum_i f_i \left|\psi_i\right|^2$ and $E = \sum_i f_i \epsilon_i$. This means that contrary to requirements in the theory of DFT $n(\mathbf{r})$ and E are no longer the true ground state density and energy, respectively. But only so small T should be used that its effects on $n(\mathbf{r})$ and E are negligible.

2.4 The functional $\mathscr{E}[n]$

Following Foulkes and Haydock [15], let us write down $E_\mathrm{s}[n]$ in an alternative way by making use of Eqs. (2.34) and (2.35):

$$E_\mathrm{s}[n_\mathrm{out}] = \sum_i \epsilon_i[n_\mathrm{out}] - \int \mathrm{d}^3\mathbf{r}\, V_\mathrm{s}[n_\mathrm{out}](\mathbf{r}) n_\mathrm{out}(\mathbf{r}) + F_\mathrm{s}[n_\mathrm{out}]. \tag{2.50}$$

As discussed, by minimizing $E[n]$ it is possible to find n_GS through the HK variational principle. Now, with $n_\mathrm{out} = n$, Eq. (2.50) is exactly equal to $E_{\rm s}[n] = T_{\rm s}[n] + F_{\rm s}[n]$, which in turn is exactly equal to $E[n]$ by definition. Therefore the variational principle still applies. The next step is to expand $E[n_{\rm out}]$ around $n_{\rm in}$ to the second order. It is a sensible thing to do for differences

$$\Delta n(\mathbf{r}) = n_{\rm out}(\mathbf{r}) - n_{\rm in}(\mathbf{r}) \tag{2.51}$$

because both $n_{\rm in}$ and $n_{\rm out}$ are supposed to be close to $n_{\rm GS}$ and due to it Δn should be small. Now the concept of functional Taylor expansion is required. For example, expansion of $F_{\rm s}[n_{\rm out}]$ to the second order reads [18]

$$\begin{aligned} &F_{\rm s}[n_{\rm out}] = E_{\rm s}[n_{\rm in} + \Delta n] \qquad (2.52)\\ =&F_{\rm s}[n_{\rm in}] + \int {\rm d}\mathbf{r}\, \left.\frac{\delta F_{\rm s}[n]}{\delta n(\mathbf{r})}\right|_{n_{\rm in}} \Delta n(\mathbf{r}) + \frac{1}{2}\iint {\rm d}\mathbf{r}{\rm d}\mathbf{r}'\, \left.\frac{\delta^2 F_{\rm s}[n]}{\delta n(\mathbf{r})\delta n(\mathbf{r}')}\right|_{n_{\rm in}} \Delta n(\mathbf{r})\Delta n(\mathbf{r}'). \end{aligned}$$

As can be seen from this equation, the functional derivatives and their integrals easily become massive and tedious to read. Thus, in accordance with [15], [16] and [19], from now on I will use the following kind of abbreviations:

$$\begin{aligned} n(\mathbf{r}) &\to n, & \int {\rm d}\mathbf{r} &\to \int, \\ n(\mathbf{r}') &\to n', & \int {\rm d}\mathbf{r}' &\to \int', \end{aligned}$$

and so on. By adopting this notation the functional mathematics become significantly clearer to read. But now back to the expansion. By inserting (2.52) into (2.50) and using $n_{\rm out} = n_{\rm in} + \Delta n$ gives us

$$E_{\rm s}[n_{\rm out}] = \sum_i \epsilon_i + F_{\rm s}[n_{\rm in}] - \int \left.\frac{\delta F_{\rm s}[n]}{\delta n}\right|_{n_{\rm in}} n_{\rm in} + \frac{1}{2}\iint' \left.\frac{\delta^2 F_{\rm s}[n]}{\delta n \delta n'}\right|_{n_{\rm in}} \Delta n \Delta n'. \tag{2.53}$$

So $E_{\mathrm{s}}[n_{\mathrm{out}}] = \mathscr{E}[n_{\mathrm{in}}] + \mathscr{O}(\Delta n^2)$, where $\mathscr{E}[n_{\mathrm{in}}]$ is the $E_{\mathrm{s}}[n_{\mathrm{out}}]$ with n_{out} formally replaced by n_{in}:

$$\begin{aligned}\mathscr{E}[n_{\mathrm{in}}] =& \sum_i \epsilon_i - \frac{1}{2}\iint' \left.\frac{\delta^2 F_{\mathrm{s}}[n]}{\delta n \delta n'}\right|_{n_{\mathrm{in}}} \Delta n \Delta n' \\ =& \sum_i \epsilon_i[n_{\mathrm{out}}] + F_{\mathrm{s}}[n_{\mathrm{in}}] - \int \left.\frac{\delta F_{\mathrm{s}}[n]}{\delta n}\right|_{n_{\mathrm{in}}} n_{\mathrm{in}}. \end{aligned} \tag{2.54}$$

Now it must be ensured that this functional $\mathscr{E}$ is stationary around the ground state density—otherwise in the self-consistent solving cycle of the KS constriction the density will not converge. So let us analyze it further. By expanding $T_{\mathrm{s}}[n_{\mathrm{in}}]$ around n_{out} and using Eq. (2.42) we arrive at

$$T_{\mathrm{s}}[n_{\mathrm{in}}] = T_{\mathrm{s}}[n_{\mathrm{out}}] + \int V_{\mathrm{s}}[n_{\mathrm{in}}]\Delta n + \frac{1}{2}\iint' \left.\frac{\delta^2 T_{\mathrm{s}}}{\delta n \delta n'}\right|_{n_{\mathrm{out}}} \Delta n \Delta n'. \tag{2.55}$$

After this using $T_{\mathrm{s}}[n] = \sum_i \epsilon_i - \int V_{\mathrm{s}} n$ for $T_{\mathrm{s}}[n_{\mathrm{out}}] = T_{\mathrm{s}}[\Delta n + n_{\mathrm{in}}]$ gives

$$T_{\mathrm{s}}[n_{\mathrm{in}}] = \sum_i \epsilon_i - \int V_{\mathrm{s}}[n_{\mathrm{in}}] n_{\mathrm{in}} + \frac{1}{2}\iint' \left.\frac{\delta^2 T_{\mathrm{s}}}{\delta n \delta n'}\right|_{n_{\mathrm{out}}} \Delta n \Delta n'. \tag{2.56}$$

Hence we have for $E_{\mathrm{s}}[n_{\mathrm{in}}] = T_{\mathrm{s}}[n_{\mathrm{in}}] + F_{\mathrm{s}}[n_{\mathrm{in}}]$

$$\begin{aligned}E_{\mathrm{s}}[n_{\mathrm{in}}] &= \sum_i \epsilon_i + F_{\mathrm{s}}[n_{\mathrm{in}}] - \int V_{\mathrm{s}} n_{\mathrm{in}} + \frac{1}{2}\iint' \left.\frac{\delta^2 T_{\mathrm{s}}}{\delta n \delta n'}\right|_{n_{\mathrm{out}}} \Delta n \Delta n' \\ &= \mathscr{E}[n_{\mathrm{in}}] + \frac{1}{2}\iint' \left.\frac{\delta^2 T_{\mathrm{s}}}{\delta n \delta n'}\right|_{n_{\mathrm{out}}} \Delta n \Delta n'. \end{aligned} \tag{2.57}$$

This means that now we have two alternative expressions for $\mathscr{E}[n_{\mathrm{in}}]$, as besides Eq. (2.54) we also have

$$\mathscr{E}[n_{\text{in}}] = E_{\text{s}}[n_{\text{in}}] - \frac{1}{2} \iint' \left. \frac{\delta^2 T_{\text{s}}}{\delta n \delta n'} \right|_{n_{\text{out}}} \Delta n \Delta n'. \tag{2.58}$$

This form was obtained by expanding T_{s} to second order in $n_{\text{out}} - n_{\text{in}}$, whereas for the first form this was done for T_{s}. With these two forms it is now possible to expand $\mathscr{E}[n_{\text{in}}]$ around n_{GS}. Namely, by adding (2.54) and (2.58) together and working to second order in small quantities

$$\Delta n_{\text{in}} = n_{\text{in}} - n_{\text{GS}} \quad \text{and} \quad \Delta n_{\text{out}} = n_{\text{out}} - n_{\text{GS}} \tag{2.59}$$

gives

$$\mathscr{E}[n_{\text{in}}] = E_{\text{GS}} + \frac{1}{2} \iint' \left. \frac{\delta^2 E_{\text{s}}}{\delta n \delta n'} \right|_{n_{\text{GS}}} \Delta n_{\text{in}} \Delta n'_{\text{out}}. \tag{2.60}$$

We now see that our functional $\mathscr{E}[n_{\text{in}}]$ can actually very well be either larger or smaller than E_{GS} even though it usually is larger since $\Delta n_{\text{in}} \sim \Delta n_{\text{out}}$. But it does not matter because it is still stationary at n_{GS}, i.e., the linear terms are absent. This means that in the self-consistent solving cycle the density should still converge to n_{GS} and energy to E_{GS}. So let us now adopt $\mathscr{E}$ as our new energy functional. Let us now first write it out explicitly into a more practical form. From Eq. (2.54) we have

$$\begin{aligned}
\mathscr{E}[n_{\text{in}}] &= \sum_i \epsilon_i - \iint' \frac{n_{\text{in}} n'_{\text{in}}}{|r - r'|} - V_{\text{xc}}[n_{\text{in}}] n_{\text{out}} + \frac{1}{2} \iint' \frac{n_{\text{out}} n'_{\text{out}}}{|r - r'|} + E_{\text{xc}}[n_{\text{out}}] \\
&= \sum_i \epsilon_i - \frac{1}{2} \iint' \frac{n_{\text{in}} n'_{\text{in}}}{|\mathbf{r} - \mathbf{r}'|} - \int V_{\text{xc}}[n_{\text{in}}] n_{\text{in}} + E_{\text{xc}}[n_{\text{in}}].
\end{aligned} \tag{2.61}$$

Finally it should be noted that even though formally the eigenenergies ϵ_i are for the density n_{out}, we can replace them with those for n_{GS} since

$$\epsilon_i[n_{\text{out}}] = \epsilon_i[n_{\text{GS}}] + \iint' \left. \frac{\delta^2 \epsilon_i[n]}{\delta n \delta n'} \right|_{n_{\text{out}}} \Delta n_{\text{out}} \Delta n'_{\text{out}}, \tag{2.62}$$

so the replacement $\epsilon_i[n_{\text{out}}] \to \epsilon_i[n_{\text{GS}}]$ does not violate the stationarity. Now it is possible for example to compute the values of $\epsilon_i[n_{\text{GS}}]$ beforehands with in principle any method.

2.5 The frozen core approximation

The KS construction includes both core and valence-electronlike solutions ($\psi_{i_{\text{c}}}$ and $\psi_{i_{\text{v}}}$, respectively). The core wavefunctions are well localized around the deep potential of the nuclei and "feel" the effects of the other atoms as comparatively weak pertubations. This is why the core-electronlike solutions should be very close to linear combinations of orthogonal free atomic core functions $\varphi_{a_{\text{c}}}$. Suppose that the difference is of order λ. Then by using the ordinary variational principle we obtain for the core energy

$$\begin{aligned}\sum_{i_{\text{c}}} \epsilon_{i_{\text{c}}} =& \sum_{i_{\text{c}}} \langle \psi_{i_{\text{c}}}| - \frac{1}{2}\nabla^2 + V_{\text{s}}(\mathbf{r})|\psi_{i_{\text{c}}}\rangle \\ =& \sum_{a_{\text{c}}} \langle \varphi_{a_{\text{c}}}| - \frac{1}{2}\nabla^2 + V_{\text{s}}(\mathbf{r})|\varphi_{a_{\text{c}}}\rangle + \mathscr{O}(\lambda^2) \\ =& T_{\text{c}} + \int n_{\text{c}} V_{\text{s}} + \mathscr{O}(\lambda^2). \end{aligned} \tag{2.63}$$

Next, since $\sum_i = \sum_{i_{\text{c}}} + \sum_{i_{\text{v}}}$, the sum over the eigenvalues ϵ_i splits into two parts and by using (2.63) and ignoring the $\mathscr{O}(\lambda^2)$ terms (2.61) becomes

$$\mathscr{E}[n] = \sum_{i_{\text{v}}} \epsilon_{i_{\text{v}}} + T_{\text{c}} + \int n_{\text{c}} V_{\text{s}}[n] - E_{\text{H}}[n] - \int V_{\text{xc}}[n]n + E_{\text{xc}}[n] + E_{\text{II}}. \tag{2.64}$$

After this the 3rd, 4th and 5th term from this equation can be simplified significantly by using $n = n_{\text{c}} + n_{\text{v}}$:

$$\begin{aligned}
&\int n_{\mathrm{c}} V_{\mathrm{s}}[n_{\mathrm{c}}+n_{\mathrm{v}}] - E_{\mathrm{H}}[n_{\mathrm{c}}+n_{\mathrm{v}}] - \int V_{\mathrm{xc}}[n_{\mathrm{c}}+n_{\mathrm{v}}]\,(n_{\mathrm{c}}+n_{\mathrm{v}}) \\
=&\int n_{\mathrm{c}} V_{\mathrm{nucl}} + \iint' \frac{n_{\mathrm{c}}\,(n_{\mathrm{c}}{}'+n_{\mathrm{v}}{}')}{|\mathbf{r}-\mathbf{r}'|} + \int n_{\mathrm{c}} V_{\mathrm{xc}}[n_{\mathrm{c}}+n_{\mathrm{v}}] \\
-&\frac{1}{2}\iint \frac{(n_{\mathrm{c}}+n_{\mathrm{v}})\,(n_{\mathrm{c}}{}'+n_{\mathrm{v}}{}')}{|\mathbf{r}-\mathbf{r}'|} - \int V_{\mathrm{xc}}[n_{\mathrm{c}}+n_{\mathrm{v}}]\,(n_{\mathrm{c}}+n_{\mathrm{v}}) \\
=&\int n_{\mathrm{c}} V_{\mathrm{nucl}} + E_{\mathrm{H}}[n_{\mathrm{c}}] - E_{\mathrm{H}}[n_{\mathrm{v}}] - \int V_{\mathrm{xc}}[n] n_{\mathrm{v}}.
\end{aligned} \tag{2.65}$$

Also $V_{\mathrm{nucl}}(\mathbf{r})$ can be divided into core and valence parts:

$$V_{\mathrm{nucl}}(\mathbf{r}) = \sum_{I}^{N} \frac{Z_I^{\mathrm{c}} + Z_I^{\mathrm{v}}}{|\mathbf{r}-\mathbf{R}_I|}. \tag{2.66}$$

Here Z_I^{c} (Z_I^{v}) is the amount of core (valence) electrons on atom I. So it is the amount of positive charge being screened out (left unscreened) by the core electrons.

Furthermore, thanks to the strong localization of the core electrons, the core density belonging to nucleus I can be written as $n_{\mathrm{c},I}(\mathbf{r}) = -\delta(\mathbf{R}_I)Z_{\mathrm{c},I}$ from the point of view of other nuclei and their core electrons. So

$$n_{\mathrm{c}}(\mathbf{r}) = -\sum_{I}^{N} \delta(\mathbf{R}_I) Z_I^{\mathrm{c}}. \tag{2.67}$$

Inserting this into the first term from (2.65) ($\int n_{\mathrm{c}} V_{\mathrm{nucl}}$) yields

$$\begin{aligned}
\int n_{\mathrm{c}} V_{\mathrm{nucl}} &= -\sum_{I,J}^{N} \int \frac{\delta(\mathbf{R}_I) Z_{\mathrm{c},I}\,(Z_J^{\mathrm{c}}+Z_J^{\mathrm{v}})}{|\mathbf{R}_I-\mathbf{R}_J|} \\
&= -\sum_{\substack{I,J \\ I\neq J}}^{N} \frac{Z_I^{\mathrm{c}}\,(Z_J^{\mathrm{c}}+Z_J^{\mathrm{v}})}{|\mathbf{R}_I-\mathbf{R}_J|} + \sum_{I}^{N} \int \frac{n_{\mathrm{c},I}(\mathbf{r}-\mathbf{R}_I)\,(Z_I^{\mathrm{c}}+Z_I^{\mathrm{v}})}{|\mathbf{r}-\mathbf{R}_I|}.
\end{aligned} \tag{2.68}$$

Here the latter term is a structure-independent constant—it does not depend on $\mathbf{R}_I$ or valence electrons—and can be ignored. All the structure-independent constants arise from interactions between the core electrons and nuclei, so neglecting them does not affect the final goal (solving the valence electron problem). Eventually it just leads to different zero-point energy.

Treating $E_{\mathrm{H}}[n_{\mathrm{c}}]$ similarly leads to

$$\frac{1}{2}\iint' \frac{n_{\mathrm{c}}n_{\mathrm{c}}'}{|\mathbf{r}-\mathbf{r}'|} = \frac{1}{2}\sum_{\substack{I,J\\I\neq J}}^{N} \frac{Z_I^{\mathrm{c}}Z_J^{\mathrm{c}}}{|\mathbf{R}_I-\mathbf{R}_J|} + \frac{1}{2}\sum_{I}^{N}\iint' \frac{n_I^{\mathrm{c}}(\mathbf{r}-\mathbf{R}_I)n_I^{\mathrm{c}}(\mathbf{r}'-\mathbf{R}_I)}{|\mathbf{r}-\mathbf{r}'|}. \tag{2.69}$$

Here the latter term is another structure-independent constant and is henceforth ignored.

Next the ion-ion interaction can be separated into a form similar with (2.68) and (2.69) by using $Z_I = Z_I^{\mathrm{c}} + Z_I^{\mathrm{v}}$:

$$E_{\mathrm{II}} = \frac{1}{2}\sum_{\substack{I,J\\I\neq J}}^{N} \frac{Z_I^{\mathrm{c}}Z_J^{\mathrm{c}}}{|\mathbf{R}_I-\mathbf{R}_J|} + \frac{1}{2}\sum_{\substack{I,J\\I\neq J}}^{N} \frac{Z_I^{\mathrm{v}}Z_J^{\mathrm{v}}}{|\mathbf{R}_I-\mathbf{R}_J|} + \sum_{\substack{I,J\\I\neq J}}^{N} \frac{Z_I^{\mathrm{c}}Z_J^{\mathrm{v}}}{|\mathbf{R}_I-\mathbf{R}_J|}. \tag{2.70}$$

Putting the Eqs. (2.68–2.70) together only leaves us one summation term:

$$\int n_{\mathrm{c}}V_{\mathrm{nucl}} + E_{\mathrm{H}}[n_{\mathrm{c}}] + E_{\mathrm{II}} = \frac{1}{2}\sum_{\substack{I,J\\I\neq J}}^{N} \frac{Z_I^{\mathrm{v}}Z_J^{\mathrm{v}}}{|\mathbf{R}_I-\mathbf{R}_J|}. \tag{2.71}$$

As the next step we can in a way "linearize" $V_{\mathrm{xc}}\left[n_{\mathrm{c}}+n_{\mathrm{v}}\right]$ and $E_{\mathrm{xc}}\left[n_{\mathrm{c}}+n_{\mathrm{v}}\right]$ so that we obtain for the xc-terms left at this point

$$
\begin{aligned}
&- \int V_{\mathrm{xc}}[n_{\mathrm{c}} + n_{\mathrm{v}}] n_{\mathrm{v}} + E_{\mathrm{xc}}[n_{\mathrm{c}} + n_{\mathrm{v}}] \\
&= - \int V_{\mathrm{xc}}\left[n_{\mathrm{c}}\right] n_{\mathrm{v}} - \int V_{\mathrm{xc}}\left[n_{\mathrm{v}}\right] n_{\mathrm{v}} + E_{\mathrm{xc}}[n_{\mathrm{c}}] + E_{\mathrm{xc}}[n_{\mathrm{v}}],
\end{aligned} \tag{2.72}
$$

where $E_{\mathrm{xc}}[n_{\mathrm{c}}]$ is also an ignorable structure-independent constant if we linearize it further, since then it does not depend on the ion positions $\mathbf{R}_I$ anymore:

$$
E_{\mathrm{xc}}[n_{\mathrm{c}}] \approx \sum_I E_{\mathrm{xc}}[n_{\mathrm{c},I}]. \tag{2.73}
$$

These linearizations are neither trivial nor straightforward, but they are well-established and theoretically justified for instance in [20].

Now, by putting all the terms together and ignoring (2.73) as well as all the other structure-independent constants, we obtain for $\mathscr{E}$

$$
\mathscr{E}[n_{\mathrm{v}}] = \sum_{i_{\mathrm{v}}} \epsilon_{i_{\mathrm{v}}} - E_{\mathrm{H}}[n_{\mathrm{v}}] - \int V_{\mathrm{xc}}[n_{\mathrm{v}}] n_{\mathrm{v}} + E_{\mathrm{xc}}[n_{\mathrm{v}}] + \frac{1}{2} \sum_{\substack{I,J \\ I \neq J}}^{N} \frac{Z_I^{\mathrm{v}} Z_J^{\mathrm{v}}}{|\mathbf{R}_I - \mathbf{R}_J|}, \tag{2.74}
$$

which is basically exactly Eq. (2.61) with all the core electron energy and density ignored through replacements $\sum_i \epsilon_i \to \sum_{i_{\mathrm{v}}} \epsilon_{i_{\mathrm{v}}}$ and $n \to n_{\mathrm{v}}$. But the KS valence eigenstates $\psi_{i_{\mathrm{v}}}(\mathbf{r})$ are still obtained from the same single-particle KS equation (2.31) that still has the core contributions:

$$
\begin{aligned}
\Big\{ &- \frac{1}{2}\nabla^2 + V_{\mathrm{nucl}}(\mathbf{r}) + V_{\mathrm{H}}[n_c(\mathbf{r})] + V_{\mathrm{H}}[n_v(\mathbf{r})] + \\
&+ V_{\mathrm{xc}}[n_c(\mathbf{r})] + V_{\mathrm{xc}}[n_v(\mathbf{r})] \Big\} \psi_{i_v}(\mathbf{r}) = \epsilon_{i_v} \psi_{i_v}(\mathbf{r}).
\end{aligned} \tag{2.75}
$$

But if also $V_{\mathrm{xc}}[n_{\mathrm{c}}]$ in the above equation is linearized, we can now replace the one-electron potential due to the frozen cores by a sum of ionic pseudopotentials [21]:

$$\left\{-\frac{1}{2}\nabla^2+\sum_I V_I^{\mathrm{ps}}(\mathbf{r}-\mathbf{R}_I)+V_{\mathrm{H}}[n_v(\mathbf{r})]+V_{\mathrm{xc}}[n_v(\mathbf{r})]\right\}\psi_{i_{\mathrm{v}}}^{\mathrm{ps}}(\mathbf{r})=\epsilon_{i_{\mathrm{v}}}\psi_{i_{\mathrm{v}}}^{\mathrm{ps}}(\mathbf{r}). \tag{2.76}$$

This way the problem becomes dependent on valence electrons only, which is excellent since all the physics of interest is there. The pseudopotentials that include $V_{\mathrm{xc}}[n_{\mathrm{c}_I}]$ can be computed beforehand. Computation of these ionic pseudopotentials is an art of its own and has been comprehensively studied for example in [22]. Nevertheless, at this point the KS construction is determined by Eqs. (2.74) and (2.76).

2.6 Second-order self-consistent charge extension

Let us first for simplicity employ notation alterations

$$\begin{aligned} i_{\mathrm{v}} &\to i, & \psi_{i_{\mathrm{v}}}^{\mathrm{ps}}(\mathbf{r}) &\to \psi_i(\mathbf{r}),\\ n_{\mathrm{v}}(\mathbf{r}) &\to n(\mathbf{r}), & \mathscr{E} &\to E. \end{aligned}$$

By explicitly calculating Eq. (2.74), we obtain with these notations

$$\begin{aligned}\mathscr{E}[n]=&\sum_i\langle\psi_i|-\frac{1}{2}\nabla^2+V_{\mathrm{ps}}+\int'\frac{n'}{|\mathbf{r}-\mathbf{r}'|}+V_{\mathrm{xc}}[n]|\psi_i\rangle\\ &-\left(\int V_{\mathrm{ps}}n+\iint'\frac{nn'}{|\mathbf{r}-\mathbf{r}'|}+\int V_{\mathrm{xc}}n\right)\\ &+\left(\int V_{\mathrm{ps}}n+\frac{1}{2}\iint'\frac{nn'}{|\mathbf{r}-\mathbf{r}'|}+E_{\mathrm{xc}}[n]\right)\\ =&\sum_i\langle\psi_i[n]|-\frac{1}{2}\nabla^2+V_{\mathrm{ps}}+\frac{1}{2}\int'\frac{n'}{|\mathbf{r}-\mathbf{r}'|}|\psi_i[n]\rangle+E_{\mathrm{xc}}[n].\end{aligned} \tag{2.77}$$

Now in the *second-order self-consistent charge extension* (SCC-DFTB), which was derived by M. Elstner et al. in 1998 [16], expands $\mathscr{E}$ to the second-order in the fluctuations around $n_0(\mathbf{r})$—an initial guess density. So now $n = n_0 + \delta n_0$:

$$\begin{aligned}
&\sum_i \langle \psi_i[n_0+\delta n_0]| \,\frac{1}{2}\int' \frac{n_0'+\delta n_0'}{|\mathbf{r}-\mathbf{r}'|}\, |\psi_i[n_0+\delta n_0]\rangle \\
=&\sum_i \langle \psi_i[n_0+\delta n_0]| \int' \frac{n_0'}{|\mathbf{r}-\mathbf{r}'|}\, |\psi_i[n_0+\delta n_0]\rangle \\
&+\frac{1}{2}\iint' \frac{\delta n_0\,(n_0'+\delta n_0)}{|\mathbf{r}-\mathbf{r}'|} - \frac{1}{2}\iint' \frac{n_0'\,(n_0+\delta n_0)}{|\mathbf{r}-\mathbf{r}'|} \\
=&\sum_i \langle \psi_i[n_0+\delta n_0]|V_{\mathrm{H}}[n_0]|\psi_i[n_0+\delta n_0]\rangle \\
&+\frac{1}{2}\iint' \frac{\delta n_0 \delta n_0'}{|\mathbf{r}-\mathbf{r}'|} - \frac{1}{2}\iint' \frac{n_0 n_0'}{|\mathbf{r}-\mathbf{r}'|},
\end{aligned} \tag{2.78}$$

where I at first took the $\delta n_0'$-term out of the brakets, then added $V_{\mathrm{H}}/2$ to there and also subtracted the corresponding term outside the brakets. The linear terms in δn_0 vanish and we are left with only second-order corrections. Now, only the expansion of the exchange-correlation energy is yet to be done. We get for $E_{\mathrm{xc}}[n_{\mathrm{in}}] = E_{\mathrm{xc}}[n_0 + \delta n_0]$

$$E_{\mathrm{xc}}[n_0+\delta n_0] = E_{\mathrm{xc}}[n_0] + \int V_{\mathrm{xc}}[n_0]\delta n_0 + \frac{1}{2}\iint' \left.\frac{E_{\mathrm{xc}}}{\delta n \delta n'}\right|_{n_0} \delta n_0 \delta n_0'. \tag{2.79}$$

By plugging this into Eq. (2.77) and arranging terms so that we get $V_{\mathrm{xc}}[n_0]$ inside the brakets (analogously as for Hartree potential in Eq. (2.78)) we arrive at the standard expanded form of the Kohn-Sham energy:

$$
\begin{aligned}
\mathscr{E}[\delta n_0] = & \underbrace{\sum_i \langle\psi_i| \left(-\frac{1}{2}\nabla^2 + V + V_{\mathrm{H}}[n_0] + V_{\mathrm{xc}}[n_0]\right) |\psi_i\rangle}_{\text{the band structure energy}} \\
& \underbrace{+ \frac{1}{2}\iint' \left(\frac{\delta^2 E_{\mathrm{xc}}[n_0]}{\delta n_0 \delta n_0'} + \frac{1}{|\mathbf{r}-\mathbf{r}'|}\right)\delta n_0 \delta n_0'}_{\text{the charge fluctuation term}} \\
& \underbrace{+ E_{\mathrm{xc}}[n_0] - \int V_{\mathrm{xc}}[n_0] n_0 - \frac{1}{2}\iint' \frac{n_0 n_0'}{|\mathbf{r}-\mathbf{r}'|} + E_{\mathrm{II}}}_{\text{the repulsion term}} \,.
\end{aligned} \tag{2.80}
$$

2.7 DFTB energy

2.7.1 Tight-binding formalism

So far the treatment has been for general valence electron densities.

Consider the valence electrons $\phi_{I_\alpha}(\mathbf{r})$ of the atom I belonging to the system in question. Assuming *tight-binding*, these valence electrons should first and foremost be tightly bound to the atom to which they belong and they should have limited interaction with pseudopotentials of the surrounding atoms. As a result their wave functions will be rather similar to the free atomic wave functions $\varphi^{\mathrm{free}}_{I_\mu}(\mathbf{r})$ that satisfy the pseudo-atom Schrödinger equation

$$
\left[-\frac{1}{2}\nabla^2 + V^{\mathrm{free}}_{\mathrm{s},I}(\mathbf{r})\right]\varphi^{\mathrm{free}}_{I_\mu}(\mathbf{r}) = \epsilon^{\mathrm{free}}_{I_\mu}\varphi^{\mathrm{free}}_{I_\mu}(\mathbf{r}), \tag{2.81}
$$

$$
V^{\mathrm{free}}_{\mathrm{s},I}(\mathbf{r}) = V^{\mathrm{ps}}_I(\mathbf{r}) + V_{\mathrm{H}}[n^{\mathrm{free}}_{0,I}](\mathbf{r}) + V_{\mathrm{xc}}[n^{\mathrm{free}}_{0,I}](\mathbf{r})\,. \tag{2.82}
$$

Due to their similarity, it makes great sense to construct the valence electron wave functions out of the orbitals of the free atoms:

$$
\phi_{I_\alpha}(\mathbf{r}) = \sum_\beta b_{I_\beta}\varphi^{\mathrm{free}}_{I_\beta}(\mathbf{r}). \tag{2.83}
$$

The valence electrons should now not be confused with the KS wave functions $\psi_i(\mathbf{r})$, since they are obtained from a single-particle potential $V_\mathrm{s}(\mathbf{r})$ with mathematical trickery and could very well be shared by several different atoms in the structure. But the total density of course still is the sum of N Kohn-Sham eigenstates lowest in energy, as is of course the sum $\sum_{I_\alpha} \phi_{I_\alpha}$. Thus also the KS wave functions can be expanded similarly to Eq. (2.83):

$$\psi_i(\mathbf{r}) = \sum_{I_\mu} c^i_{I_\mu} \varphi^\mathrm{free}_{I_\mu}(\mathbf{r}). \tag{2.84}$$

However, the higher the orbitals are in energy, the smaller their contribution in $\psi_i(\mathbf{r})$ is. Thus the computational efficiency can be improved by neglecting the higher-energy orbitals, which is particularly topical in the case of approximative but quick DFTB theory. The most compact sensible reduced basis—the *minimal basis*—only consists of the most essential orbitals. That is, for example for period II elements (for example boron, carbon and nitrogen) the $2s$ and the three orthogonal $2p$ orbitals since their valence electrons are in the $2s$ and $2p$ shells ($1s$ is occupied by the core electrons). Since there are just so few basis elements in the minimal basis, special attention to its quality should be paid when it is used. Here quality means possibility to find such expansion coefficients $c^i_{I_\mu}$ in Eq. (2.83) that $\psi_i(\mathbf{r})$ given by that equation differs from the true $\psi_i(\mathbf{r})$ as little as possible in several different relevant situations. Now, these requirements are poorly met by $\varphi^\mathrm{free}_{I_\mu}(\mathbf{r})$ for minimal basis. Therefore it is needed to introduce a better basis. A common way of doing this is to replace them with orbitals $\varphi_{I_\mu}(\mathbf{r})$ that are obtained from a KS construction similar to the free atom construction determined by Eqs. (2.81) and (2.82). In this construction a confining potential $V^\mathrm{conf}_I(\mathbf{r})$ is introduced to $V^\mathrm{free}_{\mathrm{s},I}(\mathbf{r})$:

$$\left[-\frac{1}{2}\nabla^2 + V^\mathrm{conf}_{\mathrm{s},I}(\mathbf{r})\right] \varphi_{I_\mu}(\mathbf{r}) = \epsilon_{I_\mu}\varphi_{I_\mu}(\mathbf{r}) \quad \text{and} \tag{2.85}$$

$$V^\mathrm{conf}_{\mathrm{s},I} = V^\mathrm{ps}_I(\mathbf{r}) + V_\mathrm{H}[n^\mathrm{conf}_{0,I}](\mathbf{r}) + V_\mathrm{xc}[n^\mathrm{conf}_{0,I}](\mathbf{r}) + V^\mathrm{conf}_I(\mathbf{r}). \tag{2.86}$$

The additional potential $V^\mathrm{conf}_I(\mathbf{r})$ can be interpreted as a potential mimicking the repulsive potential of the surrounding electrons. Hence its name—it is supposed to provide a potential barrier to *confine* the orbitals into smaller volume. Namely, the pseudopotential $V_I^{\mathrm{ps}}(\mathbf{r})$ approaches zero for large $|\mathbf{r}|$ leading to long "tails" in $\varphi_{I_\mu}^{\mathrm{free}}(\mathbf{r})$.

As the resulting orbitals $\varphi_\mu(\mathbf{r})$ are supposed to truly resemble the corresponding free atomic orbitals $\varphi_\mu^{\mathrm{free}}(\mathbf{r})$, $V_{\mathrm{conf}}(\mathbf{r})$ should be spherically symmetric similarly to $V_I^{\mathrm{ps}}(\mathbf{r})$ and $V_{\mathrm{xc}}[n_{0,I}^{\mathrm{conf}}](\mathbf{r})$. Otherwise there are no eigenstates of the angular quantum number l for the differential equation (2.85) and it would not make sense to talk about s and p orbitals for instance. Also from the radial part of $\varphi_\mu(\mathbf{r})$ only the tails should be cut off, so V_{conf} should be close to zero in proximity of the nucleus and grow strongly as a function of distance r.

The V_{conf}-potential is our encounter with *parametrization*. For each element in calculation a V_{conf}-potential needs to be determined and the orbitals $\varphi_\mu(\mathbf{r})$ calculated. But more about this later in Sec. 4.1.

2.7.2 The band structure term E_{BS}

The band structure (BS) energy term is the first term from Eq. (2.80):

$$E_{\mathrm{BS}} = \sum_i \langle \psi_i | H^0 | \psi_i \rangle \, . \tag{2.87}$$

It is named after band structures for historic reasons—without the second-order self-consistent charge extension part the band structures are fully determined by this term (more about band structures in Sec. 2.7.8). But since we are now dealing with SCC-DFTB, this naming is a bit delusive, but we let it be.

Now, E_{BS} can be written in the tight-binding formalism by using (2.84), and it becomes

$$E_{\mathrm{BS}} = \sum_i \sum_{I_\mu, J_\nu} c_{I_\mu}^{i*} c_{J_\nu}^{i} H_{I_\mu J_\nu}^0, \tag{2.88}$$

where $H_{I_\mu J_\nu}^0$ are the matrix elements of the H^0-matrix:

$$H^0_{I_\mu J_\nu} = \langle \varphi_{I_\mu}(\mathbf{r}-\mathbf{R}_I)|H^0|\varphi_{J_\nu}(\mathbf{r}-\mathbf{R}_J)\rangle \,. \tag{2.89}$$

The notation $\sum_{I_\mu}$ implies that the summation is carried over all the possible indices, i.e., first over all the possible orbital numbers μ related to the specific atom I and secondly over all the possible atoms I. It is thus a shorthand notation for $\sum_I \sum_{\mu \in I}$.

2.7.3 Charge fluctuation term

The charge fluctuation term, or self-consistent charge term, E_{SCC} was defined as

$$E_{\text{SCC}}[n_0 + \delta n_0] = \frac{1}{2} \iint' \left(\frac{\delta^2 E_{\text{xc}}[n_0]}{\delta n_0 \delta n_0'} + \frac{1}{|\mathbf{r}-\mathbf{r}'|} \right) \delta n_0 \delta n_0'. \tag{2.90}$$

It is the only term in Eq. (2.80) possessing the electron density (i.e., charge) fluctuations δn_0, hence the name. Its role is therefore to describe the effect of the change in the guessed input density to the value of $\mathscr{E}[n]$. We, however, already know it from atomic physics. Namely,

$$\begin{aligned} E(\Delta q) &\approx E_0 + \left(\frac{\partial E}{\partial \Delta q} \right) \Delta q + \frac{1}{2} \left(\frac{\partial^2 E}{\partial \left(\Delta q\right)^2} \right) \left(\Delta q\right)^2 \\ &= E_0 - \chi \Delta q + \frac{1}{2} U \left(\Delta q\right)^2 , \end{aligned} \tag{2.91}$$

where

$$\chi \approx (IE + EA)/2, \tag{2.92}$$

$$U \approx IE - EA, \tag{2.93}$$

and where in turn U is the *Hubbard on-site energy* (or Hubbard U) and IE and EA are the *first ionization energy* and *electron affinity* of the atom in question, respectively.

This observation provides us with a route to simplify this term enormously by making use of U—a measurable and calculable physical constant. This is very much of tight-binding fashion, where the overall goal is to try to make use of the assumption of tightly bound electrons as much as possible and replace some troublesome quantities with something that can be calculated in advance, or in other words *parametrized*. This time the troublesome quantity is essentially the E_{xc}-contribution in this term.

Another approximation in the tight-binding fashion arises from the fact that by definition the electronic densities are confined around the nuclei. Thus it makes sense to discuss *atomic volumes*. More explicitly it is possible to define a volume around an atom that "belongs" to that atom. Now, consider the real space $\mathscr{V}$ divided into volumes $\mathscr{V}_I$, related to atoms I, so that

$$\sum_I \mathscr{V}_I = \mathscr{V} \quad \text{and} \quad \int_{\mathscr{V}} = \sum_I \int_{\mathscr{V}_I} . \tag{2.94}$$

We do not need to specify these atomic volumes at any point—they should just provide some kind of heuristic picture of some volumes that belong to each nucleus. Anyway, according to this picture, the excess charge related to $\delta n_0(\mathbf{r})$ can be divided between the atomic volumes and we have for atom I

$$\Delta q_I = \int_{\mathscr{V}_I} \delta n_0(\mathbf{r}). \tag{2.95}$$

Analysis of these excess charges is known as *Mulliken charge analysis*. Anyway, in turn, the density fluctuation δn_0 can be expressed with Mulliken charges Δq_I:

$$\delta n_0(\mathbf{r}) = \sum_I \Delta q_I \delta n_I(\mathbf{r}) \quad \text{and} \tag{2.96}$$

$$\int_{\mathscr{V}_I} \delta n_I(\mathbf{r}) = 1. \tag{2.97}$$

In other words, Δq_I is simply $\delta q_{0;I}$ normalized with Δq_I. Now, together with Eqs. (2.95) and (2.96) E_{SCC} becomes

$$\begin{aligned} E_{\mathrm{SCC}} &= \sum_{IJ} \frac{1}{2} \left(\Delta q_I\right) \left(\Delta q_J\right) \int_{\mathscr{V}_I} \int'_{\mathscr{V}_J} \left(\left.\frac{\delta^2 E_{\mathrm{xc}}}{\delta n_0 \delta n'_0}\right|_{n_0} + \frac{1}{|\mathbf{r} - \mathbf{r}'|} \right) \\ &= \sum_{IJ} E^{IJ}_{\mathrm{SCC}}. \end{aligned} \tag{2.98}$$

In order to analyze this further, consider first terms with $I = J$:

$$E^{II}_{\mathrm{SCC}} = \sum_{IJ} \frac{1}{2} \left(\Delta q_I\right)^2 \int_{\mathscr{V}_I} \int'_{\mathscr{V}_I} \left(\left.\frac{\delta^2 E_{\mathrm{xc}}}{\delta n_0 \delta n'_0}\right|_{n_0} + \frac{1}{|\mathbf{r} - \mathbf{r}'|} \right) \delta n_I \delta n'_I. \tag{2.99}$$

This result should be in correspondence with our result (2.91) from the atomic physics and thus we find that

$$E^{II}_{\mathrm{SCC}} = \frac{1}{2} U_I \left(\Delta q_I\right)^2. \tag{2.100}$$

Next for different atoms ($A \neq B$) the xc-contributions will vanish since for E_{xc} it holds that $\delta^2 E_{\mathrm{xc}} / \delta n \delta n' \propto \delta(\mathbf{r} - \mathbf{r}')$. Thus the interaction is only electrostatic and these terms read

$$E^{II}_{\mathrm{SCC}} = \frac{1}{2} \left(\Delta q_I\right)^2 \int_{\mathscr{V}_I} \int'_{\mathscr{V}_J} \frac{\delta n_I \delta n'_J}{|\mathbf{r} - \mathbf{r}'|}. \tag{2.101}$$

Now recall that for a given $\mathscr{V}_I$ the density function $\delta n_I(\mathbf{r})$ describes the distribution of the "excess" charge when compared to $n_0(\mathbf{r})$. Its only restriction is Eq. (2.97) and thus in principle it could be any function that integrates to unity. However, the expression (2.101) can only be calculated if $\delta n_I(\mathbf{r})$ is known. Therefore some assumptions have to be made for its form. Firstly, it can be assumed, that their form is radial in good approximation. Secondly, in order to preserve the simplicity, we must expect it to have the same form for all the same atoms. This means that if atoms I and J are of the same element,

$$\delta n_I(\mathbf{r}-\mathbf{R}_I) = \delta n_J(\mathbf{r}-\mathbf{R}_J) \tag{2.102}$$

Thirdly, it can be shown that a Gaussian profile for δn_I is a good choice. Finally, in order to obtain the correct limit we must require that when $I = J$ the result coincides with the result for E_{SCC}^{II}. Importantly, with this way we can relate this term to the Hubbard U as well. Now, by using the symmetry of Eq. (2.102) the integral $\iint' \delta n_I \delta n'_J / |\mathbf{r}-\mathbf{r}'|$ can be evaluated. This has been done in detail in [19] as well as in [16]. Nevertheless, the final results for those calculations are

$$E_{\mathrm{SCC}} = \frac{1}{2}\sum_{IJ} \gamma_{IJ}(R_{IJ})\Delta q_I \Delta q_J, \tag{2.103}$$

$$\gamma_{IJ}(R_{IJ}) = \begin{cases} U_I, & I = J, \\ \operatorname{erf}\left(C_{IJ}R_{IJ}\right)/R_{IJ}, & I \neq J, \end{cases} \quad \text{and} \tag{2.104}$$

$$C_{IJ} = U_I U_J \sqrt{\frac{\pi}{2}\frac{1}{U_I^2 + U_J^2}}, \tag{2.105}$$

where $\operatorname{erf}(x)$ is the error function.

So instead of three-dimensional density functions $\delta n_0(\mathbf{r})$ for which we should have performed complex integrals, E_{SCC} is now given by a set of real-valued variables $\{\Delta q_I\}$. The simplification is remarkable, thanks to the tight-binding approximations. But we cannot really exploit this form yet. We should manage to express it as a function of the expansion coefficients $\{c_{I_\mu}^a\}$ just like the E_{BS}-term. So we should somehow express the Mulliken populations q_I as their function even though they contain integrals over the nonspecific atomic volumes $\mathscr{V}_I$:

$$q_I = \sum_i \int_{\mathscr{V}_I} |\psi_i(\mathbf{r})|^2 = \sum_i \sum_{A_\alpha, B_\beta} c_{A_\alpha}^{i*} c_{B_\beta}^{i} \int_{\mathscr{V}_I} \varphi_{A_\alpha}^{*}(\mathbf{r}-\mathbf{R}_A)\varphi_{B_\beta}(\mathbf{r}-\mathbf{R}_B). \tag{2.106}$$

Performing this integration directly would be a difficult task even if we had specific forms for $\mathscr{V}_A$. Thus some approximations should be made. Firstly, if $A \neq I$ and $B \neq I$ the following approximation is very reasonable:

$$\int_{\mathscr{V}_I} \varphi^*_{A_\alpha}(\mathbf{r}-\mathbf{R}_A)\varphi_{B_\beta}(\mathbf{r}-\mathbf{R}_B) = 0, \quad A \neq I, B \neq I. \tag{2.107}$$

But what if $A = I$, but $B \neq I$? Let us define the S-matrix, i.e., the *overlap integral*

$$S_{A_\alpha B_\beta} = \int \varphi^*_{A_\alpha}(\mathbf{r}-\mathbf{R}_A)\varphi_{B_\beta}(\mathbf{r}-\mathbf{R}_B). \tag{2.108}$$

Now, by means of Fig. 1 we can use the elements of the S-matrix to approximate

$$\int_{\mathscr{V}_I} \varphi^*_{A_\alpha}(\mathbf{r}-\mathbf{R}_A)\varphi_{B_\beta}(\mathbf{r}-\mathbf{R}_B) = \frac{1}{2} S_{I_\mu B_\beta}, \quad B \neq I. \tag{2.109}$$

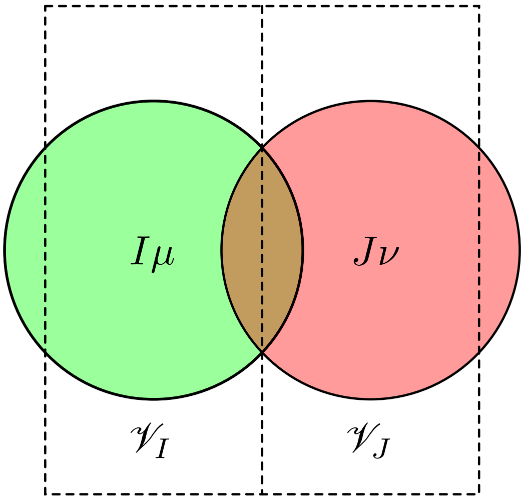

Figure 1: Overlap of the local orbitals I_μ and J_ν, in the case pictured $\mu = \nu$ (both are s-orbitals). As it can be seen, particularly in this case the approximation (2.109) is actually even exact (if also $\mathscr{V}_I$ and $\mathscr{V}_J$ are identical). Otherwise (for example in the case of $2p_x$-orbital in the origin and $2p_y$-orbital in $L, 0, 0)$ the approximation clearly fails but on the other hand in such cases the overlaps are small anyway.

Now only the case where $A = B = I$ remains. We would like to relate these terms to elements of the S-matrix as well. Hence we write

$$\int_{\mathscr{V}_I} \varphi_\alpha^*(\mathbf{r}-\mathbf{R}_I)\varphi_\beta(\mathbf{r}-\mathbf{R}_I) = XS_{I_\alpha I_\beta} = X\delta_{\alpha\beta}. \tag{2.110}$$

It is not completely intuitive what we should have for X in this case. The value $X = 1/2$ is intuitively too small, but $X = 1$ would mean that orbitals of atom I fully belong to $\mathscr{V}_I$ which would contradict with (2.109) since in that case we should have zero overlap between orbitals of neighbouring atoms. But what is certain is that X should be such that the sum of the q_I from (2.106) agree with

$$\sum_I q_I = \sum_i \langle\psi_i|\psi_i\rangle = \sum_i \sum_{A_\alpha B_\beta} c_{A_\alpha}^{i*} c_{B_\beta}^{i} S_{A_\alpha B_\beta}. \tag{2.111}$$

In other words we require correct normalization. Performing the comparison and using (2.107), (2.109) and (2.110) yields for us $X = 1$ after all. Thus, all in all by using δ-algebra we have

$$\begin{aligned}
&\int_{\mathscr{V}_I} \varphi_\alpha^*(\mathbf{r}-\mathbf{R}_A)\varphi_\beta(\mathbf{r}-\mathbf{R}_B) \\
=&\left[\frac{1}{2}\underbrace{\delta_{AI}\left(1-\delta_{BI}\right)}_{A=I,\ B\neq I}+\frac{1}{2}\underbrace{\delta_{BI}\left(1-\delta_{AI}\right)}_{B=I,\ A\neq I}+\underbrace{\delta_{AI}\delta_{BI}}_{A=B=I}\right] S_{A_\alpha B_\beta} \\
=&\frac{1}{2}\left[\delta_{AI}+\delta_{BI}\right] S_{A_\alpha B_\beta}.
\end{aligned} \tag{2.112}$$

Inserting this into Eq. (2.106), performing some index changes and using the property $S^*_{A_\alpha B_\beta} = S_{B_\beta A_\alpha}$ and the relation $z + z^* = 2\,\mathfrak{Re}(z)$ we obtain for $\Delta q_I = q_I - q_I^0$ (where q_I^0 is the valence electron count of atom I)

$$\begin{aligned}\Delta q_I =& \frac{1}{2}\sum_i \left[\sum_{\alpha,B_\beta} c^{i*}_{I_\alpha} c^i_{B_\beta} S_{I_\alpha B_\beta} + \sum_{A_\alpha,\beta} c^{i*}_{A_\alpha} c^i_{I_\beta} S_{A_\alpha I_\beta}\right] - q^0_I \\ =& \frac{1}{2}\sum_i \sum_{\mu,A_\alpha} \left[c^{i*}_{I_\mu} c^i_{A_\alpha} S_{I_\mu A_\alpha} + c^i_{I_\mu} c^{i*}_{A_\alpha} S^*_{I_\mu A_\alpha}\right] - q^0_I \\ =& \sum_i \sum_{\mu,A_\alpha} \mathfrak{Re}\left(c^{i*}_{I_\mu} c^i_{A_\alpha} S_{I_\mu A_\alpha}\right) - q^0_I.\end{aligned} \tag{2.113}$$

Thus all in all we have managed to express this E_{SCC}-term only as a function of $\{c^i_{I_\mu}\}$ despite its very complex first form (2.90).

2.7.4 Repulsive energy term

The third and last line of the SCC-DFTB energy is the repulsive energy term

$$E_{\mathrm{rep}} = E_{\mathrm{II}} - E_{\mathrm{H}}[n_0] + E_{\mathrm{xc}}[n_0] - \int V_{\mathrm{xc}}[n_0] n_0. \tag{2.114}$$

It chiefly consists of the ion-ion repulsive energy E_{II}, hence the name. The term $E_{\mathrm{H}}[n_0]$ is the screening of the ion-ion repulsion due to the initial valence electron density n_0 and the last two terms are many-body effects associated with n_0.

Now, something needs to be done to these terms. Let us postulate that all of these can be expressed as a sum of pairwise repulsive functions depending only on the distances of the atom pairs:

$$E_{\mathrm{rep}} = \sum_{I<J} V^{IJ}_{\mathrm{rep}}(R_{IJ}). \tag{2.115}$$

According to Eq. (2.9) the ion-ion repulsion term E_{II} is of this form by definition. Also $E_{\mathrm{H}}[n_0]$ can be shown to be exactly of this form if we assume that the atomic initial densities n_0^I are spherically symmetric (consistently with Δq_I in E_{SCC}). So, we have

$$n_0(\mathbf{r}) = \sum_I n_0^I(\mathbf{r} - \mathbf{R}_I). \tag{2.116}$$

Plugging this into the definition of E_{H} (2.44) gives

$$\begin{aligned}
E_{\mathrm{H}}[n_0] = \frac{1}{2}\iint' \frac{n_0(\mathbf{r})n_0(\mathbf{r}')}{|\mathbf{r}-\mathbf{r}'|} &= \frac{1}{2}\iint' \sum_{IJ} \frac{n_0^I(\mathbf{r}-\mathbf{R}_I)n_0^J(\mathbf{r}'-\mathbf{R}_J)}{|\mathbf{r}-\mathbf{r}'|} \\
=& \sum_{I<J}\iint' \frac{n_0^I(\mathbf{r}-\mathbf{R}_I)n_0^J(\mathbf{r}'-\mathbf{R}_J)}{|\mathbf{r}-\mathbf{r}'|} + \frac{1}{2}\sum_I \iint' \frac{n_0^I(\mathbf{r}-\mathbf{R}_I)n_0^I(\mathbf{r}'-\mathbf{R}_I)}{|\mathbf{r}-\mathbf{r}'|} \\
=& \sum_{I<J}\iint' \frac{n_0^I(\mathbf{r})n_0^J(\mathbf{r}')}{|\mathbf{r}-\mathbf{r}'+\mathbf{R}_{IJ}|} + \frac{1}{2}\sum_I \iint' \frac{n_0^I(\mathbf{r})n_0^I(\mathbf{r}')}{|\mathbf{r}-\mathbf{r}'|} \\
=& \sum_{I<J} f_{IJ}(R_{IJ}) + (\text{structure-independent constant})\,,
\end{aligned} \tag{2.117}$$

where f_{IJ} is some unknown function, which most importantly only depends on the distance R_{IJ} between the atoms I and J and the element of I and J. The structure-independent constant *should* be further ignored, since it is of the form $\sum_I f_I$ instead of $\sum_{IJ} f_{IJ}(R_{IJ})$. It also *can* be ignored since it is structure-independent, (i.e., independent of R_{IJ}), and thus only affects the indifferent zero energy level.

Also the two xc-terms can be argumented to be of the form (2.115) similarly to $E_{\mathrm{H}}[n_0]$ if we have

$$V_{\mathrm{xc}}[n_0] = \sum_I V_{\mathrm{xc}}[n_0^I], \tag{2.118}$$

i.e., the V_{xc}-functional is *linear*. This is of course not the case, but is a reasonable approximation similarly to linearization of V_{xc} in the frozen-core approximation part.

The V_{rep}-functions should also be short-ranged. Firstly, from Eq. (2.117) we see how $E_{\text{H}}[n_0]$ screens out the ion-ion repulsions in larger distances since

$$\sum_{I<J} \iint' \frac{n_0^I(\mathbf{r}) n_0^J(\mathbf{r}')}{|\mathbf{r} - \mathbf{r}' + \mathbf{R}_{IJ}|} \to \sum_{I<J} \frac{Z_I^{\text{v}} Z_J^{\text{v}}}{R_{IJ}} = E_{\text{II}} \quad \text{for large } R_{IJ}. \tag{2.119}$$

Secondly also the xc-contribution terms cancel each other when distances grow.

after all for each atom pair (I, J) we have a *universal* function $V_{\text{rep}}^{IJ}(\mathbf{R}_{IJ})$. For a system with n different elements, a total of $(n^2 + n)/2$ different V_{rep}-functions exist. Their forms are not calculated—they should be simply constructed in such a way that the results given by E_{DFTB} are consistent with those of DFT, experiments etc. In other words they should be parametrized. This is not a simple task and will be discussed in detail in chapter 4. But after the parametrization the calculation of this repulsion term happens practically in zero time.

2.7.5 Solving the DFTB energy

From now on let us assume that the coefficients $c_{I_\mu}^i$ and the functions in the basis set $\{\varphi_\mu\}$ (and hence also $H^0_{I_\mu J_\nu}$ and $S_{I_\mu J_\nu}$) are real. By combining the real versions of Eqs. (2.88), (2.103), (2.113) and (2.115) the DFTB energy reads

$$E = \sum_i \sum_{I_\mu, J_\nu} c_{I_\mu}^i c_{J_\nu}^i H^0_{I_\mu J_\nu} + \frac{1}{2} \sum_{I,J} \gamma_{IJ}(R_{IJ}) \Delta q_I \Delta q_J + \sum_{I<J} V_{\text{rep}}^{IJ}(R_{IJ}), \tag{2.120}$$

$$\Delta q_I = \sum_i \sum_{\mu, A_\alpha} \left(c_{I_\mu}^i c_{A_\alpha}^i S_{I_\mu A_\alpha} \right) - q_I^0, \tag{2.121}$$

where γ_{AB} is defined by Eq. (2.104). So we have managed to reduce the original problem of KS construction including multidimensional differential equations into this purely algebraic problem of finding the stationary point of a function of multiple variables (expansion coefficients $c_{I_\mu}^i$).

This kind of problem is best solved through the method of *multiple Lagrange multipliers*. Its theory tells us that in a *stationary* point of a function $f(x_1, \dots, x_N)$ the following equations hold:

$$\nabla_x f(x_1, \dots, x_N) - \sum_i^M \lambda_i \nabla_x g_i(x_1, \dots, x_N) = 0 \quad \text{and} \tag{2.122}$$

$$g_i(x_1, \dots, x_N) = 0 \quad \forall i, \tag{2.123}$$

where $g_i(x_1, \dots, x_N)$ are the constraint functions and λ_i are the Lagrange multipliers themselves.

In our case this method is particularly appropriate, since as discussed in the derivation of the energy functional $\mathscr{E}$ (2.120), it is no longer assumed to be minimized by n_{GS}. It is rather only assumed to be stationary at n_{GS}. So in the correct density $\mathscr{E}$ might actually be in a local maximum.

Nevertheless, now the functions constraining the expansion coefficients $c^i_{I_\mu}$ are the KS wave function inner products $\langle \psi_i | \psi_j \rangle = \delta_{ij}$. Also naturally we must have $c^i_{I_\mu} \in [0, 1]$. Now, writing Eqs. (2.122) and (2.123) down in our case yields

$$\frac{\partial}{\partial c^p_{I_\mu}} E - \sum_i e_i \frac{\partial}{\partial c^p_{I_\mu}} \langle \psi_i | \psi_j \rangle = 0 \quad \forall c^a_{I_\mu} \quad \text{and} \tag{2.124}$$

$$\langle \psi_i | \psi_j \rangle = \delta_{ij} \quad \forall i, j, \tag{2.125}$$

I have labeled the undefined Lagrange multipliers as e_a since in this case it should physically have dimension of energy. Nevertheless, it now only remains to work out the c-dependencies of these equations. Starting from the E_{BS} term, we get

$$
\begin{aligned}
\frac{\partial}{\partial c^p_{I_\mu}} E_{\mathrm{BS}} =& \frac{\partial}{\partial c^p_{I_\mu}} \sum_b \sum_{A_\alpha, B_\beta} c^a_{A_\alpha} c^a_{B_\beta} H^0_{A_\alpha B_\beta} \\
=& \sum_b \sum_{A_\alpha, B_\beta} \left(\delta_{ap} \delta_{I_\mu A_\alpha} c^a_{B_\beta} + c^a_{A_\alpha} \delta_{ap} \delta_{I_\mu B_\beta} \right) H^0_{A_\alpha B_\beta} \\
=& \underbrace{\sum_{B_\beta} c^a_{B_\beta} H^0_{I_\mu B_\beta}}_{B_\beta \to J_\nu} + \underbrace{\sum_{A_\alpha} c^a_{A_\alpha} H^0_{A_\alpha I_\mu}}_{A_\alpha \to J_\nu} = 2 \sum_{J_\nu} c^a_{A_\alpha} H^0_{I_\mu J_\nu},
\end{aligned}
\tag{2.126}
$$

where in the last step I used the symmetricity of H^0.

Next with completely identical steps we obtain for the inner products

$$
\frac{\partial}{\partial c^a_{I_\mu}} \langle \psi_a | \psi_a \rangle = \frac{\partial}{\partial c^a_{I_\mu}} c^a_{A_\alpha} c^a_{B_\beta} S_{A_\alpha B_\beta} = 2 \sum_{J_\nu} S_{I_\mu J_\nu}.
\tag{2.127}
$$

The derivative of the E_{SCC} is the most complex one. First of all, we need to calculate the derivative of Δq_I:

$$
\begin{aligned}
\frac{\partial(\Delta q_A)}{\partial c^a_{I_\mu}} &= \frac{\partial(q_A - q^0_A)}{\partial c^a_{I_\mu}} = \frac{\partial}{\partial c^a_{I_\mu}} \sum_b \sum_{\alpha, J_\nu} c^b_{A_\alpha} c^b_{J_\nu} S_{A_\alpha, J_\nu} \\
=& \sum_b \sum_{\alpha, J_\nu} \left(\delta_{ab} \delta_{I_\mu A_\alpha} c^b_{J_\nu} + c^b_{A_\alpha} \delta_{ab} \delta_{I_\mu J_\nu} \right) S_{A_\alpha, J_\nu} \\
=& \delta_{IA} \sum_{J_\nu} c^a_{J_\nu} S_{\mu_A J_\nu} + \sum_\alpha c^a_{A_\alpha} S_{A_\alpha I_\mu}.
\end{aligned}
\tag{2.128}
$$

With this result the derivative of the whole E_{SCC} can be calculated:

$$
\begin{aligned}
\frac{\partial E_{\mathrm{SCC}}}{\partial c^{a}_{I_\mu}} &= \frac{\partial}{\partial c^{a}_{I_\mu}} \left(\frac{1}{2} \sum_{AB} \gamma_{AB} \Delta q_A \Delta q_B \right) \\
=& \frac{1}{2} \sum_{AB} \gamma_{AB} \left[\frac{\partial (\Delta q_A)}{\partial c^{a}_{I_\mu}} \Delta q_B + \Delta q_A \frac{\partial (\Delta q_B)}{\partial c^{a}_{I_\mu}} \right] \\
=& \frac{1}{2} \sum_{B,J_\nu} \gamma_{IB} c^{a}_{J_\nu} S_{I_\mu J_\nu} \Delta q_B + \underbrace{\frac{1}{2} \sum_{A_\alpha,B} \gamma_{AB} c^{a}_{A_\alpha} S_{A_\alpha I_\mu} \Delta q_B}_{A_\alpha \to J_\nu} \\
+& \frac{1}{2} \sum_{A,J_\nu} \gamma_{AI} c^{a}_{J_\nu} S_{I_\mu J_\nu} \Delta q_A + \underbrace{\frac{1}{2} \sum_{A,B_\beta} \gamma_{AB} c^{a}_{B_\beta} S_{B_\beta I_\mu} \Delta q_A}_{B_\beta \to J_\nu} \\
=& \underbrace{\frac{1}{2} \sum_{B,J_\nu} \left(\gamma_{IB} + \gamma_{JB} \right) c^{a}_{J_\nu} S_{I_\mu J_\nu} \Delta q_B}_{B \to K} + \underbrace{\frac{1}{2} \sum_{A,J_\nu} \left(\gamma_{AI} + \gamma_{AJ} \right) c^{a}_{J_\nu} S_{I_\mu J_\nu} \Delta q_A}_{A \to K} \\
=& \sum_{J_\nu} c^{a}_{J_\nu} \left[S_{I_\mu J_\nu} \sum_{J} \left(\gamma_{IK} + \gamma_{JK} \right) \Delta q_J \right],
\end{aligned}
\tag{2.129}
$$

where in the last step I used the symmetricity of γ and S. Now, by plugging Eqs. (2.126), (2.127) and (2.129) into (2.124) and (2.125) gives us the final forms of the KS equations in the tight-binding formalism:

$$
\sum_{J_\nu} c^{a}_{J_\nu} \left(H_{I_\mu J_\nu} - e_a S_{I_\mu J_\nu} \right) = 0 \quad \forall a, I_\mu, \tag{2.130}
$$

where

$$
H_{I_\mu J_\nu} = H^{0}_{I_\mu J_\nu} + \frac{1}{2} S_{I_\mu J_\nu} \sum_{J} \left(\gamma_{IK} + \gamma_{JK} \right) \Delta q_J \tag{2.131}
$$

and in these Eqs. the c-coefficients are restricted through

$$\sum_{I_\mu,J_\nu} c^a_{I_\mu} c^a_{J_\nu} S_{I_\mu J_\nu} = 1 \quad \forall a. \tag{2.132}$$

For a total of N valence electrons in the system and M orbitals in the minimal bases of all the different elements we have $NM/2$ different c-coefficients (factor $1/2$ is for degenerated spin). Each of them has its own equation in (2.130). Also we have $N/2$ undetermined Lagrange multipliers e_a and $N/2$ different Eqs. from (2.132). Hence in total we have here $(NM + N)/2$ variables and equations. After the $\{c^i_{I_\mu}\}$ have been solved, they can be plugged in to Eqs. (2.120) and (2.121) to yield the final value for E_{DFTB}.

Eqs. (2.130) and (2.132) are the KS equation equivalents in the DFTB. Albeit they are mathematically very different to the KS equations, they have the same physics in the background and they have to be solved similarly, i.e., self-consistently: from an initial guess of $\{c^a_{J_\nu}\}$ we obtain $H_{I_\mu J_\nu}$ which we can plug into (2.130) to yield new set of $\{c^a_{J_\nu}\}$ and so on until self-consistency is achieved. With this method also the convergence problems are similar with KS equations [19]. But without the E_{SCC} term $\Delta q_J = 0$ and Eqs. (2.130) and (2.131) become very simple and convergence is not a problem anymore.

2.7.6 Calculation of the overlap matrix S

Computation of the overlap matrix elements

$$S_{I_\mu J_\nu} = \langle \varphi_{I_\mu}(\mathbf{r} - \mathbf{R}_I) | \varphi_{J_\nu}(\mathbf{r} - \mathbf{R}_J) \rangle = \int \varphi^*_{I_\mu}(\mathbf{r} - \mathbf{R}_I) \varphi_{J_\nu}(\mathbf{r} - \mathbf{R}_J) \tag{2.133}$$

can be simplified considerably. Namely, it can be reduced to a linear combination of S-matrices with another orbital at origin and another at $R\hat{\mathbf{z}}$ with $R = |\mathbf{R}_J - \mathbf{R}_I|$:

$$S_{I_\mu J_\nu} = \sum_{I_\alpha J_\beta} C_{I_\alpha J_\beta} \int \varphi^*_{I_\alpha}(\mathbf{r}) \varphi_{J_\beta}(\mathbf{r} - R\hat{\mathbf{z}}) = \sum_\tau C_\tau S_\tau(R). \tag{2.134}$$

To see this, let us first make a linear transformation of space $\mathbf{r} \to \mathbf{r} - \mathbf{R}_I$ or $\mathbf{r} \to \mathbf{r} - \mathbf{R}_J$. The transform should be chosen so that the orbital with lower principal quantum number n (or with lower angular momentum quantum number l if both orbitals have the same n) ends up in the origin. After this let us make a rotation Γ that rotates the system so that the other orbital gets into $R\hat{\mathbf{z}}$. Obviously the final value of the integrand (2.133) remains unaltered under these transformations if we rotate the orbitals with Γ as well.

Now, firstly s-orbitals are spherically symmetric and hence they need not be rotated at all. But the p-orbitals are not spherically symmetric. They however have the rotational symmetries $p_y(\mathbf{r}) = \Gamma_z(\pi/2)p_x(\mathbf{r})$ and $p_z(\mathbf{r}) = \Gamma_y(\pi/2)p_x(\mathbf{r})$ as well as $\Gamma_i(\theta)p_i(\mathbf{r}) = p_i(\mathbf{r})$ for $i = x, y, z$ and for any θ. So under rotations these functions behave exactly like the space coordinates x, y and z. Thus the p-orbitals in a way form a basis in a "p-space" (like x, y and z form a basis in Euclidean space) and a "p-vector" $\mathbf{p}$ can be rotated similarly to $\mathbf{r}$.

There exists an infinite amount of different rotations that yield the desired result, i.e., the orbital that is not in the origin ends up in $R\hat{\mathbf{z}}$. Different rotations might leave the orbitals in different orientations though, but in such a way that the amount of overlap does not change. Now, consider an example of such a rotation $\Gamma_1 = \Gamma_y(-\alpha_{yz})\Gamma_x(-\alpha_{xz})$, where Γ_y and Γ_x are rotations with respect to the y-axis and x-axis, respectively, α_{yz} is the angle between $\mathbf{R}$ and the yz-plane, and α_{xz} is the angle between $\mathbf{R}$ and the xz-plane. It is a straightforward procedure to find that Γ_1 reads

$$\Gamma_1 = \begin{bmatrix} \sqrt{1-x^2} & -\frac{xy}{\sqrt{1-x^2}} & -\frac{xz}{\sqrt{1-x^2}} \\ 0 & \frac{z}{\sqrt{1-x^2}} & -\frac{y}{\sqrt{1-x^2}} \\ x & y & z \end{bmatrix} \tag{2.135}$$

where x, y and z are the components of the unit direction vector $\mathbf{R}/|\mathbf{R}|$. Now Γ_1 rotates for example $p_x(\mathbf{r}) = (1,0,0)_p$ in the following way:

$$\begin{aligned} \Gamma_1 p_x(\mathbf{r}) = &\begin{bmatrix} \sqrt{1-x^2} & -\frac{xy}{\sqrt{1-x^2}} & -\frac{xz}{\sqrt{1-x^2}} \\ 0 & \frac{z}{\sqrt{1-x^2}} & -\frac{y}{\sqrt{1-x^2}} \\ x & y & z \end{bmatrix} \begin{pmatrix} 1 \\ 0 \\ 0 \end{pmatrix}_p = \begin{pmatrix} \sqrt{1-x^2} \\ 0 \\ x \end{pmatrix}_p \\ =&\sqrt{1-x^2}p_x(\mathbf{r}) + x p_z(\mathbf{r}). \end{aligned} \tag{2.136}$$

Similarly

$$\Gamma_1 p_y(\mathbf{r}) = -\frac{xy}{\sqrt{1-x^2}} p_x(\mathbf{r}) + \frac{z}{\sqrt{1-x^2}} p_y(\mathbf{r}) + y p_z(\mathbf{r}). \tag{2.137}$$

Now, by using symmetries

$$\int \mathrm{d}^3\mathbf{r}\, s^*(\mathbf{r}) p_j(\mathbf{r} - R\hat{\mathbf{z}}) = 0, \quad \text{if } i \neq z \quad \text{and} \tag{2.138}$$

$$\int \mathrm{d}^3\mathbf{r}\, p_i^*(\mathbf{r}) p_j(\mathbf{r} - R\hat{\mathbf{z}}) = 0, \quad \text{if } i \neq j, \tag{2.139}$$

we can see just for example that

$$S_{sp_x}(R) = x S_{sp\sigma}(R), \tag{2.140}$$

$$S_{p_x p_y}(R) = x^2 S_{pp\sigma}(R) + (1-x^2) S_{pp\pi}(R) \quad \text{and} \tag{2.141}$$

$$S_{p_x p_y}(R) = xy S_{pp\sigma}(R) - xy S_{pp\pi}(R), \tag{2.142}$$

where

$$S_{sp\sigma}(R) = \int \mathrm{d}^3\mathbf{r}\, s^*(\mathbf{r}) p_z(\mathbf{r} - R\hat{\mathbf{z}}), \tag{2.143}$$

$$S_{pp\sigma}(R) = \int \mathrm{d}^3\mathbf{r}\, p_z^*(\mathbf{r}) p_z(\mathbf{r} - R\hat{\mathbf{z}}), \quad \text{and} \tag{2.144}$$

$$S_{pp\pi}(R) = \int \mathrm{d}^3\mathbf{r}\, p_x^*(\mathbf{r}) p_x(\mathbf{r} - R\hat{\mathbf{z}}). \tag{2.145}$$

The integrals (2.143–2.145) are examples of the *Slater-Koster (SK) integrals*. They have been named after the basic σ and π bonding situations (for example $S_{sp\sigma}$ is the overlap integral of σ-bond between s and p-orbitals). The coefficients determining the contributions of these integrals in the matrix elements of S, as in Eqs. (2.140–2.142), are the *Slater-Koster coefficients*. Now we can rewrite Eq. (2.134) as

$$S_{I_\mu J_\nu} = \sum_\tau C_\tau S_\tau(R), \tag{2.146}$$

where τ labels all the different bonding situations, e.g. $pp\pi$, many of which are zero by symmetry. As there are more orbitals than just the s and p orbitals, there are more bonding situations than just the ones discussed so far. For example with d-orbitals also the δ-bond comes into play.

A comprehensive collection of the Slater-Koster coefficients was first listed by J. C. Slater and G. F. Koster in 1954 [23]. With the notation used here they are also listed in [19]. Now these Slater-Koster tables allow rapid computation of $S_{I_\mu J_\nu}$ since the SK integrals can be computed in advance. Details of their computation are discussed in [19].

The SK integrals are pairwise like the V_{rep}-functions and therefore there exist own SK integrals for each element pair. But for V_{rep}-functions we have also $V_{\text{rep}}^{IJ} = V_{\text{rep}}^{JI}$, which is in general not the case for SK integrals. Hence, in general we actually have two different SK integrals for each element pair, unless the pair is of same element or there is rotational symmetry present (for example $S_{pp\sigma}$ and $S_{pp\pi}$). But for example for $S_{ps\sigma}$ there are no such symmetries and we have two different integrals for it in the heteroelemental case.

2.7.7 Calculation of the Hamiltonian matrix $H[n_0]$

The Hamiltonian matrix elements $H^0_{I_\mu J_\nu}$ read

$$H^0_{I_\mu J_\nu} = \langle \varphi_{I_\mu}(\mathbf{r} - \mathbf{R}_I) | H[n_0] | \varphi_{J_\nu}(\mathbf{r} - \mathbf{R}_J) \rangle = \int \varphi^*_{I_\mu}(\mathbf{r}) H^0[n_0] \varphi_{J_\nu}(\mathbf{r} - \mathbf{R}_{IJ}). \tag{2.147}$$

To determine them more explicitly, we now need the exact form of $H^0[n_0(\mathbf{r})]$, for which we need to consider what the initial density guess $n_0(\mathbf{r})$ actually is. In principle we could choose it to be nearly any density that is reasonably close to the true $n(\mathbf{r})$, but it is preferable to have n_0 to be the true density in the limit $R_{IJ} \to \infty$ for all I, J. Then we must have

$$n_0(\mathbf{r}) = \sum_I n_{0,I}^{\text{free}}(\mathbf{r} - \mathbf{R}_I) \quad \text{and} \tag{2.148}$$

$$H[n_0] = -\frac{1}{2}\nabla^2 + V_s^{\text{free}}[n_0]. \tag{2.149}$$

Above the orbitals $\varphi_{I_\mu}^{\text{free}}(\mathbf{r})$ contributing to $n_{0,I}^{\text{free}}(\mathbf{r} - \mathbf{R}_I)$ are from the KS construction for the free atoms, i.e., Eqs. (2.81–2.82) and $V_s^{\text{free}}[n_0]$ is the KS single particle potential producing the initial free atom density n_0.

Now, for $I = J$ the matrix elements of H^0 read $\langle \varphi_{I_\mu} | -\frac{1}{2}\nabla^2 + V_s^{\text{free}}[n_0] | \varphi_{I_\nu} \rangle$. Consistently with previously used approximations we can consider the orbitals to be localized within $\mathscr{V}_I$ and hence we can also ignore all the potential of $V_s^{\text{free}}[n_0]$ that is not in $\mathscr{V}_I$—that part of the potential would have negligible contributions to the matrix element integrand. Now, the potential left unignored thus only produces $n_{0,I}^{\text{free}}$ through the KS equations, and hence this potential must be $V_{\text{s},I}^{\text{free}}$ from Eq. (2.82). This is called the *one-center approximation*. The orbitals φ_{J_ν} are eigenstates for the KS Hamiltonian with this potential and thus these matrix elements become $\delta_{\mu\nu}\epsilon_\mu$. However, this would lead to a situation where in the discussed limit of infinite separation the initial density would be the correct density but the initial energy would be $\sum_i \sum_{I_\mu} c_{I_\mu}^i \epsilon_\mu$. So to obtain the correct final energy in this limit, approximation $\epsilon_\mu \approx \epsilon_\mu^{\text{free}}$ should be made. Luckily this approximation is not particularly crude, since the free and confined orbitals are not far from one another in density and as discussed, for small density changes energies change quadratically.

Next, for the non-diagonal matrix elements (for which $I \neq J$) we can similarly to the previous case argue that the *two-center approximation*, where $V_s^{\text{free}}[n_0] = V_{\text{s},I}^{\text{free}} + V_{\text{s},I}^{\text{free}}$, is sufficient. Therefore these matrix elements now read $\langle \varphi_{I_\mu} | -\frac{1}{2}\nabla^2 + V_{\text{s},I}^{\text{free}} + V_{\text{s},I}^{\text{free}} | \varphi_{J_\nu} \rangle$. This form can be further simplified by using the fact that the orbitals φ_{I_μ} are eigenstates for $-\frac{1}{2}\nabla^2 + V_{\text{s},I}^{\text{conf}}$. Now comparing Eqs. (2.82) and (2.86) shows that we can rewrite $V_{\text{s},I}^{\text{free}}$ as $V_{\text{s},I}^{\text{conf}} - V_{\text{conf},I}$ and therefore by operating with $-\frac{1}{2}\nabla^2 + V_{\text{s},I}^{\text{conf}}$ to the left gives $\epsilon_\mu S_{I_\mu J_\nu}(\mathbf{R}_{IJ}) + \langle \varphi_{I_\mu} | V_{\text{s},J} - V_{\text{conf},I} | \varphi_{J_\nu} \rangle$. We could have also operated with $-\frac{1}{2}\nabla^2 + V_{\text{s},J}^{\text{conf}}$ to the right to obtain a bit different equivalent form. In [19] both of these two forms are used to improve the numerical accuracy in the integration. Nevertheless, all in all we have obtained for $H_{I_\mu J_\nu}^0$

$$H^0_{I_\mu J_\nu} = \begin{cases} \delta_{\mu\nu}\epsilon_\mu, & \text{if} I = J, \\ \epsilon_\mu S_{I_\mu J_\nu} + \int \left(V_{\mathrm{s},J} - V_{\mathrm{conf},I}\right) \varphi^*_{I_\mu}\varphi_{J_\nu}, & \text{if} I \neq J. \end{cases} \tag{2.150}$$

Finally, the integral $\int \left(V_{\mathrm{s},J} - V_{\mathrm{conf},I}\right) \varphi^*_{I_\mu}\varphi_{J_\nu}$ in the non-diagonal case can be decomposed into a linear combination of Slater-Koster integrals similarly to the S matrix—the only difference between these cases is the potential V_s or V_conf centered at either of the ions. And since it is spherically symmetric, angular properties are equal in both cases and thus Slater-Koster transformations apply for H as well. So similarly to the S case, calculation of the H^0 matrix can be made rapid by computing the H^0-Slater-Koster integrals beforehand and then applying the SK transformation rules in the simulation.

2.7.8 Periodic boundary conditions

So far we have only considered tight-binding within a finite amount of atoms. But for example hexagonal boron nitride layers and nanotubes are best modelled as infinite periodic lattices. In such case the nuclear potential $\widetilde{V}_\mathrm{nucl}$ can be constructed by repeating the atomic potential

$$\widetilde{V}_\mathrm{nucl}(\mathbf{r}) = \sum_{I,\mathbf{T}} V_{\mathrm{nucl},I}(\mathbf{r} - \mathbf{T}) \tag{2.151}$$

where the sum runs over atoms I belonging to the unit cell and lattice vectors $\mathbf{T}$. The crystal Hamiltonian is

$$\widetilde{H}(\mathbf{r}) = -\frac{1}{2}\nabla^2 + \widetilde{V}_\mathrm{nucl}(\mathbf{r}) \tag{2.152}$$

and its eigenstates $\widetilde{\psi}_{i;\mathbf{k}}(\mathbf{r})$ have the Bloch form

$$\widetilde{\psi}_{i;\mathbf{k}}(\mathbf{r}) = \mathrm{e}^{\mathrm{i}\mathbf{k}\cdot\mathbf{r}} u_i(\mathbf{r}), \tag{2.153}$$

where $u_i(\mathbf{r})$ has the same periodicity with $\widetilde{V}_{\mathrm{nucl}}(\mathbf{r})$, i.e., $u(\mathbf{r}+\mathbf{T}) = u(\mathbf{r})$ for every $\mathbf{T}$. Now we want the basis functions $\widetilde{\varphi}_{\mu;\mathbf{k}}(\mathbf{r})$ to have the Bloch form as well, since otherwise their linear combination would not be a Bloch function. Also, it would be convenient if this basis would be related to the previously used basis $\varphi_{I_\mu}(\mathbf{r})$ that satisfies the pseudoatom equation (2.85). This can be done by extending the pseudoatom eigenstates $\varphi_\mu(\mathbf{r})$ to the whole crystal in the following way:

$$\widetilde{\varphi}_{\mu;\mathbf{k}}(\mathbf{r}) = \frac{1}{\sqrt{N}} \sum_{\mathbf{T}} \mathrm{e}^{\mathrm{i}\mathbf{k}\cdot\mathbf{T}} \varphi_\mu(\mathbf{r}-\mathbf{T}). \tag{2.154}$$

It can be seen readily that $\widetilde{\varphi}_{\mu;\mathbf{k}}(\mathbf{r}+\mathbf{T}_0) = \mathrm{e}^{\mathrm{i}\mathbf{k}\cdot\mathbf{T}_0}\widetilde{\varphi}_{\mu;\mathbf{k}}(\mathbf{r})$. That is, when the physical location in real space is shifted by $\mathbf{T}_0$, only the phase of the wave function will be changed. In other words it is of the Bloch form (2.153) as required. It is also easily seen that $\langle \widetilde{\varphi}_{\mu;\mathbf{k}} | \widetilde{\varphi}_{\nu;\mathbf{k}} \rangle = \delta_{\mu\nu}$. Now, the KS wave functions read with this basis as

$$\widetilde{\psi}_{i;\mathbf{k}}(\mathbf{r}) = \sum_\mu c^i_{\mu;\mathbf{k}} \widetilde{\varphi}_{\mu;\mathbf{k}}(\mathbf{r}). \tag{2.155}$$

In this new basis the elements of the S-matrix (now labeled as $\widetilde{S}$) become

$$\begin{aligned} \widetilde{S}_{\mu\nu;\mathbf{k}} &= \frac{1}{N} \sum_{\mathbf{T},\mathbf{T}'} \mathrm{e}^{\mathrm{i}\mathbf{k}\cdot(\mathbf{T}'-\mathbf{T})} \int \varphi_\mu(\mathbf{r}-\mathbf{T})\varphi_\nu(\mathbf{r}-\mathbf{T}') \\ &= \frac{1}{N} \sum_{\mathbf{T},\mathbf{T}+\mathbf{T}''} \mathrm{e}^{\mathrm{i}\mathbf{k}\cdot\mathbf{T}''} \int \varphi_\mu(\mathbf{r}-\mathbf{T})\varphi_\nu(\mathbf{r}-\mathbf{T}-\mathbf{T}'') \\ &= \sum_{\mathbf{T}''} \mathrm{e}^{\mathrm{i}\mathbf{k}\cdot\mathbf{T}''} \int \varphi_\mu(\mathbf{r})\varphi_\nu(\mathbf{r}-\mathbf{T}) = \sum_{\mathbf{T}} \mathrm{e}^{\mathrm{i}\mathbf{k}\cdot\mathbf{T}} S_{\mu\nu}(\mathbf{T}). \end{aligned} \tag{2.156}$$

Next, for the H^0-matrix $\widetilde{H}^0_{\mu\nu;\mathbf{k}} = \langle \widetilde{\varphi}_{\mu;\mathbf{k}}(\mathbf{r}) | \widetilde{H}[n_0] | \widetilde{\varphi}_{\nu;\mathbf{k}}(\mathbf{r}) \rangle$ we obtain with identical steps

$$\widetilde{H}^0_{\mu\nu;\mathbf{k}} = \sum_{\mathbf{T}} \mathrm{e}^{\mathrm{i}\mathbf{k}\cdot\mathbf{T}} H^0_{\mu\nu}(\mathbf{T}). \tag{2.157}$$

Finally, by respectively substituting H^0 and S from Eqs. (2.130–2.132) with $\widetilde{H}^0$ and $\widetilde{S}$ we obtain

$$\sum_{\nu} c^i_{\nu;\mathbf{k}} \left(\widetilde{H}_{\mu\nu;\mathbf{k}} - e_{i;\mathbf{k}} \widetilde{S}_{\mu\nu;\mathbf{k}} \right) = 0 \quad \forall i, \mu \quad \text{and} \tag{2.158}$$

$$\sum_{\mu,\nu} c^i_{\mu;\mathbf{k}} c^i_{\nu;\mathbf{k}} \widetilde{S}_{\mu\nu;\mathbf{k}} = 1 \quad \forall i, \tag{2.159}$$

where

$$\widetilde{H}_{\mu\nu} = H^0_{\mu\nu} + \frac{1}{2} S_{I_\mu J_\nu} \sum_J \left(\gamma_{IK} + \gamma_{JK} \right) \Delta q_J. \tag{2.160}$$

The Mulliken charges can be also calculated with the substitution $S_{I_\mu J_\nu} \rightarrow \widetilde{S}_{\mu\nu;\mathbf{k}}$. However, now we have charge fluctuations for several different $\mathbf{k}$. Hence it is necessary to introduce a summation for $k = |\mathbf{k}|$ from 0 to k_{F}, i.e., *the Fermi wave vector* (remember that $T = 0$ is assumed). Now, from Eq. (2.113) we obtain

$$\Delta q_I = \sum_i \sum_{\mu, A_\alpha} \sum_{k=0}^{k_{\mathrm{F}}} c^i_{\mu;\mathbf{k}} c^i_{A_\alpha;\mathbf{k}} \widetilde{S}_{I_\mu A_\alpha;\mathbf{k}} - q^0_I. \tag{2.161}$$

After the c-coefficients have been solved, calculating the DFTB-energy is not as straightforward as previously. The band structure term that now reads

$$E_{\mathrm{BS}} = \sum_i \sum_{\mu,\nu} \sum_{k=0}^{k_{\mathrm{F}}} c^i_{\mu;\mathbf{k}} c^i_{\nu;\mathbf{k}} H^0_{\mu\nu} \tag{2.162}$$

is not much more complex than before but the E_{SCC}-term

$$E_{\mathrm{SCC}} = \frac{1}{2} \sum_{IJ}^{\text{unit cell}} \sum_{\mathbf{T}} \gamma_{IJ}(|\mathbf{R}_{IJ} - \mathbf{T}|) \Delta q_I \Delta q_J \tag{2.163}$$

has become trickier. But there do exist standard methods for computing the infinite sum over all translations $\mathbf{T}$, e.g. the Ewald summation [24]. The sum over ions I and J should only go through the ions within the unit cell, since now we should consider the E_{DFTB} per unit cell. Lastly, when we are considering E_{rep}, we must take into account that the repulsive potential energy of two atoms in neighbouring unit cells should be divided evenly between their unit cells. Now, it is easily seen that the formula

$$E_{\mathrm{rep}} = \frac{1}{2} \sum_{IJ}^{\text{unit cell}} \sum_{\mathbf{T}} V_{\mathrm{rep}}^{IJ}(|\mathbf{R}_{IJ} - \mathbf{T}|) \tag{2.164}$$

gives the correct E_{rep} with a special case definition $V_{\mathrm{rep}}(0) = 0$. Now, this formula is very easy to compute, since due to the short-rangedness of the repulsions there are only few terms in the summation.

3 Boron nitride nanostructures

3.1 Hexagonal boron nitride layer

As discussed, the BN nanostructures are based on the hexagonal graphene-like honeycomb structure. The simplest such structure is the hexagonal boron nitride layer (h-BN). Its geometry is defined by the lattice vectors $\mathbf{a}$ and the atom position vectors R within the unit cell. They can be defined in various different but equivalent ways, but in this thesis I use the following configuration for the lattice vectors

$$\mathbf{a}_1 = a\,(1, 0, 0)\,, \tag{3.1}$$

$$\mathbf{a}_2 = a\left(-\frac{1}{2}, \frac{\sqrt{3}}{2}, 0\right) \quad \text{and} \tag{3.2}$$

$$\mathbf{a}_3 = c\,(0, 0, 1)\,. \tag{3.3}$$

Now the position vectors for boron and nitrogen ($\mathbf{R}_{\mathrm{B}}$ and $\mathbf{R}_{\mathrm{N}}$, respectively) read

$$\mathbf{R}_{\mathrm{B}} = a\,(0, 0, 0) \quad \text{and} \tag{3.4}$$

$$\mathbf{R}_{\mathrm{N}} = a\left(0, \frac{1}{\sqrt{3}}, 0\right). \tag{3.5}$$

These vectors are visualized in Fig. 2. The lattice is then obtained by repeating the unit cell infinitely in each direction. The lattice vectors $\mathbf{T}$ are now of the form $\mathbf{T} = n_1\mathbf{a}_1 + n_2\mathbf{a}_2 + n_2\mathbf{a}_2$

The reciprocal lattice is defined through the usual relation

$$\mathbf{b}_k = \frac{2\pi\epsilon_{ijk}}{V_{\mathrm{uc}}}\mathbf{a}_i \times \mathbf{a}_j, \tag{3.6}$$

where $V_{\mathrm{uc}} = a^2c\sqrt{3}/2$ is the volume of the unit cell. Now we can see why also for the single h-BN layer it was necessary to define the third lattice

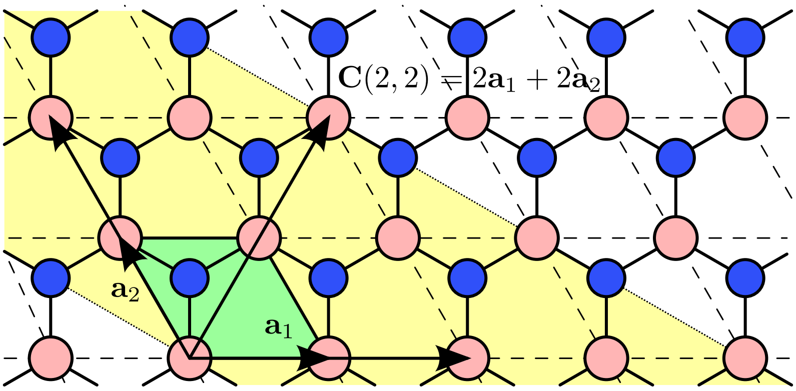

Figure 2: BN honeycomb network with lattice vectors $\mathbf{a}_1$ and $\mathbf{a}_2$ as well as the two-atom unit cell spanned by them (in green). The definition of the chirality vector $C(n,m)$ is clarified with an example for $C(2,2)$: The lines bordering the yellow area are perpendicular to the $C(2,2)$. The yellow area is rolled and its borders connected to form the tube. Positions of the different B and N atoms can be labeled as $\mathbf{R}_{\mathrm{B}}(i,j) = \mathbf{R}_{\mathrm{B}} + i\mathbf{a}_1 + j\mathbf{a}_2$ and $\mathbf{R}_{\mathrm{N}}(i,j) = \mathbf{R}_{\mathrm{B}} + i\mathbf{a}_1 + j\mathbf{a}_2$, respectively.

vector $\mathbf{a}_3$. Nevertheless, now with the definitions (3.1–3.3) the reciprocal space unit vectors become

$$\mathbf{b}_1 = \frac{2\pi}{a}\left(1, \frac{1}{\sqrt{3}}, 0\right), \tag{3.7}$$

$$\mathbf{b}_2 = \frac{2\pi}{a}\left(0, \frac{2}{\sqrt{3}}, 0\right) \quad \text{and} \tag{3.8}$$

$$\mathbf{b}_3 = \frac{2\pi}{c}\left(0, 0, 1\right). \tag{3.9}$$

They are visualized in Fig. 3 along with the so-called *special symmetry points* Γ, M, K and K'. It can be seen from the picture that $\mathbf{M} = \mathbf{b}_2/2$, $\mathbf{K} = (2\mathbf{b}_1 - \mathbf{b}_2)/3$ and $\mathbf{K}' = (\mathbf{b}_1 + \mathbf{b}_2)/3$. Thus we have

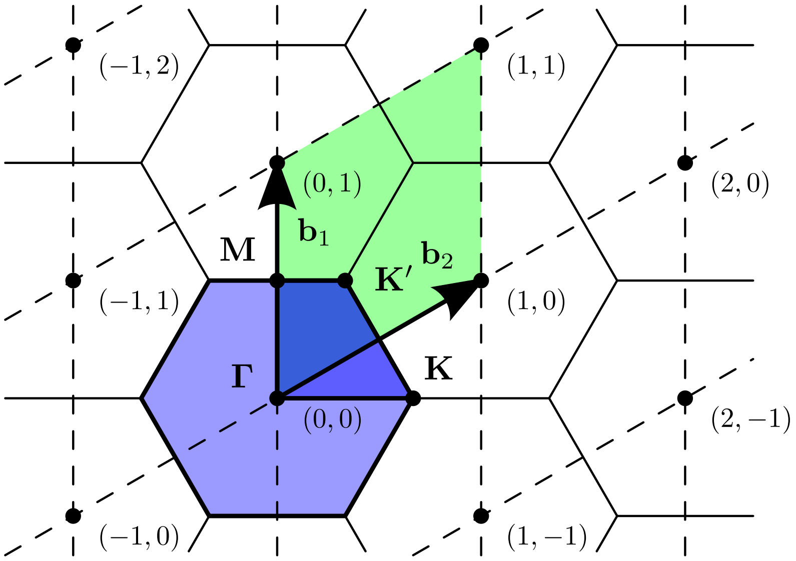

Figure 3: The reciprocal lattice vectors $\mathbf{b}_1$ and $\mathbf{b}_2$ as well as the reciprocal unit cell (in green). The hexagons represent the Brillouin zones, first of which is coloured in blue. Also its first quarter, which is adequate in describing the whole 1st Brillouin zone due to symmetry reasons, is highlighted in darker blue. Also the special symmetry points are shown.

$$\mathbf{\Gamma} = \frac{2\pi}{a}\left(0, 0, 0\right), \tag{3.10}$$

$$\mathbf{M} = \frac{2\pi}{a}\left(0, \frac{1}{\sqrt{3}}, 0\right), \tag{3.11}$$

$$\mathbf{K} = \frac{2\pi}{a}\left(\frac{2}{3}, 0, 0\right) \quad \text{and} \tag{3.12}$$

$$\mathbf{K}' = \frac{2\pi}{a}\left(\frac{1}{3}, \frac{1}{\sqrt{3}}, 0\right). \tag{3.13}$$

3.2 Boron nitride nanotubes

After defining the lattice, the nanotubes can be defined through so-called *Chirality vector*

$$C(n, m) = n\mathbf{a}_1 + m\mathbf{a}_2, \quad n > m. \tag{3.14}$$

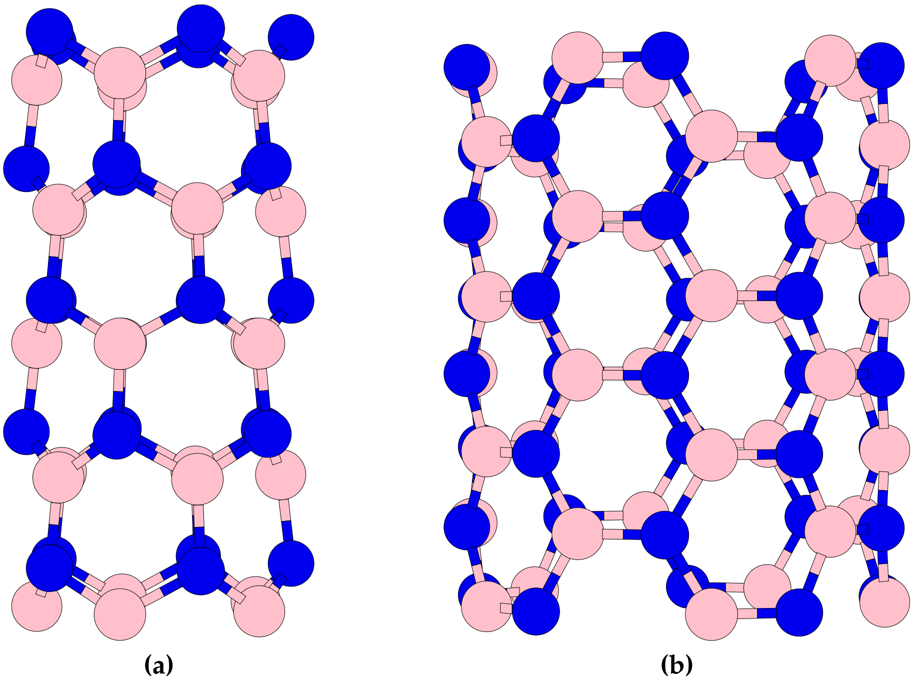

Figure 4: Examples of (a) zigzag and (b) armchair BNNTs for $n = 5$. Their unit cells have been repeated 3 and 5 times, respectively. So it is seen that for constant n the unit cell of the zigzag/armchair BNNT is long/short and narrow/wide.

It specifies the way in which the layer is wrapped into tubular form. Fig. 2 demonstrates how this is done through an example for $C(2,2)$. The NTs obtained by using the $C(n,m)$ are referred to as (n,m) BNNTs. The special cases of $(n,0)$ and (n,n) nanotubes are called *zigzag* and *armchair* nanotubes, respectively. Fig. 4 shows examples of zigzag and armchair tubes for $n = 5$. In this thesis, as well as in most computational papers, only these cases are considered due to the simplicity of their unit cells. Besides, when BNNTs are synthesized, they commonly end up in either zigzag or armchair form. A unit cell of $(n,0)$ or (n,n) BNNT consists of $4n$ atoms. However, there are some underlying rotational symmetries—there are only three different kinds of bonds in chiral NTs, and in zigzag and armchair NTs this number is reduced to just two. Consequently, in zigzag and armchair BNNTs the B and N atoms lay in their own cylinder levels with slightly different radii. Due to these symmetries the $4n$-atom unit cell can be simplified greatly by revisiting the standard Bloch theorem and applying the rotational symmetry [25, 26]. However, this theory is not utilized in this work. It only applies to perfect NTs and with defected ones this symmetry cannot be employed.

As nanotubes are quasi-one-dimensional there are periodic boundary conditions only in one direction ($\hat{\mathbf{z}}$-direction in this thesis) and thus the $\mathbf{k}$-space is one-dimensional as well. The reciprocal lattice is defined with

$$\mathbf{b} = \frac{2\pi}{l}\left(0, 0, 1\right), \tag{3.15}$$

where l is the length of the BNNT. The only symmetry points are $\Gamma = 0$ and $\mathbf{X} = \mathbf{b}/2$.

3.3 Elastic properties of BN nanostructures

This section is based on R. Feynman's classic book [27]. Now, *Young's modulus*, or *elastic modulus*, is a measure of the stiffness of an elastic material and is used to chararacterize materials. Any material obeys *Hooke's law* for small enough stretchings. It states that the force and the stretching caused by it are linearly related. Now, consider an object of initial length l_0 and initial cross-section area A_0. Thus it has initial volume $V_0 = l_0 A_0$. Under stretching of $l - l_0$ the object resists the change with certain force $F(l - l_0) = \mathrm{d}E/\mathrm{d}\left(l - l_0\right) = \mathrm{d}E/\mathrm{d}l$. According to Hooke's law the correspondence between the stretching and the force is linear:

$$F(l - l_0) = K(l - l_0). \tag{3.16}$$

But here the constant K (*the spring constant*) as well as $F(l - l_0)$ are extensive physical properties, i.e., they depend on the size and shape of the structure in question. However, Eq. (3.16) can be manipulated by defining *strain* ϵ and stress σ:

$$\epsilon = \frac{l - l_0}{l_0} \quad \text{and} \tag{3.17}$$

$$\sigma = \frac{1}{V_0}\frac{\mathrm{d}E}{\mathrm{d}\epsilon} = \frac{1}{A_0}\frac{\mathrm{d}E}{\mathrm{d}l}. \tag{3.18}$$

The result of this manipulation reads

$$\sigma = Y\epsilon, \tag{3.19}$$

where Y is a material-dependent constant—Young's modulus. Note that it indeed is only material-dependent instead of being also size-dependent, i.e., it is an intensive physical quantity. Also note that the stretching in one direction induces shrinkage in the other directions, and that all the above equations assume this, though not explicitly written down.

However, as the BN nanostructures are one atom layer thick, the concept of cross-section area is rather vague. Particularly the thickness h_0 of the structures can not be defined indisputably. Luckily we can define so-called *modified Young's modulus* Y_s, which relates to Y through

$$Y_\mathrm{s} = Yh_0 \tag{3.20}$$

and thus is independent of the thickness of the object. Therefore

$$\frac{h_0}{V_0}\frac{\mathrm{d}E}{\mathrm{d}\epsilon} = Y_\mathrm{s}\epsilon. \tag{3.21}$$

Now, for the h-BN layer unit cell we have $V_0 = l_0 w_0 h_0$, where w_0 is the initial width of the object, and for nanotubes we can approximate $V_0 = 2\pi r_0 l_0 h_0$, where r_0 is the initial radius of the tube. Thus for h-BN and BNNTs Eq. (3.21) becomes

$$\frac{1}{l_0 w_0}\frac{\mathrm{d}E}{\mathrm{d}\epsilon} = Y_\mathrm{s}\epsilon \quad \text{and} \tag{3.22}$$

$$\frac{1}{2\pi r_0 l_0}\frac{\mathrm{d}E}{\mathrm{d}\epsilon} = Y_\mathrm{s}\epsilon, \tag{3.23}$$

respectively. These equations still define Y_s as structure-independent and material-specific constant for single h-BN layer and single-walled BNNT.

Anyhow the obtained modified moduli can be converted back into ordinary Young's modulus through (3.20) by using the usual thickness value $h_0 = 3.33\,\text{Å}$ [28], which is the interplanar thickness of h-BN layers.

In general it is possible to have strains in any direction and there also are shear-type strains. Thus strain becomes a tensor of 2nd order. Also stress is a tensor of 2nd order. These two are then related (similarly to Eq. (3.19)) through

$$\sigma_{ij} = \sum_{kl} C_{ijkl}\epsilon_{kl}, \tag{3.24}$$

where the 4th rank tensor C is the *elasticity tensor*. Only one of its components is Young's modulus. Another physical quantity appearing in the components of C is *the Poisson's ratio* ν. If the strain is applied to the $\hat{\mathbf{x}}$-direction, the system experiences shrinking in the other directions and ν is defined as

$$\nu = -\frac{\epsilon_y}{\epsilon_x} = -\frac{\epsilon_z}{\epsilon_x}. \tag{3.25}$$

Above I have for simplicity denoted strain (stress) in $\hat{\mathbf{i}}$-direction as ϵ_i (σ_i) instead of ϵ_{ii} (σ_{ii}). This is because I will not cover any situations with shear strains or stresses in this thesis, so all the strains and stresses will be of the type ϵ_{ii} or σ_{ii}.

4 DFTB parametrization

In this section I shall go in more detail to the theory and practical construction of DFTB parametrization—particularly from the viewpoint of BN-parametrization and HOTBIT, which is the code with which I have performed the BN-parametrization in this thesis (see the next section).

4.1 The V_{conf}-potential and the x-parameters

Now the V_{conf}-potential determining the confinement of the orbitals φ_μ through Eq. (2.85) should be determined. As discussed, V_{conf} should be close to zero in proximity of the nucleus and grow (strongly) as a function of distance r. Thus in the Taylor expansion of $V_{\text{conf}}(r)$ the linear term should be ruled out and therefore $V_{\text{conf}}(|\mathbf{r}|)$ is of the form

$$V_{\text{conf}}(|\mathbf{r}|) = \left(\frac{|\mathbf{r}|}{r_0}\right)^2 \tag{4.1}$$

at its simplest, e.g. under the first-order approximation. This form is also a sufficient approximation in our case. Namely, the majority of the error from the minimal basis $\{\varphi_\mu\}$ anyhow comes from its small size and thus endless fine-tuning of its elements φ_μ by adding more and more higher-order terms into V_{conf} is not sensible. Therefore we adapt the form (4.1). Next, it has been observed [19] that in practice usually the optimal is of the order $2r_{\text{cov}}$, where r_{cov} is the *covalent radius* of the element in question. Therefore we write

$$V_{\text{conf}}(|\mathbf{r}|) = \left(\frac{|\mathbf{r}|}{2xr_{\text{cov}}}\right)^2, \tag{4.2}$$

where x is a new parameter with default value 1. It may be substantially larger than 1 too since it only means that the pseudoatomic orbitals φ_μ are closer to the free orbitals $\varphi_\mu^{\text{free}}$, but it should not be significantly smaller, since then the V_{conf} deforms the orbitals too much. A sensible range is $x \gtrsim 0.6$.

4.2 The U-parameters

The derivation of the E_{SCC} term in Sec. 2.7.3 made use of the Hubbard on-site energy and expressed E_{SCC} in terms of it. However this physical constant might be taken as a parameter as well—deviating its value from the true Hubbard U does not cause anything illegal. It thus can be used to fine-tune the value of E_{SCC}. But usually its value is not needed to change and this will be the case in my work as well.

The quality of given set of x- and U-parameters should be inspected by first computing with these parameter values in some chosen test systems such physical quantities that do not depend on E_{rep} and then comparing them to references. In practice this kind of quantities are the equilibrium band structures for periodic systems (for example the h-BN layer). This is because when the Fermi energy is diminished from the BS energies, the contributions from both E_{rep} and the zero-point energy vanish. So, after deciding some values for the x- and U-parameters and computing the confined orbitals for the chosen x, one should calculate the band structures in the test systems (with geometries from reference literature) both with DFTB and LDA-DFT. The better the correspondence, the better choices the values of x- and U-parameters were.

4.3 The V_{rep}-potentials

The repulsion functions $V_{\mathrm{rep}}(R)$ should provide *transferability* of the parametrization in very different bonding situations and in systems of various scales. Thus they should be constructed in such a way that the difference between DFTB and DFT energies is minimized *on average*. In practice this happens by selecting a set of *reference systems* with as comprehensive selection of different bonding situations as possible and minimizing this difference in these systems.

Also the x- and U-parameters alter the V_{rep}-functions, since they affect the E_{BS} and E_{SCC} energy terms. And they can do this differently for different reference systems. Thus tweaking of x- and U-parameters is an important part of parametrization of the V_{rep}-potentials. This also complicates the process of the DFTB parametrization, and it is not necessarily a straightforward task.

4.3.1 Requirements for the V_{rep}-potentials

Often all the possible bonding situations are not covered by the reference systems used in the parametrization. Thus even if good V_{rep}-functions were found for the used reference systems, it would not guarantee transferability for systems with different bonding situations. For such cases there however does exist a set of requirements and rules of thumb that suggest good quality and transferability of V_{rep}-functions:

1. The V_{rep}-functions should be short-ranged as discussed in the previous section. If the construction of the V_{rep}-potentials leads to them having long "tails", it implies a large error in $E_{\mathrm{BS}} + E_{\mathrm{SCC}}$. This is because the long-ranged interaction energies should originate from the single-particle interactions (through matrix elements of S and H^0) only.

   Therefore for each V_{rep}-function there should exist a relatively short limit distance called the *cutoff distance* R_{cut} so that for $R > R_{\mathrm{cut}}$ we would have $V_{\mathrm{rep}} \equiv 0$. This limit should not be much larger than the typical equilibrium bond length.

2. They should decrease *strictly monotonically* from ∞ to 0 in the range $0 < R < \infty$. After all, we can think of them as generalized ion-ion repulsion potentials and odd non-monotonic behavior would be unphysical. Moving two ions closer to each other should not decrease E_{rep}. Such unphysical behavior of V_{rep}-functions would more likely lead into problems with other systems than the used reference systems. In other words the transferability of the parametrization would probably be poor.

3. The previous requirement for the mathematical form of V_{rep}-functions is not actually enough. For good transferability we should also require for $\mathrm{d}V_{\mathrm{rep}}(R)/\mathrm{d}R$ (e.g. the *repulsion forces* between the atom pairs) *strictly monotonic* growth from $-\infty$ to 0 for $0 < R < \infty$. This is because these forces also have a physical meaning as generalized ion-ion repulsion forces and odd behavior of these forces would most likely lead into bad transferability also in this case and with the same arguments.

If these requirements are not filled, it suggests that the values of x- and U-parameters should be improved, or in the worst case proper DFTB parametrization can not be done at all for the elements in question.

4.3.2 Reference systems

Now, in the construction of the V_{rep}-functions their individual contributions to $E_{\mathrm{rep}} = \sum_{IJ} V_{\mathrm{rep}}^{IJ}(R_{IJ})$ should be separated in general, since there are several different V_{rep}-functions for different kinds of interactions (with an exception for homoelemental systems). This is obtained for example by using reference systems with only one kind of repulsion interactions (for example in the case of BN-parametrization only B–B bonds, N–N bonds or B–N bonds) and then parametrizing the V_{rep}-functions one by one. The simplest such system is the dimer, i.e., the two-atom molecule with the bond length R. For them $E_{\mathrm{rep}}(R) = V_{\mathrm{rep}}(R)$ and thus to satisfy $E_{\mathrm{ref}} = E_{\mathrm{DFTB}}$ we simply obtain for dimers

$$V_{\mathrm{rep}}(R) = E_{\mathrm{ref}}(R) - \left[E_{\mathrm{BS}}(R) + E_{\mathrm{SCC}}(R)\right]. \tag{4.3}$$

The simplest single-bond-type reference systems after the dimer are obtained by generalizing the dimer into systems with N *equal* bond lengths R instead of just one (for example the h-BN lattice). For those kinds of systems we have $E_{\mathrm{rep}} = N V_{\mathrm{rep}}(R)$ and thus

$$V_{\mathrm{rep}}(R) = \frac{1}{N}\left[E_{\mathrm{ref}}(R) - \left[E_{\mathrm{BS}}(R) + E_{\mathrm{SCC}}(R)\right]\right]. \tag{4.4}$$

However, for example in lattices there is of course an infinite amount of different R_{IJ} for each atom I. But if they are above the R_{cut} they do not contribute to the E_{rep} and hence it is allowed to have atomic distances larger than R_{cut} in reference systems. So if we are using a lattice as a reference system, we should be careful in keeping R_{cut} shorter than the second smallest neighbor distance of given interaction type. For example for h-BN lattice and B-N interactions R_{cut} should be shorter than the 3rd nearest neighbor distance as with the 2nd nearest neighbor distances the interaction types are either B–B or N–N.

Also it is possible to use systems with several kinds of interactions if all but one V_{rep}-function is already parametrized. In this case an equation similar to (4.4) can be obtained.

At this point construction of the V_{rep}-potentials is already doable: By determining the reference system energies $E_{\text{ref}}(R)$ for a collection of reference systems and with a set of different R, we obtain sets of data points from Eq. (4.4) (with $N = 1$ for dimers). Then the V_{rep}-functions can be *fitted* to these data points. However, this is not the ideal way to fit the repulsions. Instead, a better result is usually obtained if the fitting is performed to the *force* data points $\mathrm{d}V_{\text{rep}}(R)/\mathrm{d}R$. They are obtained from Eq. (4.4) through differentiation and read

$$V'_{\text{rep}}(R) = \frac{1}{N}\left[E'_{\text{ref}}(R) - [E'_{\text{BS}}(R) + E'_{\text{SCC}}(R)]\right]. \tag{4.5}$$

Now the repulsion potentials can be recovered from the repulsion forces through integration.

There are numerous reasonings behind this complication. First of all, it is not necessarily seen at the first glance from the V_{rep}-functions itself whether or not $\mathrm{d}V_{\text{rep}}(R)/\mathrm{d}R$ grows monotonically as required. But from $\mathrm{d}V_{\text{rep}}(R)/\mathrm{d}R$ it is naturally easily seen. Secondly, the reference energies might not have the same zero-point energy with DFTB energies and the Eq. (4.4) would apply only after taking this difference into account. But with forces the zero-point energy vanishes due to the differentiation and (4.5) always applies. Thirdly, the force approach allows more reference system types and hence it allows to take into account a broader range of different bonding situations.

For instance for the equilibrium systems we have $E'_{\text{ref}}(R_0) = 0$ by definition for the equilibrium bond length R_0 and Eq. (4.5) becomes

$$V'_{\text{rep}}(R_0) = -\frac{1}{N}\left[E'_{\text{BS}}(R_0) + E'_{\text{SCC}}(R_0)\right]. \tag{4.6}$$

With this it is possible to obtain a force fitting points from experimental equilibrium bond lengths.

It is also possible to use general single-bond-type structures (with arbitrary bond lengths) as reference systems. The force data points are obtained by minimizing the total difference of DFTB and reference forces (more details in [19]).

Also, with the force approach reference systems are even allowed to contain several bond types whose $V_{\rm rep}$-functions are yet to be parametrized. This is possible by selecting just a subset of bonds where the only unknown bond type is the one under parametrization. It is allowed to have other bond types though (if their $V_{\rm rep}$ is already constructed). Now, if the lengths of these bonds are kept constant, the force contributions from these constant bonds vanish through differentiation (just like the zero-point energy). After this, the force differences should be minimized as before: If all the bond lengths are equal, an equation similar to Eq. (4.5) can be derived. And if there are different bond lengths, the differences between reference and DFTB forces can be minimized similarly to the non-subset case.

4.3.3 Fitting to the force data point sets

In this thesis only equal bond length cases in non-subset situations (Eqs. (4.5) and (4.6)) will be employed. In practice these equations can be used in several different ways. And now in this subsection I describe how the usage of these equations is implemented in HOTBIT and how they are therefore used in this thesis.

Firstly, in the non-equilibrium case one should compute a repulsion potential data point set $\{V_{\rm rep}(R_a)\}$ with Eq. (4.4). After this a smooth spline of 3rd order is fitted to this data point set internally in HOTBIT. And the repulsion force data point set $\{V'_{\rm rep}(R_a)\}$ is obtained as a derivative of this spline at points $\{R_a\}$.

Secondly, in the equilibrium case Eq. (4.5) is directly employed. To determine $E'_{\rm BS}(R_0)+E'_{\rm SCC}(R_0)$, computation of $E_{\rm BS}+E_{\rm SCC}$ is performed at both R_0 and $R_0+\Delta R$ for a small ΔR and the derivative is approximated as a slope between these two energies.

After calculating the force data point sets, also the fitting of the force repulsions to them is parametrized in HOTBIT. More accurately, the fit for the repulsion force $F(R) = {\rm d}V_{\rm rep}(R)/{\rm d}R$ is obtained through minimizing the functional

$$S[F(R)] = \sum_i \left(\frac{V'_{\mathrm{rep},i} - F(R_i)}{\sigma_i} \right)^2 + \lambda^2 \int^{R_{\mathrm{cut}}} \mathrm{d}R \, [F''(R)]^2 \tag{4.7}$$

with a constraint $F(R_{\mathrm{cut}}) = 0$. Above the new parameters are firstly λ, which is the smoothness parameter of the fit—increasing λ makes the curvature more expensive resulting in a smoother fit. Secondly, the set of parameters $\{\sigma_i\}$ are the weights for each reference system set i—increasing σ_i results into fit following data points of system i more closely. These parameters should now be tuned until a fit that follows the force data points in an eye-satisfying way and also satisfies the discussed requirements. After this $V_{\mathrm{rep}}(R)$ is recovered through the following integration:

$$V_{\mathrm{rep}}(R) = -\int_R^{R_{\mathrm{cut}}} \mathrm{d}R \, F(R). \tag{4.8}$$

5 HOTBIT—the DFTB code

The HOTBIT code [29], written by Pekka Koskinen, is capable of creating DFTB parametrizations and utilizing them in calculations. It is written in PYTHON for clarity and transparency albeit resulting in slightly slower performance when compared to C++ , for instance. But due to the lightness of the used DFTB theory, it is still remarkably fast. This code is used as an implementation to ASE (Atomistic Simulation Environment) [30], which also is a PYTHON -based code. As per its name, it is designed for setting up and simulating all kinds of atomic problems.

5.1 Usage of HOTBIT

A HOTBIT calculator is initialized in a following way:

```
calc = Hotbit(
  elements={'B':'B.elm',          #Element file for B
            'N':'N.elm'},         #Element file for N
  tables  ={'BB':'rep_BB.par',   #BB-interaction parameter file
            'BN':'rep_BN.par',   #BN-interaction parameter file
            'NN':'rep_NN.par'},#NN-interaction parameter file

  SCC=True,                       #SCC-DFTB is used
  gamma_cut=1e9,                  #E_SCC-term integration cutoff
  width=0.1                       amount of the Fermi smearing
  txt='output.cal',               #output file of calculations
  rs='k'                          #periodic k-point calculation
  kpts=(20,20,1),                 #the k-point sampling
)
```

This features the setting I have mostly used in my calculations. Firstly `B.elm` and `N.elm` are the *element files* for B and N, respectively. These files include firstly the Hubbard U for the element in question. Secondly they include from the unconfined pseudopotential calculation (2.81) the eigenenergies $\epsilon_{2s}^{\text{free}}$ and $\epsilon_{2p}^{\text{free}}$. They are needed in the computation of $H^0_{I_\mu,nuJ}$ (see Eq. (2.150)). The `.par`-files are the parametrization functions containing the SK integrals and V_{rep}-functions. The parameter `gamma_cut` sets the limit in the integration of the E_{SCC}-term Eq. (2.163) with the periodic boundary conditions. In my calculations I used values between

$10^9 - 10^{12}$ and I found them sufficient in my tests. HOTBIT employs the thermal broadening (see the discussion in Sec. 2.3.2). Strength of it is characterized by parameter `width`, which is the width of the Fermi occupation (i.e., width of f defined by Eq. (2.49)) in eVs. In the used units ($k_\mathrm{B} = 1$) it equals to T and its default value is $0.1\,\mathrm{eV}$.

This particular calculator is for some pseudo-2D structure, since the k-point sampling is two-dimensional. It can be attached to this 2d structure with

```
BNstructure.set_calculator(calc)
```

5.2 Notes about HOTBIT

Here I have gathered a list of miscellaneous notes about the theory employed by HOTBIT and practical issues related to the usage of HOTBIT (and ASE):

1. The ASE version 3.6.0. is preferred to be used with HOTBIT, since at the time HOTBIT was coded, it was the ASE version available. The newer versions might have some compatibility issues.
2. The units defined by Eqs. (2.1–2.8) are used internally by HOTBIT. But since HOTBIT is an ASE calculator, the units viewed from outside are electronvolts and Ångströms. This has to be taken into account with values of U and r_cov—they have to be given to HOTBIT in Hartrees and Bohrs, respectively.
3. HOTBIT uses internally the reciprocal lattice defined by Eq. (3.6) in the k-point calculations. Consequently also Eqs. (3.7–3.15) apply. But in ASE the reciprocal vectors are defined in such a way that $\left|\mathbf{b}_i^\mathrm{ASE}\right| = 1\ \forall i$. This induces relations $\mathbf{k}^\mathrm{ASE} = \sqrt{3}a/(4\pi)\,\mathbf{k}^\mathrm{HB}$ for 2D h-BN structures (a is the lattice parameter) and $\mathbf{k}^\mathrm{ASE} = l/(2\pi)\,\mathbf{k}^\mathrm{HB}$ for BNNTs (l is the length of the tube). This has to be taken into account for example when plotting DFTB band structures to the same figure with band structures computed with ASE with other calculators.

6 Construction of BN-parametrization

Table 1: The used values of U and r_{cov}. The value for U has been calculated from IE and EA with Eq. (2.93). In the parametrization the U in Ha and r_{cov} in Bohr should be used as discussed in the precious section.

	IE(eV) [31]	EA(eV) [32]	U		r_{cov} [33]	
			(eV)	(Ha)	(Å)	(Bohr)
B	8.294	0.277	8.017	0.295	0.84	1.59
N	14.527	0.072	14.455	0.531	0.71	1.34

Table 1 features the values of U and r_{cov} used in my parametrization. I chose not to alter U at all, and I just employed the default U-values shown in this table. Also the used values for r_{cov} read there. However, it afterwards turned out that I accidentally had used the r_{cov} in eV instead of Bohrs. Luckily this mistake did not have any effect on the final parametrization since due to this I only thought I was dealing with $1/0.529 = 1.890$ times larger x-parameters than I really was. In the following I will however keep my erroneous x-parameter notation so now the x-parameters are defined through $V_{\text{conf}}(|\mathbf{r}|) = [|\mathbf{r}|/(2 \cdot 0.529 \cdot x r_{\text{cov}})]^2$ instead of $V_{\text{conf}}(|\mathbf{r}|) = [|\mathbf{r}|/(2 x r_{\text{cov}})]^2$, which is the Eq. (4.2).

6.1 The x-parameters

As discussed in Sec. 4.3.1, the quality of different x-parameters should first be compared based on their effects on the band structures. More explicitly, the general matching between the DFTB and reference (LDA-DFT) energy bands implies that the minimal basis set $\{\varphi_\mu\}$ is of good quality. In this sense all the bands are equally important in seeking the good x-parameters. But on the other hand the band structures are not only a tool for finding the optimal x-parameters. They also are an application of the parametrization and in that sense the valence and conduction bands and the band gap E_{gap} are particularly important. Thus, all in all, when judging the quality of x-parameters from the point of view of band structures, all the bands but particularly the conduction and valence bands and E_{gap} are important.

In my work I used as the only reference band structure system the h-BN layer with $a = 2.50$ Å [14] as the reference value for the lattice constant. All BN nanostructures are based on this layer and therefore good correspondence between the DFT and DFTB band structures probably ensures that they are good also for other BN nanostructures—such as BN nanotubes. Hence making the x-parameter comparisons only based on the h-BN band structures should be enough.

I studied a quite broad range of $x = (x_\mathrm{B}, x_\mathrm{N})$, since the sensible range for x-parameters is from ~ 0.6 to infinity[2]—the lower bound is explained by the fact that too tight confinement results in $\{\varphi_\mu\}$ too different from $\{\varphi_\mu^\mathrm{free}\}$ and hence unphysical and the infinity limit just leads to $\{\varphi_\mu\} = \{\varphi_\mu^\mathrm{free}\}$. Now, the results of my experimentings with different x-parameters are presented in Fig. 5. Only a selected array of $(x_\mathrm{B}, x_\mathrm{N})$ in a bit narrow range is shown, but the general behavior should be well visible. It is seen that modifying the x-parameters around the default values does not have particularly drastic effects on the band structures and clearly for any pair $(x_\mathrm{B}, x_\mathrm{N})$ perfect match between the DFTB and LDA-DFT band structures is not found. But some x-parameter values are certainly better than others, so analyzing the effects of changing x_B and x_N to the h-BN BS properties can be done. And it seems that luckily these effects are somewhat systematic and linear and the contributions from x_B and x_N can be approximately separated. This simplifies the process of choosing the final x-parameters as their effects can be considered independently.

When it comes to variation of x_B, first of all the four lowest bands seem to mostly retain their shape, but increasing x_B shifts these bands lower in the energy as a whole. As the result the valence band ends up in too low energy when compared to DFT. This increases the DFTB-E_gap, since the conduction band is hardly altered by changes in x_B. The conduction band is also too low in energy (even strongly and for any x_B), so lowering the valence band when increasing x_B improves the DFTB-E_gap—even for $(x_\mathrm{B}, x_\mathrm{N}) = (3.0, 2.0)$ we only have $E_\mathrm{gap} = 4.35$ eV whereas the experimental E_gap is ~ 5 eV. Considering all this, larger x_B should be preferred but also low x_B might be an option if it provides better V_rep-functions.

Next, x_N has even less influence on the h-BN BS. Bands from 2nd to 4th seem not to be altered by it nearly at all, but increasing it improves the first band. On the other hand, lowering it improves the conduction band around the Γ-point as well as the higher bands in general. Hence based on this analysis it is difficult to deduce the best x_N and it really does not rule

---

[2] Now with my mistake from ~ 1 to infinity.

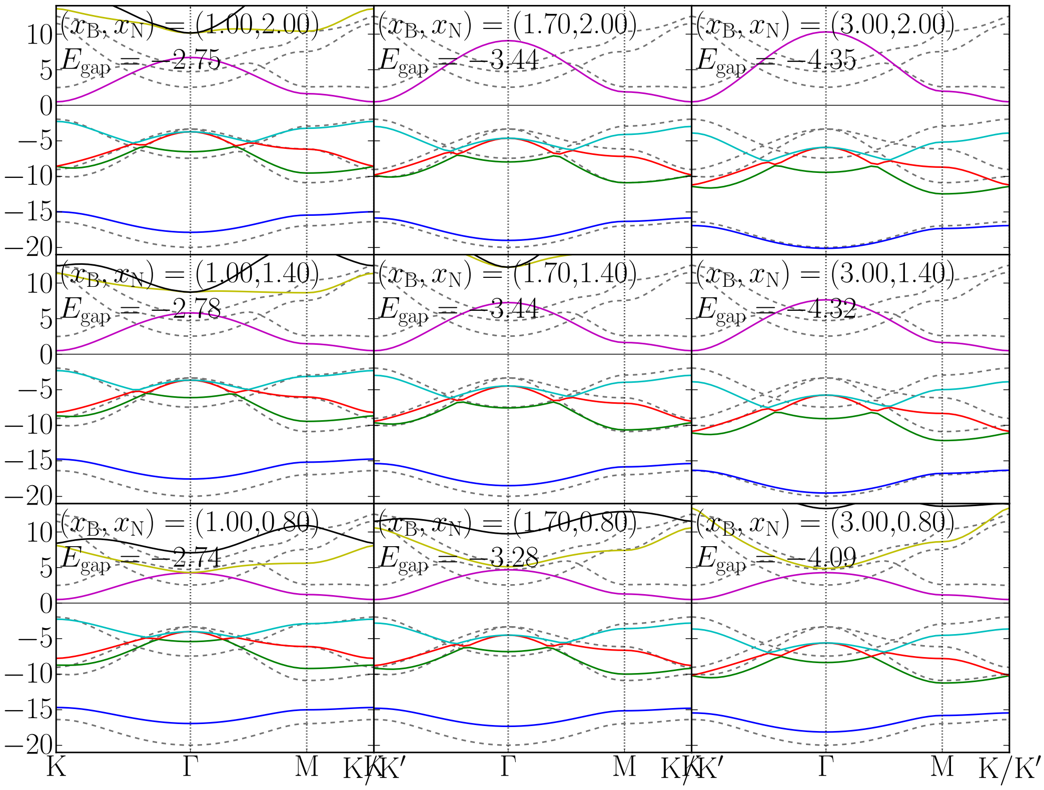

Figure 5: Band structure of the h-BN layer for several values for (x_B, x_N)—DFTB bands in solid coloured and LDA-DFT in grey dashed. There are 4 valence electron positions in the h-BN unit cells (three from B and one from N) and thus the four lowest bands are the normally occupied valence bands. In singular, valence band refers to the highest of them (the 4th band) and conduction band refers to the band above it (the 5th band).

out any value for it from a sensible range. Thus the final value for x_N is left to be decided by the quality of V_{rep}-parametrizations.

In the numerical calculation of the band structures I experimented with different settings with both DFTB and DFT (e.g. the Fermi width), but they had little influence on the results. With DFT I even tried more advanced xc-functionals than the V_{xc}^{LDA}, but the results were again similar.

6.2 Parametrization of the repulsion potentials $V_{\mathrm{rep}}(R)$

Now, for BN-parametrization B–B, N–N and B–N interactions each need their own V_{rep}-function. In order to construct them, one needs to specify the reference systems and calculate the reference forces there at first.

6.2.1 The used reference systems

The selection of possible reference systems for BB-V_{rep} is not particularly large. Aside the dimer (B_2 molecule), the other possible reference systems include at least other small boron clusters. But the eventual use of this parametrization will be in BN nanostructures where one boron atom is bonded to one other boron atom at maximum (and even then only in special cases as in the h-BN network there are only B–N interactions). Meanwhile in boron clusters there are several B–B bonds per boron atom and thus there are interactions that in a way are not represented in BN nanostructures with one B–B interaction. Of course, though, the B–B interactions in BN nanostructures are also affected by the surrounding B–N bonds. They could be taken into account at their simplest by constructing a three-atom cluster from two boron and one nitrogen atom. In such case we will have two B–N interactions and one B–B one. The effect of the B–N interactions could be taken into account by keeping them constant when changing the B–B bond length or by performing the fitting for B–N interactions first so that the BN-V_{rep} would be known.

After all, I use as reference systems for BB-V_{rep} only equilibrium and non-equilibrium dimers. With the equilibrium dimer the equilibrium bond length $R_0 = 1.59\,\text{Å}$ was used and $V'_{\mathrm{rep}}(R_0)$ was computed as described earlier. With the non-equilibrium dimer $E(\mathrm{B}_2)$ was calculated with LDA DFT with degenerated spin.

For the NN-V_{rep} I used exactly similar reference systems with same reasonings. For the equilibrium dimer the experimental bond length $R_0 = 1.0977\,\text{Å}$ [34] was employed.

Finally for the BN-V_{rep} I used firstly the non-equilibrium BN dimer similarly to the BB- and NN-V_{rep}. But instead of the equilibrium BN dimer I used as an equilibrium structure the h-BN layer. It is a very relevant structure for the BN-V_{rep} since the eventual usage of this parametrization will be in structures based on h-BN and thus it will be important to take it into account in the parametrization of the BN-V_{rep}.

6.2.2 The BB-repulsion fitting

It was immediately evident that there are going to be problems with the parametrization for the BB-V_{rep}. For instance for the initial guess ($x_{\mathrm{B}} = 1.0$) a parametrization that followed the reference force points violated each and every requirement for V_{rep} and V'_{rep} listed in Sec. 4.3.1. This is visualized in Fig. 6: the reference force points form a large S-curve and as a result a fit following the reference force points would be slightly long-ranged, $V'_{\mathrm{rep}}(R)$ would be positive around $R = 1.6\,\text{Å}$, $V'_{\mathrm{rep}}(R)$ would not grow monotonically and also $V_{\mathrm{rep}}(R)$ would not decrease monotonically. Due to this improving x_{B} was crucially important. Luckily, after some examining of different values of x_{B} it turned out that for high x_{B} a much better (although still not excellent) BB-V_{rep} can be found. The best layouts for the reference force points were found around $x_{\mathrm{B}} = 1.8$, which I eventually chose for the final value of x_{B}. This value also agrees well with the preferences set for x_{B} based on the band structure considerations.

The final BB-V_{rep} repulsion fitting with said $x_{\mathrm{B}} = 1.8$ is presented in Fig. 7. As can be seen, the major S-curve has smoothed down significantly resulting in an enormously better parametrization fitting when comparing to Fig. 6. In the fitting I have slightly factitiously cut the repulsion at $R_{\mathrm{cut}} = 2.0\,\text{Å}$ to avoid the long-rangedness of the BB-V_{rep} and to be sure that the BB-V'_{rep} is strictly monotonous. This means that for large R we in a way approximate forces that are based on the dimer reference system to zero even though they are in the range of $(1-2)\,\text{eV}/\text{Å}$, which is really not neglible. However, it must be remembered that all the reference points come from $E'_{\mathrm{DFT}}(R) - [E'_{\mathrm{BS}}(R) + E'_{\mathrm{SCC}}(R)]$ and thus include errors from $E'_{\mathrm{BS}}(R) + E'_{\mathrm{SCC}}(R)$ that naturally are notable due to the minimal basis and other approximations as well. The adjustment of x_{B} only minimizes the error from the minimal basis and some of the error is inevitably left. And this error should not be compensated with BB-V_{rep}—it would be conceptually dubious and it would not probably work anyway in practice—the fitting is based only on the dimer reference system. And now, since around $(1.8-2.0)\,\text{eV}/\text{Å}$ the strong monotonical growth of the reference points comes to its end and for larger distances the forces' values settle down to a smallish value, it implies that the short-ranged E_{rep} comes to its

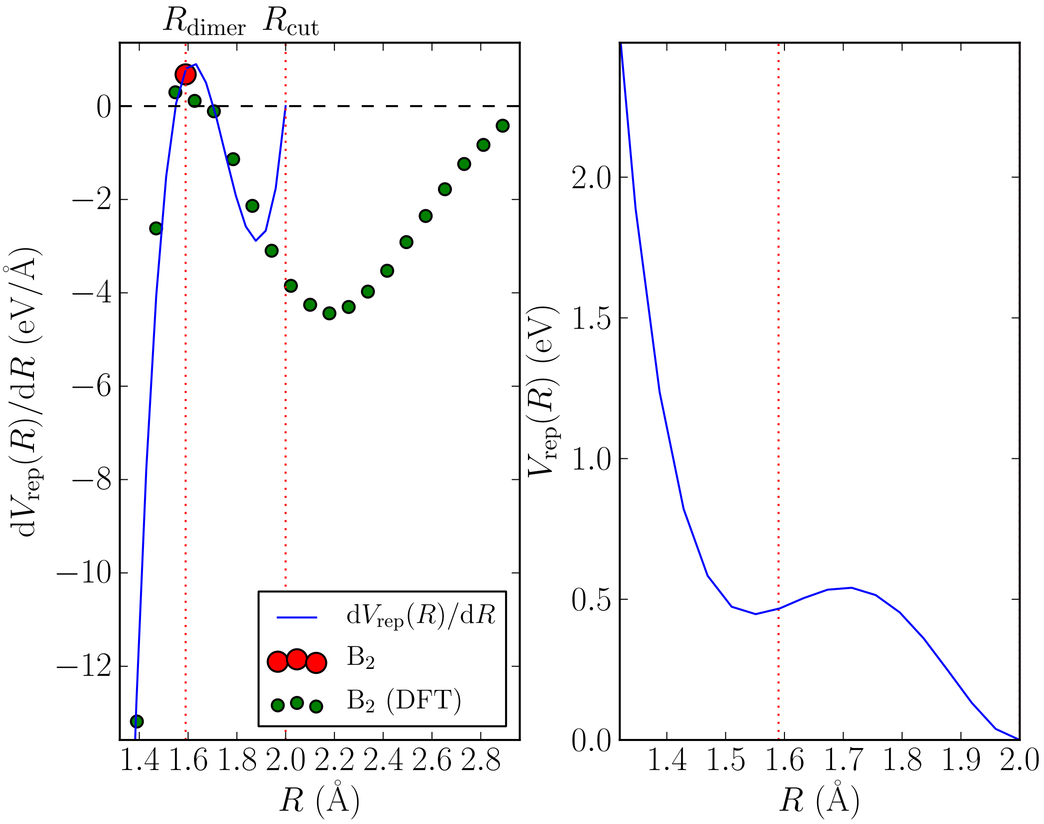

Figure 6: An unsatisfying parametrization for the B–B repulsions (with $x_{\mathrm{B}} = 1.0$—the default value). The green dots are the non-equilibrium dimer force points from LDA-DFT calculations and the red dot is the equilibrium dimer with experimental bond length.

end there and rest of the difference $E'_{\mathrm{DFT}}(R) - [E'_{\mathrm{BS}}(R) + E'_{\mathrm{SCC}}(R)]$ comes from errors in $E'_{\mathrm{BS}}(R)$ and $E'_{\mathrm{SCC}}(R)$. And thus cutting of $V_{\mathrm{rep}}(R)$ already at 2.0 Å is justified.

Otherwise the fitting process was simple. An eye-satisfying curve was easy to obtain. The fitting parameters related to the Eq. (4.7) are listed in Tab. 3.

This fitting of BB-V_{rep} provided an excellent example of the benefits of fitting to the repulsion forces instead of directly to the repulsion potential. Namely, it was difficult to find a value for the x_{B} that did not violate the preference for monotonically increasing BB-$V'_{\mathrm{rep}}(R)$.

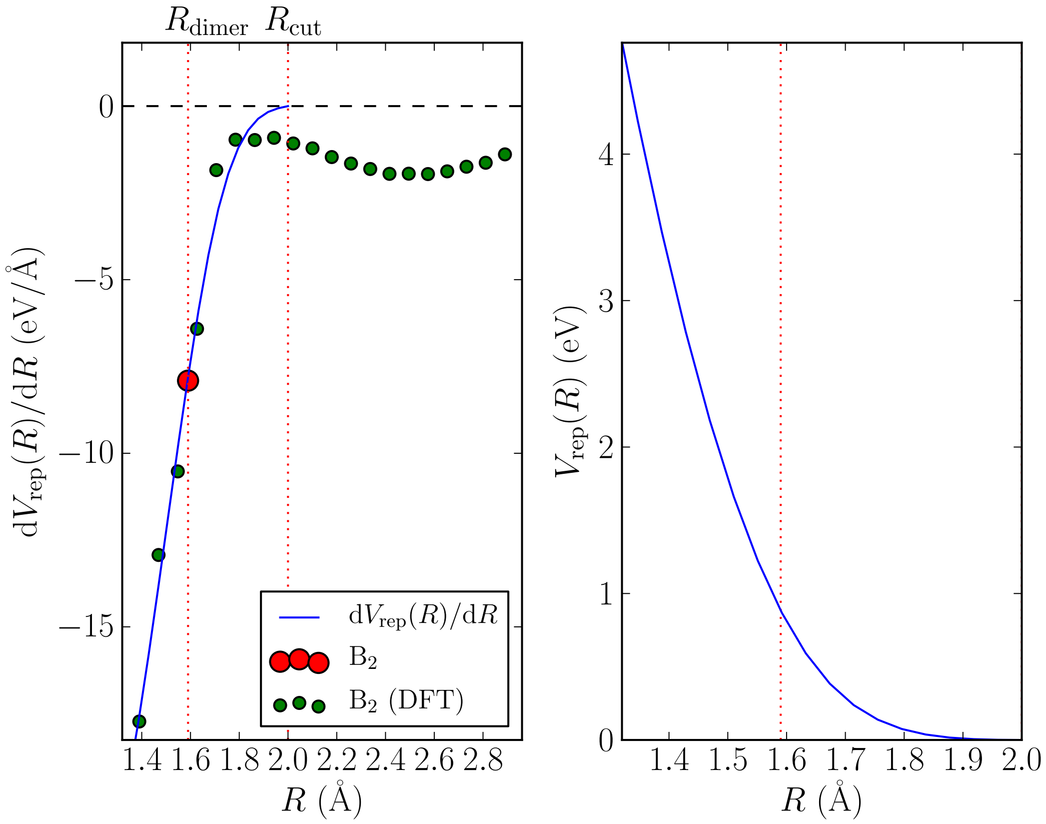

Figure 7: The final parametrization for the B–B repulsions (with $x_{\mathrm{B}} = 1.8$). Also the calculated reference force points for $R > R_{\mathrm{cut}}$ are shown in this picture, but naturally they haven't been taken into account in the fitting.

6.2.3 The NN-repulsion fitting

Unlike for BB-V_{rep}, for the NN-V_{rep} a parametrization of good quality was possible to perform practically in any case (for any x_{N}). For instance for $x_{\mathrm{N}} = 1.0$ (which I eventually chose to be the final x_{N}) and $x_{\mathrm{N}} = 2.0$ the repulsion fits are shown in Figs. 8 and 9, respectively. As can be seen, in both cases the force reference points formed a nice smooth monotonically growing curve. It also nicely approached zero for large bond lengths when $x_{\mathrm{N}} = 2.0$. For $x_{\mathrm{N}} = 1.0$ it goes slightly over zero implying a small error in E'_{BS} and E'_{SCC}. But all in all, similarly to the band structures, this consideration did not rule out any values for x_{N} and thus in the decision for its eventual value $x_{\mathrm{N}} = 1.0$ the biggest emphasis was put on its effects on the quality of the BN-V_{rep}-parametrization.

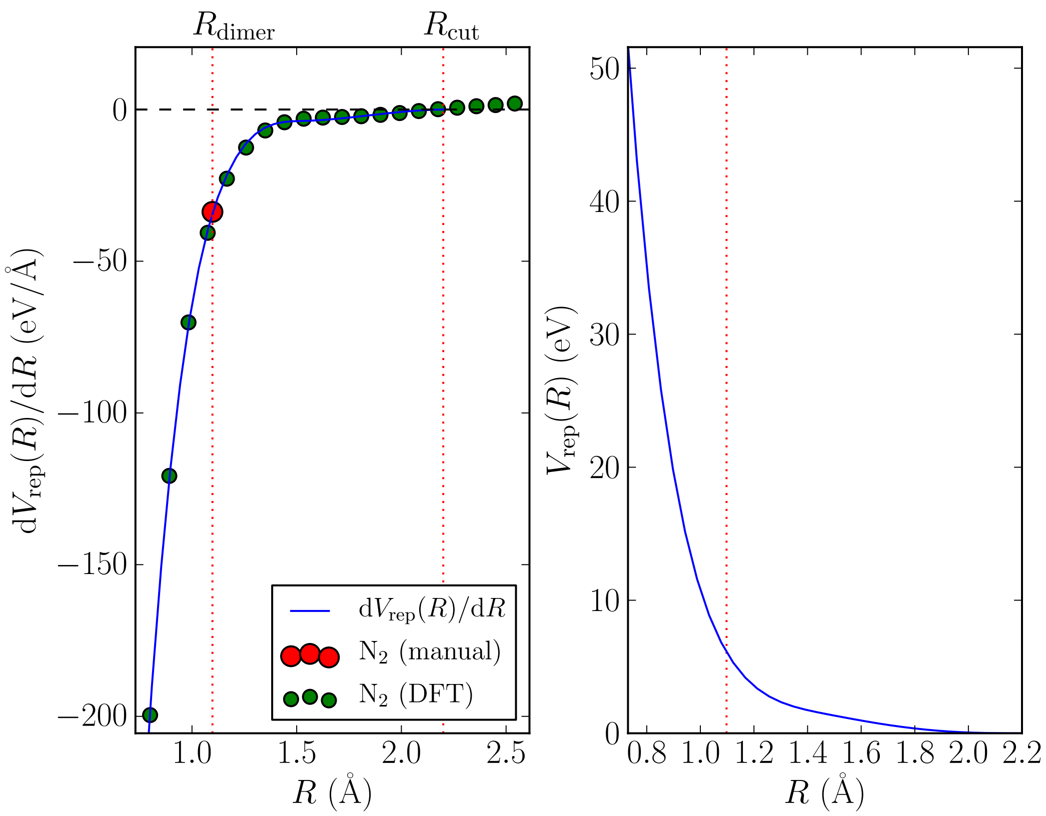

Figure 8: The final parametrization for the N–N repulsions (with $x_{\text{N}} = 1.0$—the default value).

6.2.4 The BN-repulsion fitting

In the BN-V_{rep} both x_{B} and x_{N} affect the configuration of the reference force points. But for the BB-V_{rep} $x_{\text{B}} = 1.8$ was optimal and the band-structure considerations suggested a high x_{B} as well. And meanwhile for the x_{N} hardly any preferences were found. Thus, in the parametrization of BN-V_{rep} I chose $x_{\text{B}} = 1.8$ for the initial guess and only modified x_{N}. A clear behavior stemming from x_{N} was found. Comparing the final parametrization (in Fig. 10) to a parametrization with high x_{N} (in Fig. 11—$x_{\text{N}} = 2.0$) shows that increasing x_{N} improved the error of $E'_{\text{BS}}(R) + E'_{\text{SCC}}(R)$ (based on dimers), since for large R the force reference points were closer to zero. On the other hand, decreasing x_{N} improved the alignment of the equilibrium h-BN force point with the dimer reference force points. This suggested good transferability as two different systems agreed in V'_{rep}. For the final value $x_{\text{N}} = 1.0$ these two desirable effects were compromised,

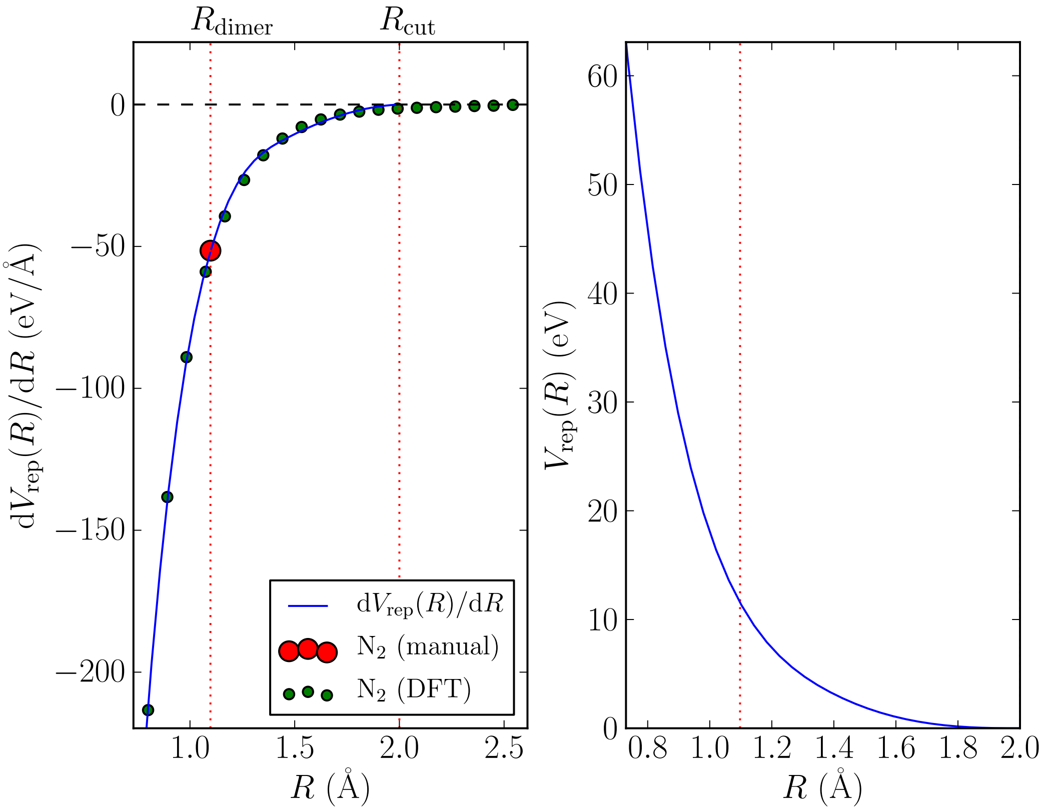

Figure 9: Another parametrization for the N–N repulsions (with $x_{\mathrm{N}} = 2.0$).

with emphasis being on the latter effect. Based on it, it might have been justifiable to choose even smaller x_{N} (0.9 or perhaps even 0.8). But based on the band structures, I also wanted to compromise between the quality of the lowest band (improved by higher x_{N}) and the quality of the conduction band (improved by smaller x_{N}) and thus this most neutral value of $x_{\mathrm{N}} = 1.0$ seemed to be the best possible choice. And also decreasing x_{N} slightly decreased the quality of NN-V_{rep} as explained in the previous section.

Now, since for $x = (1.8, 1.0)$ the fitting was reasonably satisfying, I chose not to alter x_{B} anymore. It would have led to reduced quality in BB-V_{rep}, but after all the quality of BN-V_{rep} would have been by far more important as the BN nanostructures are based on the BN bonds. Anyway, now I was luckily able to choose x_{B} so that it allowed both reasonably good BB-V_{rep} and BN-V_{rep} parametrizations.

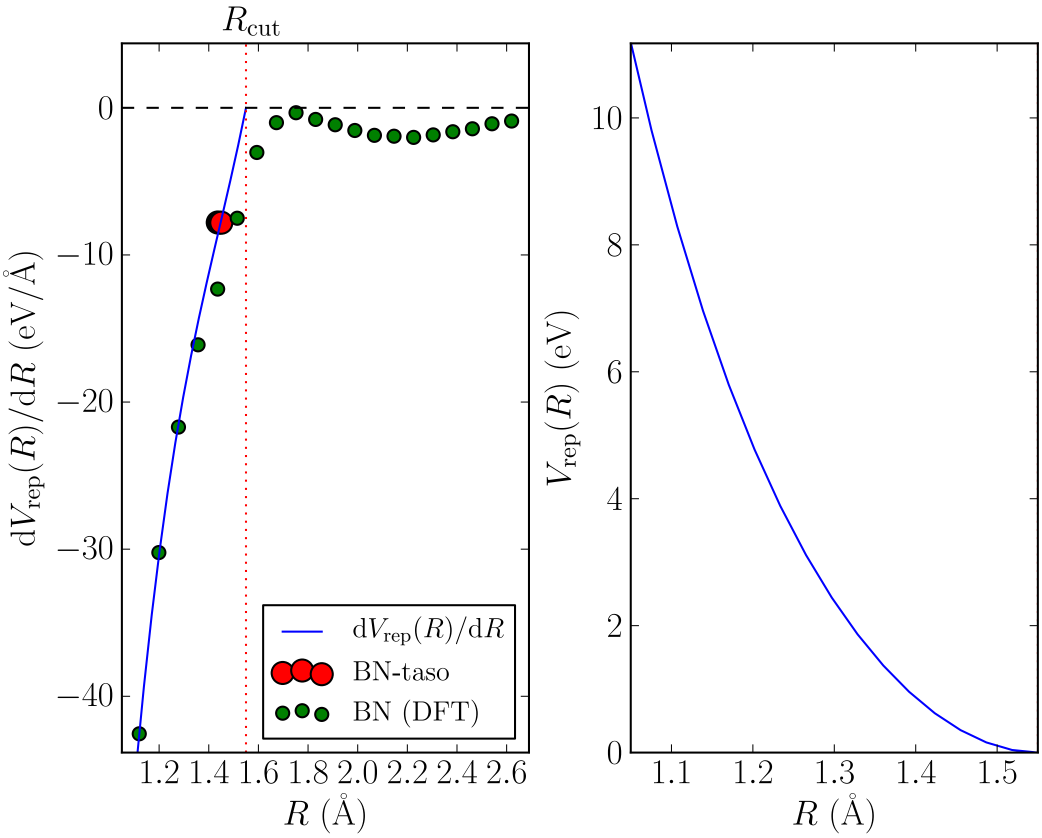

Figure 10: The final parametrization for the B–N repulsions (with $x_{\mathrm{B}} = 1.8$ and $x_{\mathrm{N}} = 2.0$).

6.3 The final parameters

To quickly sum up the parametrization I have aggregated all the parameters used to achieve my BN-parametrization in Tabs. 2 and 3.

Table 2: The final set of x-parameters. Both the erroneous and corrected values are shown. Also for r_0, which is defined by Eqs. (4.1) and (4.2), the correct value is shown both in Ångstroms and Bohrs.

	x		r_0	
	Erroneous	Real	(Å)	(Bohr)
B	1.8	0.952	1.600	3.024
N	1.0	0.529	0.751	1.420

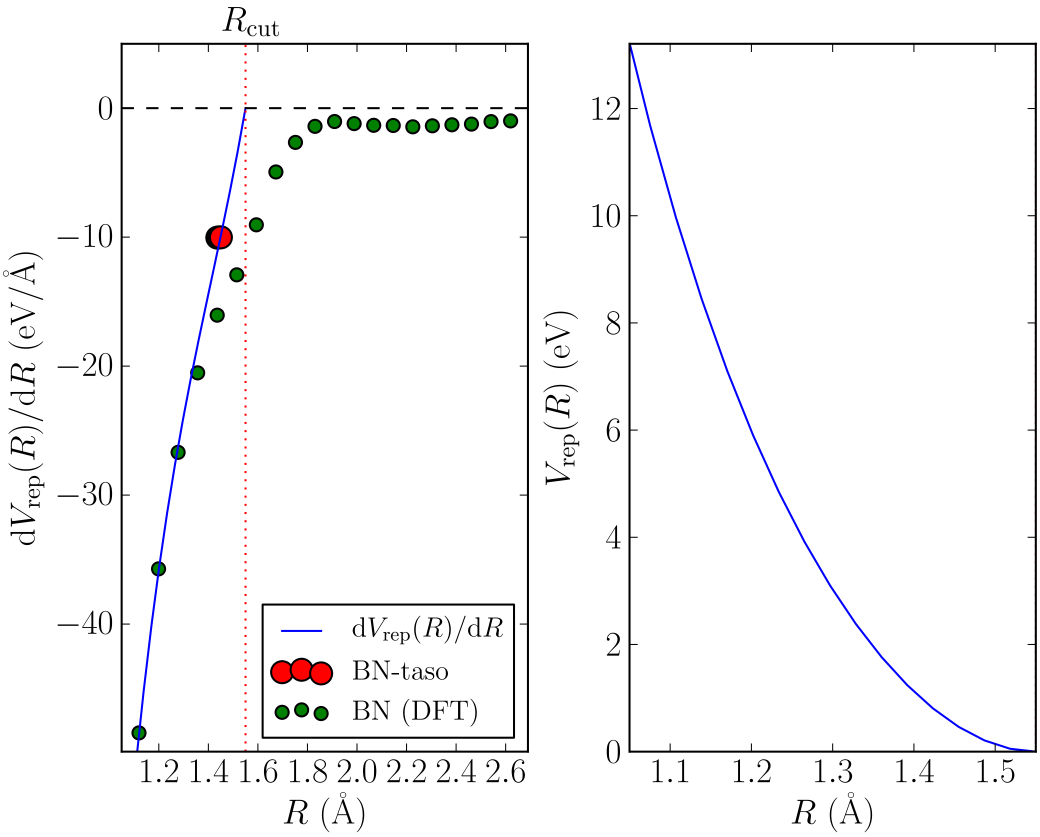

Figure 11: Another parametrization for the B–N repulsions (with $x_{\rm B} = 1.8$ and $x_{\rm N} = 2.0$).

Table 3: The final set of fitting parameters for $V_{\rm rep}$ parameter functions.

	$R_{\rm cut}$ (Å)	λ	Reference system weights σ		
			Dimer (DFT)	Dimer (Exp.)	Lattice (Exp.)
BB-$V_{\rm rep}$	2.0	0.55	1.0	1.0	
NN-$V_{\rm rep}$	2.2	3.0	2.0	1.0	
BN-$V_{\rm rep}$	1.55	40.0	1.0		2.0

6.4 Slater-Koster tables

Finally I present the Slater-Koster tables (both for S- and H^0-matrices) for $x = (1.8, 1.0)$ in Figs. 12–14. The points in these tables have range from $R = 1$ Bohr (0.53 Å) to $R = 8$ Bohr (4.23 Å) with intervals of 0.1 Bohr (0.053 Å). As it can be seen, the tables of different interactions resemble one another quite much.

The valence electrons are for both B and N in the 2nd electron shell and thus the SK tables consist of integrals between $2s$ (labeled simply as s) and $2p_i$ (labeled simply as p) orbitals. By symmetry both S and H are zero for $\tau = ss\pi$ and $ss\pi$, so there exist tables that are different from zero only for $ss\sigma$, $sp\sigma$, $pp\sigma$ and $pp\pi$.

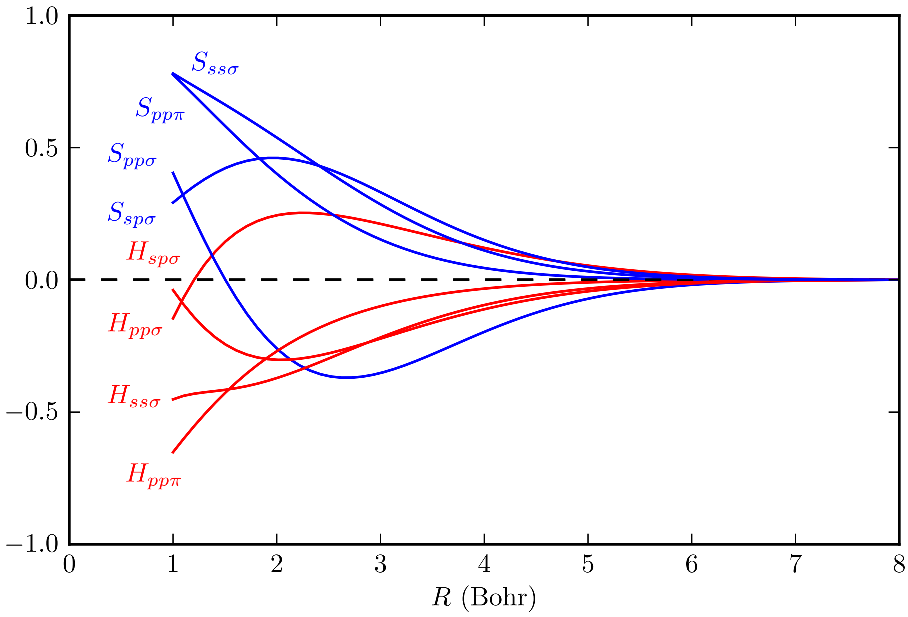

Figure 12: The Slater-Koster tables for boron–boron.

For $ss\sigma$, $pp\sigma$ and $pp\pi$ we have equality between the B–N and N–B cases due to symmetry both for S and H—if we interchange the elements in the S and H integrals (which means interchanging the radial parts), the system can be rotated in such a way that it is reduced to the original case. But with $sp\sigma$ this is naturally not possible.

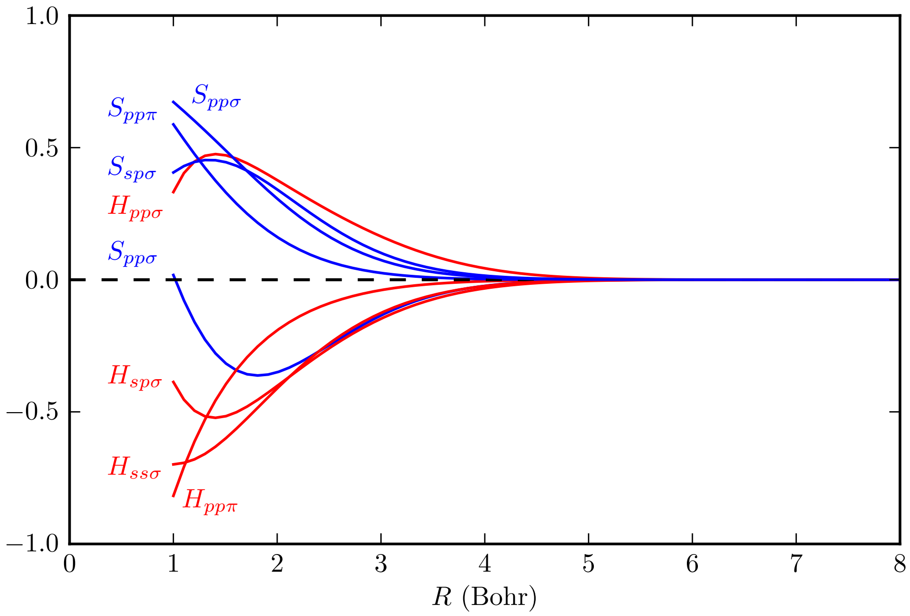

Figure 13: The Slater-Koster tables for nitrogen–nitrogen.

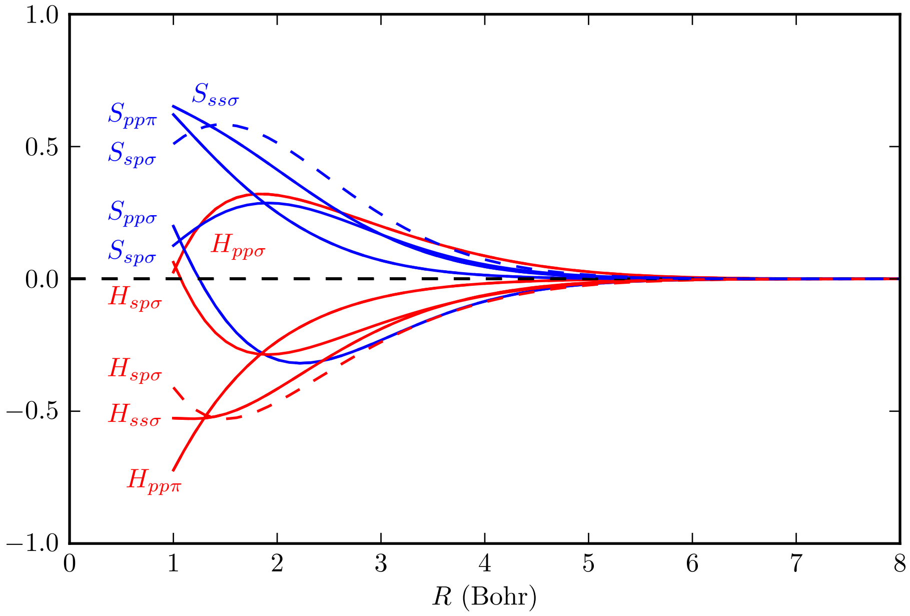

Figure 14: The Slater-Koster tables for boron–nitrogen (solid lines) and nitrogen–boron (dashed lines). If the dashed lines are missing for some N–B interaction, then this interaction equals to the corresponding B–N interaction.

7 DFTB parametrization benchmarking results

In this section I shall present the results of my DFTB computations of properties of various different BN nanostructures and benchmark those results against DFT results found from literature or calculated by me.

7.1 The band structures

7.1.1 The h-BN layer band structures

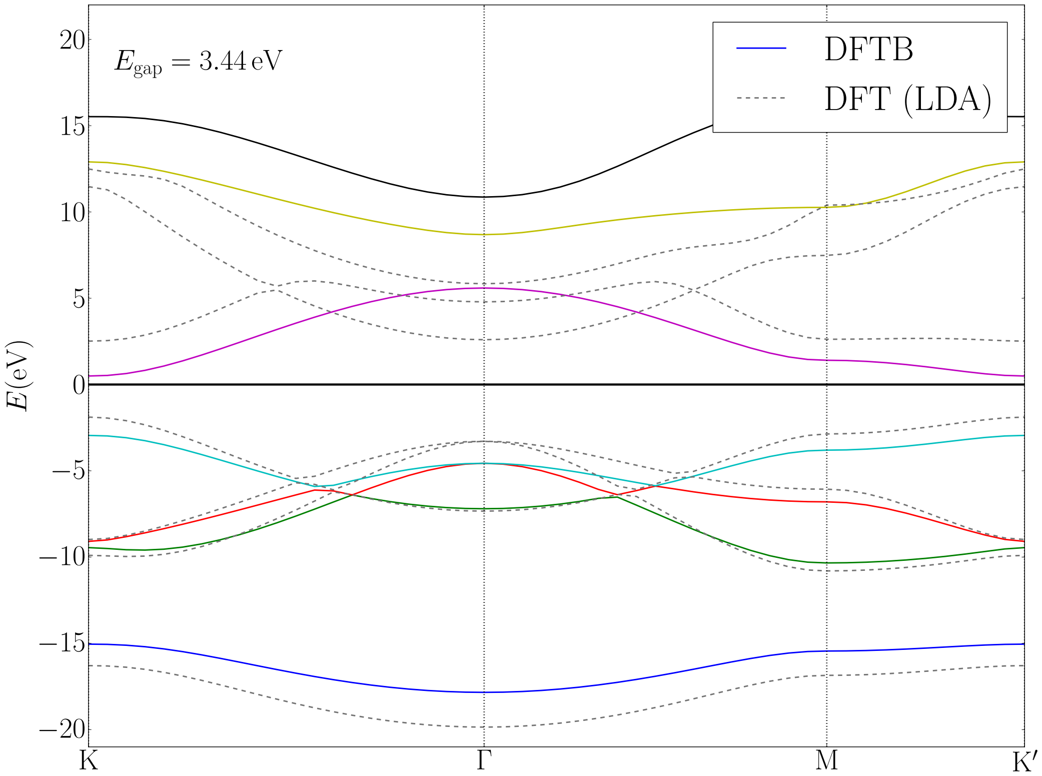

Figure 15: Band structure of the h-BN layer (the seven bottommost bands shown). Compare to Fig. 5, where the same band structures are shown for different x- and U-parameters.

The band structure of h-BN was discussed already in the parametrization section since it was used as an indicator for properly chosen U- and x-parameters. Nevertheless, I present the h-BN BS for the final x- and U-

parameters in Fig. 15. Here the same fixed lattice constant $a = 2.507$ Å has been used as before. The final obtained E_{gap} was 3.44 eV.

7.1.2 The BNNT band structures

As with the BN layer, I wanted the used nanotube structures to be fixed with geometries from references. However, constructing NT structures from reference structural parameters is not quite as trivial since the symmetry properties of zigzag and armchair nanotubes allow for them two different bond lengths r_1 and r_2 (as discussed in Sec 3.2). But I have used for simplicity the average of these two bond lengths ($\overline{r} = (r_1 + r_2)/2$) in my structures as common bond length. This makes the tubes a lot easier to construct but does not affect the band structures much. Besides, I computed the LDA-DFT data myself, so both LDA-DFT and DFTB results have been calculated in the same structures. Therefore the exact geometries of these structures are not greatly relevant. Moreover, studies with GGA-DFT by Jian-Feng Jia et al. [35] show that for armchair BNNTs $\Delta r = r_2 - r_1 \approx 0$ (see also Tab. 4) whereas for small and medium zigzag tubes Δr is relatively big (at largest it is 0.092 Å for $(3, 0)$-NT). Thus when using $\overline{r}$ with armchair BNNTs there is in practice no deviation from the correct situation. Hence I decided to calculate band structures for a set of armchair nanotubes with $\overline{r}$. The used values are listed in Tab. 4. For the Monkhorst-Pack sampling I used 20 k-points for DFTB computations, but only 10 for LDA-DFT in order to reduce the computational effort. I performed the DFT computation with GPAW code [36, 37] and used the plane wave mode with energy cutoff parameter $E_{\mathrm{cut}} = 200$ (in atomic units).

Table 4: Structural parameters of NTs used in BS computations. More explicitly this table lists amount of atoms in unit cell (N), amount of valence bands in BS (N_{v}), mean of the different bond lengths r_1 and r_2 in the NT ($\overline{r}$) and difference of these bond lengths (Δr). The values of r_1 and r_2 are taken from [35], where they also have been defined more explicitly.

NT	N	N_{v}	$\overline{r}$ (Å)	Δr (Å)
(2,2)	8	16	1.4645	0.001
(3,3)	12	24	1.4470	0.006

However, I encountered convergence problems both with DFT and DFTB computations so I ended up calculating the band structures only for few

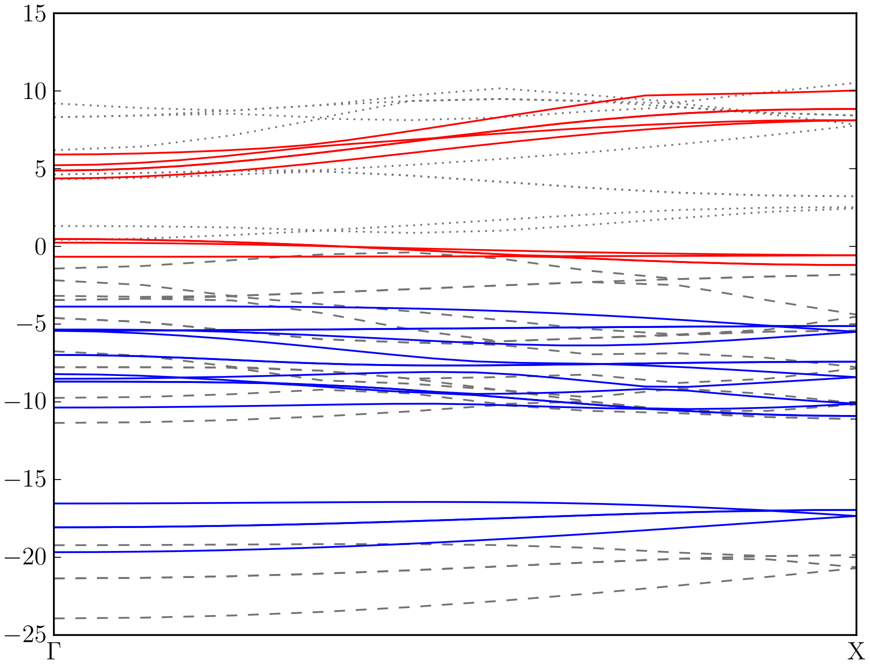

Figure 16: Band structure of (2,2) BN nanotube (25 bottommost bands shown). Blue: valence bands, red: conduction bands and grey dashed: LDA-DFT.

smallest possible armchair NTs. As a result (see Figs. 16 and 17) there is no band gap seen at all. Even though the BNNTs are typically high band gap insulators, in this extremely low and in practice perhaps unrealistic limit they seem to be (semi)conducting.

7.2 Elastic properties of the h-BN layer

I have also determined for the h-BN monolayer the most relevant elastic properties—the reduced Young's modulus Y_s as well as the Poisson's ratio σ—and compared the results to those of K. N. Kudin et al. [38]. In their paper they have used the gradient corrected PBE E_{xc}-functional.

Even though due to the hexagonal symmetry h-BN should have similar elastic properties in each direction (i.e., it should be isotropic), Kudin et al. have computed Y_s and ν in both $\hat{\mathbf{x}}$- and $\hat{\mathbf{y}}$-directions. (that is, under strain

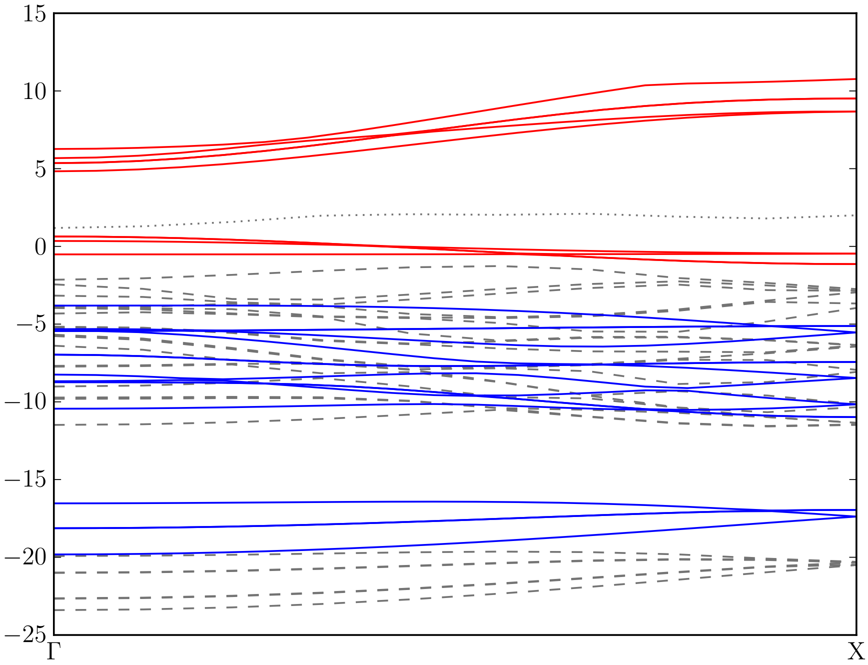

Figure 17: Band structure of (3,3) BN nanotube (25 bottommost bands shown). Blue: valence bands, red: conduction bands and grey dashed: LDA-DFT.

ϵ_x or ϵ_y, respectively). As expected, they have obtained the same results in both cases. Also I determined these quantities in both directions.

To be exact Kudin et al. have actually considered h-BN only as a limit case since their paper is actually primarily a NT study. This is why they refer to h-BN as $(\infty, 0)$ and (∞, ∞) BNNTs. In my case (for h-BN layer oriented as in Fig. 2) the former case refers to strain applied in the y-direction and the latter case refers to strain applied in the x-direction.

7.2.1 Methodology

First I created an initial symmetric h-BN monolayer unit cell with unit cell vectors (3.1–3.3) and position vectors (3.4–3.5). As the value for a I used the optimum a-value. I found it by first creating a set of unit cells with different lattice constants a and with large c (to be exact $30\,\text{Å}$) to ensure a large enough vacuum in the z-direction. Then i computed the energies of these structures. It was evident that $E(a)$ behaved quadratically (as expected based on Sec. 3.3). So I performed a quadratical fit for the energy:

$$E(a) = C_2 a^2 + C_1 a + C_0. \tag{7.1}$$

From this it was easy to deduce the optimal lattice constant a_0:

$$a_0 = -\frac{C_1}{2C_2}. \tag{7.2}$$

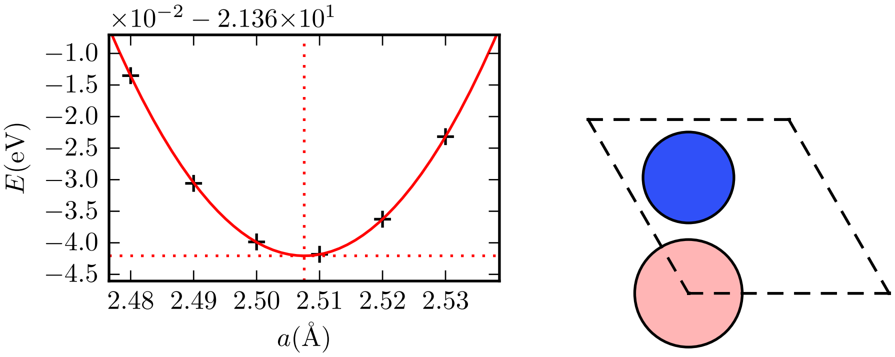

(a) The parabolic fit performed to find out the a_0. The dotted lines represent the value for the optimal lattice parameter and the energy of the unit cell for that value.

(b) The final optimal symmetric h-BN unit cell, i.e., unit cell with $a = a_0$.

Figure 18: Evaluation of the optimal symmetric unit cell (a) and the final result (b). The optimal value for the lattice constant was found to be $a = 2.508\,\text{Å}$.

This gave the result $a_0 = 2.508\,\text{Å}$.

However, there exists such an issue that optimized periodic systems[3] tend to have certain asymmetries when computed with DFTB[4]. For example

---

[3] With this I mean systems optimized with ASE's BFGS method by using HOTBIT as the calculator. The BFGS method first computes the forces acting on each atom and then manipulates their positions in an attempt to find energetically more favourable configuration, and repeats this until forces acting on the atoms are reasonably small.

[4] Or at least with HOTBIT—I am not sure what is the reason behind this. But I reckon that this might be in some way consequent of the atoms being located exactly in the edge of the unit cell—under BFGS they can move only to one direction at the edge.

for h-BN layer the perfectly symmetric configuration with lattice parameter a_0 (shown in Fig. 18b) is not the energy minimum of the system. I found that for the symmetric unit cell forces of $0.0825\,\mathrm{eV/Å}$ are found and minimizing the forces yields a configuration $36.6\,\mathrm{\mu eV}$ lower in energy. For this result I used $(20 \times 20 \times 1)$ k-points in each direction, and one might think of this being consequent from too sparse Monkhorst-Pack k-point sampling even though already this sampling is quite dense. But the results remain nearly unchanged even for exaggeratively dense k-point mesh $(100 \times 100 \times 1)$—then these numbers read $0.0823\,\mathrm{eV/Å}$ and $36.4\,\mathrm{\mu eV}$. These differences might seem negligible, but as it turns out, when the unit cell is stretched, the energy difference can grow so large that they greatly affect Y_s and ν. But it is unclear which of these ways is more “correct”. Thus I will perform the computations both in the symmetric and the BFGS-optimized case.

Now back to the computations. After making the symmetric unit cell with $a = a_0$ I chose a set of different λ_x ($\lambda_x = \epsilon_x + 1 = l_x/l_{x,0}$ is the *stretch ratio* in the x-direction) and applied them to the optimal unit cell. This kind of stretching is a source for stresses in the transverse (y) direction and they had to be relaxed. It had to be done manually[5], so for each λ_x I chose a set of λ_y and applied them to the structures stretched with λ_x. After applying the λ-tensors to the structure the lattice and position vectors were then given by

$$\mathbf{a}_1' = a\,(\lambda_x, 0, 0)\,, \tag{7.3}$$

$$\mathbf{a}_2' = a\left(-\frac{\lambda_x}{2}, \frac{\sqrt{3}\lambda_y}{2}, 0\right), \tag{7.4}$$

$$\mathbf{R}_\mathrm{B}' = a\,(0, 0, 0) \quad \text{and} \tag{7.5}$$

$$\mathbf{R}_\mathrm{N}' = a\left(0, \frac{\lambda_y}{\sqrt{3}}, 0\right). \tag{7.6}$$

Then I computed the dimensions l_x and l_y of the stretched unit cell. They are the length of the unit cell in the $\hat{\mathbf{x}}$-direction and in the $\hat{\mathbf{y}}$-direction, respectively. They are defined as

---

[5] With ASE it could in principle have been done automatically, but this feature is not (at the time of writing this work) implemented to HOTBIT. More explicitly, the stress tensors that are used in this dynamical altering of the unit cell dimensions within optimization calculation, are not supported by HOTBIT.

$$l_x = a'_{1,x} = a\lambda_x \quad \text{and} \tag{7.7}$$

$$l_y = a'_{2,y} = a\frac{\sqrt{3}\lambda_y}{2}. \tag{7.8}$$

After this I computed the energy $E(l_x, l_y)$ of each of these structures with my HOTBIT parametrization. Then I performed a parabolic fit similar to the fit in Eq. (7.1) for E as a function of l_y and for fixed l_x. From this fit I deduced similarly to Eq. (7.2) the l_y yielding the situation for which $\sigma_y = 0$. This l_y is dependent on l_x so I mark it as $l_y(l_x)|_{\sigma_y=0}$. Also $E(l_x)|_{\sigma_y=0} \equiv E(l_x, l_y|_{\sigma_y=0}))$ (i.e., the energy at this point) was given from the fitting constants by

$$E(l_x)|_{\sigma_y=0} = -\frac{C_1^2}{4C_2} + C_0. \tag{7.9}$$

I repeated this for each l_x to obtain a set of $l_y(l_x)|_{\sigma_y=0}$ as well as $E(l_x)|_{\sigma_y=0}$. Then I performed another parabolic fit for $E(l_x)|_{\sigma_y=0}$ as a function of l_x:

$$E(l_x)|_{\sigma_y=0} = P_2 l_x^2 + P_1 x + P_0. \tag{7.10}$$

From this fit I obtained $l_{x,0}$ (the equilibrium l_x) similarly to Eq. (7.2). I also made a linear fit for $l_y|_{\sigma_y=0}$ as a function of l_x:

$$l_y(l_x)|_{\sigma_y=0} = L_1 l_x + L_0. \tag{7.11}$$

From this fit I deduced $l_{y,0}$ (the value of equilibrium l_y) through

$$l_{y,0} = L_1 l_{x,0} + L_0. \tag{7.12}$$

Now by using the Eqs. (3.22), (3.25), (7.10) and (7.11) as well as the equality

$$\mathrm{d}\epsilon = \mathrm{d}l\,\frac{\mathrm{d}\epsilon}{\mathrm{d}l} = \frac{\mathrm{d}l}{l_0} \tag{7.13}$$

it was possible to compute Y_s and ν from these fits:

$$Y_\mathrm{s} = \frac{1}{l_{x,0}l_{y,0}}\frac{\mathrm{d}^2\,E(\epsilon_x)|_{\sigma_y=0}}{\mathrm{d}\epsilon_x^2} = \frac{l_{x,0}}{l_{y,0}}\frac{\mathrm{d}^2\,E(l_x)|_{\sigma_y=0}}{\mathrm{d}l_x^2} = 2\frac{l_{x,0}}{l_{y,0}}P_2 \quad \text{and} \tag{7.14}$$

$$\nu = -\frac{\mathrm{d}\epsilon_y}{\mathrm{d}\epsilon_x} = -\frac{l_{x,0}}{l_{y,0}}\frac{\mathrm{d}\;l_y(l_x)|_{\sigma_y=0}}{\mathrm{d}l_x} = -\frac{l_{x,0}}{l_{y,0}}L_1. \tag{7.15}$$

I have demonstrated all these described steps for both symmetric and BFGS-optimized cases in Fig. 19. As it is seen, there are significant systematic differences between these two cases—for $l_{x,0}$ and $l_{y,0}$ are different in both of these cases. This is also the reason why I did not use values of Eqs. (7.7) and (7.8) with $\lambda_x = \lambda_y = 0$ for $l_{x,0}$ and $l_{y,0}$.

I also repeated this process in the reverse case, i.e., with ŷ-direction as the axial direction and x̂-direction as the transverse direction.

This methodology allowed the computation of Y_s and ν in a quite straightforward and conceptually simple way (i.e., in low level of theory without the need to consider the explicit form of the 4th rank elasticity tensor).

The reference study by Kudin et al. employed 64 k-points along the shorter translational vector of their four-atom unit cell and proportionally smaller number along the longer vector. They relaxed the structures until the forces acting on ions were $0.0005\,\mathrm{eV\,Å^{-1}}$ at maximum.

In my calculations I employed 40 different k-points in both directions. In the BFGS optimizations the maximum force per ion that I allowed was $0.01\,\mathrm{eV\,Å^{-1}}$. So my computations were not in this sense as accurate as the reference study computations, but according to my testings they should be more than sufficient (i.e., increasing accuracy here would not change the results in practice). I could probably have performed these computations with equal values with the reference study though because the calculations were quite rapid.

Finally I also carried out several tests to ensure that the symmetric unit

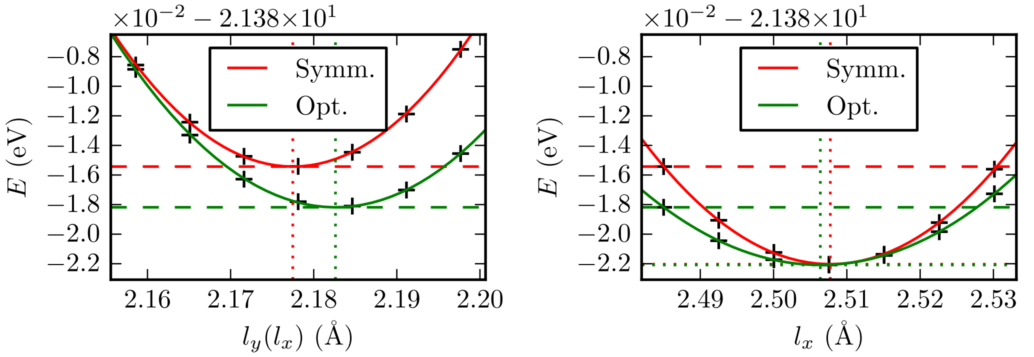

(a) An example fit for $E(l_y)|_{l_x}$, i.e., DFTB energy as a function of l_y for a fixed l_x (here $l_x \approx 2.485$ Å). The coordinates $l_y(l_x)|_{\sigma_y=0}$ and $E(l_x)|_{\sigma_y=0}$ of the minimum of the parabola are also pictured as dashed lines and they represent the situation strainless in the y-direction.

(b) Quadratical fits for $E(l_x)|_{\sigma_y=0}$. The leftmost fitting point ($l_x \approx 2.485$ Å) is from the fit shown in (a) and rest of the points are from similar fits. Also $l_{x,0}$ and $E(l_{x,0})$ are pictured with dashed lines.

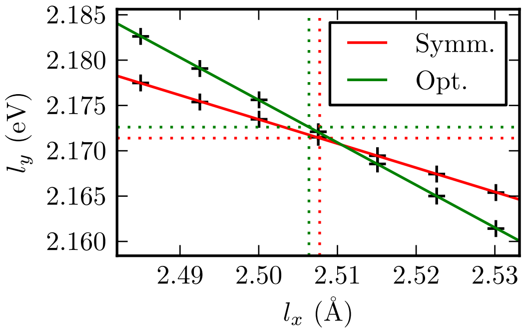

(c) Linear fit for $l_y|_{\sigma_y=0}$ as a function of l_x. The leftmost fitting points (again for $l_x \approx 2.485$ Å) are obtained from the fit shown in (a) and the rest of the points are from similar fits. Also $l_{x,0}$ and $l_{x,0}$ are pictured with dashed lines. The values for $l_{x,0}$ are from the fit shown in (b).

Figure 19: The fitting process to compute Y_s and ν of h-BN layer in the $\hat{x}$-direction. These quantities are obtained from fits in Figs 19b and 19c, respectively. In the graphs there are pictured both the case with geometrically symmetric unit cell and the case where the (erroneous) forces in this unit cell have been relaxed with the BFGS optimization method leading to asymmetric configuration.

cells I studied truly were symmetric. For example I checked for each structure that the following symmetry properties hold (see Fig. 2 for notation):

$$
\begin{aligned}
|\mathbf{R}_{\mathrm{N}}(0,0) - \mathbf{R}_{\mathrm{B}}(0,1)| &= |\mathbf{R}_{\mathrm{N}}(0,0) - \mathbf{R}_{\mathrm{B}}(1,1)|\,, \\
|\mathbf{R}_{\mathrm{B}}(0,0) - \mathbf{R}_{\mathrm{N}}(0,-1)| &= |\mathbf{R}_{\mathrm{B}}(0,0) - \mathbf{R}_{\mathrm{N}}(-1,-1)|\,.
\end{aligned}
$$

7.2.2 Obtained results

The results for the studied elastic constants are presented in Tab. 5. The difference between the symmetric and the BFGS-optimized case is bafflingly clear. Interestingly in the BFGS-optimized case Y_{s} is reasonably close to the reference result but ν definitely is not, whereas for the symmetric case the situation reverses.

Table 5: DFTB and reference DFT Y_{s} and ν for h-BN layer. As h-BN is strictly not isotropic Strain in both x and y directions is

Strain direction	Y_{s}(TPa nm)			ν		
	DFTB	DFT [38]	Err. (%)	DFTB	DFT [38]	Err. (%)
x̂ (BFGS)	315	271	16	0.541	0.211	156
ŷ (BFGS)	315	271	16	0.540	0.211	156
x̂ (symm.)	473	271	75	0.308	0.211	46
ŷ (symm.)	477	271	76	0.310	0.211	47

7.3 Properties of the BN nanotubes

Here I have computed various mechanical properties for a group of zigzag and armchair BNNTs and benchmarked them against DFT calculations by B. Baumeier et al. from their 2007 paper [39]. Firstly, what comes to geometry of the tubes, I have computed the diameter d and the *radial buckling constant* β of the tubes. The radius is defined in the reference study as

$$
r = \frac{1}{2}\left(r_{\mathrm{B}} + r_{\mathrm{N}}\right), \tag{7.16}
$$

where d_B and d_N are the diameters of the boron and nitrogen cylinders, respectively.[6] The radial buckling constant is defined as the difference of the radii of these cylinders:

$$\beta = r_\mathrm{N} - r_\mathrm{B}. \tag{7.17}$$

Secondly I computed some elastic properties, namely the reduced Young's modulus Y_s and the *elastic strain energy per atom* e_s, which is defined as

$$e_\mathrm{s} = \frac{1}{N} E(\mathrm{BNNT}) - \frac{1}{2} E(\mathrm{BN}_\mathrm{cell}). \tag{7.18}$$

To put it simply, it is the energy per atom required to roll a h-BN sheet into tubular form.

7.3.1 Methodology

In my computations I proceeded similarly to the methodology of the previous section—first I created an initial guess for the equilibrium structure for every tube type studied and then scaled them in the z-direction with different scales and relaxed them by again employing the ASE's BFGS method. This yielded for each studied tube type a total of 16 structures with slightly different unit cell lengths l in the z-direction. Then I determined the average radii r_B and r_N of each of these structures. The used method for this was to first calculate the location of the tube axis $(\overline{x}, \overline{y})$ by averaging the x and y-coordinates of all the nuclei (both B and N) in the unit cell. After this $\overline{r}_\mathrm{B}$ and $\overline{r}_\mathrm{N}$ were given as the arithmetic means of distances of the B and N atoms from this axis, respectively.

Since in this case there were periodic boundary conditions only in the direction of the axial strain, the shear stresses did not affect the unit cell dimensions as in the previous case and computations were in that sense much more simple. I only had to perform one parabolic fit for $E(l)$, and

---

[6] As already discussed in Sec. 3.2, in zigzag and armchair BNNTs the B and N atoms lay in their own cylinder levels with slightly different radii.

one linear fit for $r(l)$. These fits then yielded the equilibrium unit cell length l_0 and energy $E_0 = E(l_0)$ and the equilibrium tube radius $r_0 = r(l_0)$. After this Y_s and ν were obtained from Eqs. (3.23) and (3.25) through

$$Y_\mathrm{s} = \frac{1}{2\pi r_0 l_0} \frac{\mathrm{d}^2 E(\epsilon_z)|_{\sigma_\perp = 0}}{\mathrm{d}\epsilon_z^2} = \frac{l_0}{2\pi r_0} \frac{\mathrm{d}^2 E(l)|_{\sigma_\perp = 0}}{\mathrm{d}l_x^2} = \frac{l_0}{\pi r_0} P_2 \quad \text{and} \tag{7.19}$$

$$\nu = -\frac{\mathrm{d}\epsilon_\perp}{\mathrm{d}\epsilon_z} = -\frac{l_0}{r_0} \frac{\mathrm{d}\, r(l)|_{\sigma_\perp = 0}}{\mathrm{d}l} = -\frac{l_0}{r_0} L_1, \tag{7.20}$$

where P_2 and L_1 are similar fitting constants as in the previous section.

In the Brillouin zone integrations I used 20 k-points in the $\hat{\mathbf{z}}$-direction. This should be a sufficient amount for unit cell lengths of $\sim 4.3\,\text{Å}$ (for zigzag) and $\sim 2.5\,\text{Å}$ (for armchair). The BFGS process was continued until all the forces were under $0.01\,\mathrm{eV/Å}$.

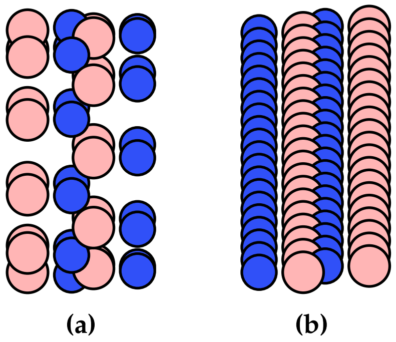

Figure 20: The structures used for the computation of elastic strain energy: (a) is a BFGS-optimized BNNT and (b) is a BFGS-optimized h-BN layer supercell obtained by repeating the minimal h-BN layer unit cell 20×2 times. It tries to replicate unfold BNNTs as well as possible.

Due to the issue related to energy differences between symmetric and optimized periodic structures that was discussed on page 80, when Eq. (7.18) is used for computing the elastic strain energy, both energy of the BNNT and the h-BN layer should be coming from BFGS-optimized structures. But it turned out that it is not enough. If the minimal BFGS-optimized h-BN unit cell was used, even negative E_s was obtained for the largest BNNT. The reason for this is that there also are some scaling issues with periodic structures.[7] Hence the comparison of the BNNT and the h-BN layer should be done also for structures of similar size. Moreover, the same amount of k-points should be used in calculations for them. I have used for the BN layer a supercell that has been obtained by repeating the minimal unit cell 20×2 times (see Fig. 20b). As the result it has equal width to the BNNT. Its long length is to mimic the unwrapped BNNT. I also used only one k-point in that direction, since it makes it effectively one-dimensional, as the BNNT is. In the width direction I used an equal amount of k-points (20).

7.3.2 Obtained results

The obtained results as well as the reference values are presented in Tab. 6 (the geometric properties) and Tab. 7 (the elastic properties). Moreover, Tab. 8 features the DFTB results for the Poisson's ratio. Firstly, the diameters are in very good agreement with the DFT results but the buckling constants not so much. This error for β is not so alarming because just a small deviation in $r_{\mathrm{B}}/r_{\mathrm{N}}$ leads to big relative error in β. In my opinion it is actually well done for DFTB to predict the correct buckling behavior, i.e., $r_{\mathrm{N}} > r_{\mathrm{B}}$ instead of $r_{\mathrm{N}} < r_{\mathrm{B}}$.

What comes to the Young's moduli, they are in accordance with Y_{s} of the BN layer in the BFGS-optimized case (see Tab. 5), i.e., $315\,\mathrm{TPa\,nm}$. Namely, when the diameter of the tubi is increased and the elastic strain energy decreases, $Y_{\mathrm{s}}(\mathrm{BNNT}) \rightarrow Y_{\mathrm{s}}(\mathrm{BN\ layer})$. To be exact, for $(15, 15)$ BNNT Y_{s} is actually already $6\,\mathrm{TPa\,nm}$ larger than $Y_{\mathrm{s}}(\mathrm{BN\ layer})$, which is unphysical result. But since the difference is only $6\,\mathrm{TPa\,nm}$, this is a minor glitch and probably due to numerical errors, and is not worrisome. Also for $(15, 15)$ BNNT $Y_{\mathrm{s}}(\mathrm{BNNT})$ the DFT reference result is $8\,\mathrm{TPa\,nm}$ larger than the DFT reference result for $Y_{\mathrm{s}}(\mathrm{BNNT})$. The errors to the DFT results are of the same order as in the case BN layer. But what is perplexing, is that whereas the reference study found that Y_{s} approximately only depends on d, my DFTB computations also found notable chirality-dependence. More explicitly for armchair BNNTs I obtained $(15 - 30)$TPa nm larger results than for

---

[7] When unit cells of periodic structures are repeated say, (n_x, n_y, n_z) times, energy of the system should scale accordingly (i.e., become $n_x n_y n_z$-fold). However, with DFTB/HOTBIT there is some issue causing this not to be exactly the case, and according to my tests this problem occurs even with dense k-point samplings. Thus, if the energies of different periodic structures are compared, they should be of the same size. Otherwise the comparison might lead to significant errors.

Table 6: Diameter d and radial buckling parameter β of various BNNTs. Both DFTB results and DFT reference values are presented and compared to each others.

(N, M)	d(Å)			β(Å)		
	DFTB	DFT [39]	Err. (%)	DFTB	DFT [39]	Err. (%)
$(4, 0)$	3.38	3.35	0.9	0.205	0.149	38
$(5, 0)$	4.13	4.08	1.3	0.168	0.122	38
$(6, 0)$	4.91	4.83	1.6	0.140	0.101	38
$(7, 0)$	5.69	5.60	1.5	0.120	0.085	42
$(8, 0)$	6.47	6.37	1.6	0.105	0.073	44
$(9, 0)$	7.26	7.15	1.5	0.094	0.064	46
$(10, 0)$	8.05	7.99	0.7	0.084	0.057	47
$(15, 0)$	12.02	11.85	1.4	0.055	0.037	50
$(4, 4)$	5.61	5.49	2.3	0.122	0.089	37
$(5, 5)$	6.98	6.87	1.6	0.096	0.068	42
$(6, 6)$	8.35	8.23	1.5	0.080	0.055	46
$(7, 7)$	9.73	9.59	1.5	0.069	0.046	49
$(8, 8)$	11.11	10.95	1.4	0.060	0.040	50
$(9, 9)$	12.49	12.31	1.4	0.053	0.036	47
$(10, 10)$	13.86	13.67	1.4	0.048	0.032	49
$(15, 15)$	20.77	20.48	1.4	0.032	0.022	43

zigzag BNNTs with equal diameter. This is illustrated in Fig. 21.

It is noteworthy that also Kudin et al. [38] have studied Y_s of some same BNNTs as Baumeier et al. [39]. They obtained for $(7, 0)$ BNNT $255\,\mathrm{TPa\,nm}$, for $(4, 4)$ BNNT $258\,\mathrm{TPa\,nm}$ and for $(7, 7)$ BNNT $267\,\mathrm{TPa\,nm}$.[8] These values are $3.0\,\%$, $3.7\,\%$ and $2.9\,\%$ smaller than those in [38], respectively. This means that these two DFT studies are in reasonably good agreement with each other and hence it was sensible to compare $Y_\mathrm{s}(\mathrm{BN\ layer})$ to [38] and $Y_\mathrm{s}(\mathrm{BNNT})$ to [39].

My DFTB parametrization clearly underestimates the elastic strain energy values for each BNNT studied. This is most likely partly related to the discussed vaguenesses of E_DFTB when unlike structures are compared. This

---

[8] In their paper there are some minor glitches concerning units and definition of Y_s, but they also have reported $\mathrm{d}^2E/\mathrm{d}\epsilon^2$ as well as all the other quantities needed to deduce Y_s, which allowed me to recalculate their Y_s and verify that I was reading their tables correctly.

Table 7: Young's modulus and strain energy per atom e_s of various BNNTs. Both DFTB results and DFT reference values are presented and compared to each others.

(N, M)	Y_s(TPa nm)			e_s(eV)		
	DFTB	DFT [39]	Err. (%)	DFTB	DFT [39]	Err. (%)
$(4, 0)$	230	227	1.1	0.356	0.479	−25.7
$(5, 0)$	251	246	2.0	0.228	0.301	−24.4
$(6, 0)$	266	259	2.9	0.157	0.218	−27.8
$(7, 0)$	275	263	4.5	0.115	0.171	−32.9
$(8, 0)$	282	267	5.6	0.087	0.140	−38.0
$(9, 0)$	288	269	6.9	0.068	0.118	−42.7
$(10, 0)$	293	273	7.4	0.054	0.102	−47.0
$(15, 0)$	304	278	9.3	0.023	0.063	−64.1
$(4, 4)$	304	268	13.6	0.118	0.168	−29.7
$(5, 5)$	309	272	13.5	0.077	0.123	−37.7
$(6, 6)$	312	274	14.0	0.054	0.096	−43.3
$(7, 7)$	315	275	14.6	0.041	0.080	−48.3
$(8, 8)$	317	276	15.0	0.033	0.069	−52.0
$(9, 9)$	319	277	15.2	0.028	0.061	−54.7
$(10, 10)$	315	278	13.4	0.024	0.055	−56.9
$(15, 15)$	321	279	14.9	0.015	0.041	−63.7

Table 8: Poisson's ratio ν of various BNNTs. Only DFTB results are presented.

(N, M)	ν	(N, M)	ν
$(4, 0)$	0.09	$(4, 4)$	0.14
$(5, 0)$	0.11	$(5, 5)$	0.17
$(6, 0)$	0.13	$(6, 6)$	0.21
$(7, 0)$	0.15	$(7, 7)$	0.25
$(8, 0)$	0.17	$(8, 8)$	0.28
$(9, 0)$	0.19	$(9, 9)$	0.32
$(10, 0)$	0.21	$(10, 10)$	0.36
$(15, 0)$	0.31	$(15, 15)$	0.54

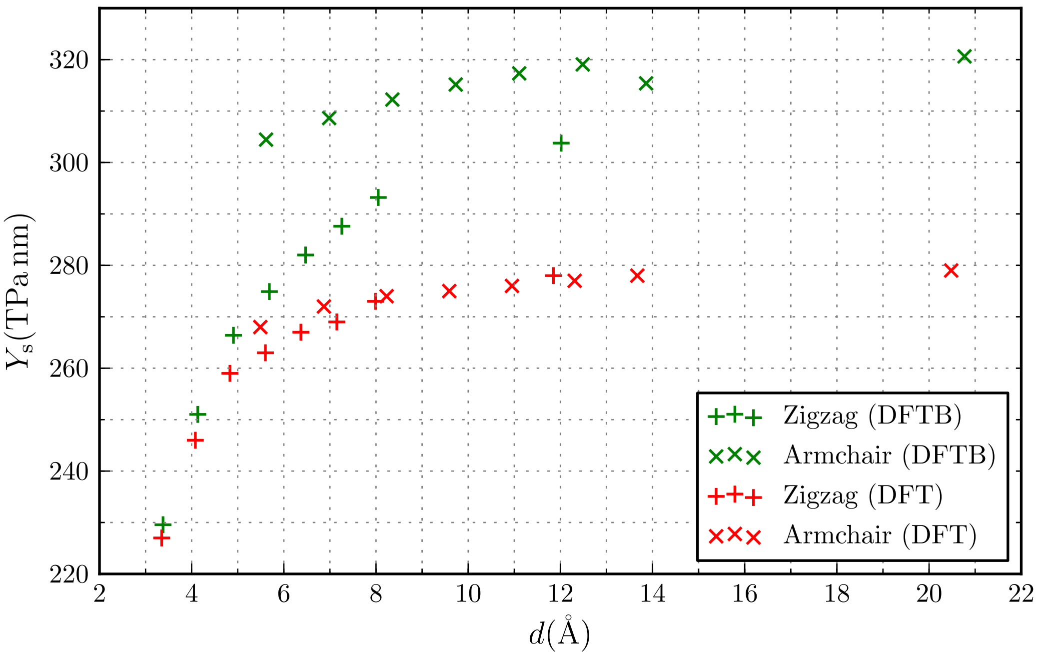

Figure 21: Relationship between Y_s and d for BNNTs for both DFTB and DFT reference [39] results.

time energies of BNNTs were compared to energy of a BN layer and they are inevitably quite a different type of structures even though I tried to mimic the BNNTs as well as possible with my BN layer.

Lastly, according to my results, ν is very small for small BNNTs, but for large BNNTs it seems to approach the overly big value obtained for h-BN in the BFGS-optimized case. Baumeier et al. have not studied ν, but Kudin et al. have. Their results for ν were 0.244 for $(7,0)$ BNNT, 0.217 for $(4,4)$ BNNT and 0.213 for $(7,7)$ BNNT. Differences of my results to these are $-38\,\%$, $-37\,\%$ and $15\,\%$, respectively. They also studied the $(12,0)$ BNNT and obtained $\nu = 0.226$ for it, and it can be deduced by interpolating that error of my results are $\sim 0\,\%$. So it seems that whereas in Ref. [38] the Poisson's ratio was found to be approximately constant, I found strong diameter dependence and obtained way too small (large) values for small (large) BNNTs.

Also another SCC-DFTB study about this precise subject exists. In their 1998 paper Hernández et al. [40] have computed d, β, Y_s, e_s and ν for various BNNTs. Interestingly, all of their results are close to the DFT results. Only their diameter values were slightly worse than mine. Performance of their BN parametrization regarding β, e_s and ν is quite staggering considering all the troubles my parametrization had with them.

7.4 Vacancy defects on a h-BN layer

Defects, where there is an atom or a small atom cluster missing, are known as *vacancy defects*. Next I will study their *formation energies* E_form on a h-BN layer under strain. For the reference paper I have chosen a study by Kuzubov et al. [41], where formation energies of vacancies in h-BN have been calculated with PBE-DFT. The considered vacancies include single boron and nitrogen vacancies ($\mathrm{V_B}$ and $\mathrm{V_N}$, respectively) as well as double vacancies ($\mathrm{V_{BN}}$). In these defects also the *chemical potential* $\mu(\mathrm{X})$ of the separated atom(s) X needs to be taken into account. This potential depends on the chemical environment into which X is to detach. Therefore the formation energy $E_\mathrm{form}(\mathrm{X})$ reads as follows:

$$E_\mathrm{form}\left(\mathrm{X}\right) = E\left(\mathrm{X}\right) - E_0 + \mu(\mathrm{X}), \tag{7.21}$$

where $E\left(\mathrm{X}\right)$ is the energy of the structure with atom(s) X and E_0 is the energy of the original undefected structure. As used in [41], the chemical potentials for $\mathrm{V_B}$, $\mathrm{V_N}$ and $\mathrm{V_{BN}}$ are

$$\begin{aligned} \mu\left(\mathrm{B}\right) &= E(\mathrm{BN_{cell}}) - \frac{1}{2}E(\mathrm{N_2}), && (7.22)\\ \mu\left(\mathrm{N}\right) &= E(\mathrm{BN_{cell}}) - \frac{1}{12}E(\mathrm{B_{12}}) \quad \text{and} && (7.23)\\ \mu\left(\mathrm{B}+\mathrm{N}\right) &= E(\mathrm{BN_{cell}}), && (7.24) \end{aligned}$$

respectively. Above $\mathrm{BN_{cell}}$ is the two atom unit cell of a h-BN layer unit cell (as in Fig. 2), $\mathrm{N_2}$ is the nitrogen molecule and $\mathrm{B_{12}}$ is a boron cluster that according to the reference paper is the most stable boron phase.

The above chemical potential definitions are not fully clear to me, but I suppose that the reasonings behind these potentials are as follows: since $\mu\left(\mathrm{B}+\mathrm{N}\right) = E(\mathrm{BN_{cell}})$, it is thought that the separated BN-pair joins the edge of another BN layer and for example forming a BN dimer molecule is not an option. So the chemical environment of the BN layer is thought to be full of other BN layers, perhaps they all are in some solution. Next, $\mu\,(\mathrm{B}) = E(\mathrm{BN}_{\mathrm{cell}}) - E(\mathrm{N}_2)/2$ implies that when two boron atoms eject from the system, they share two nitrogens from a N_2 molecule and then join another BN layer. So it is thought that the environment in this case is rich in both N_2 molecules and BN layers. Similarly to the case of $\mu\,(\mathrm{N})$ it is thought that the environment is rich in both B_{12} molecules and BN layers. If I am correct, all these definitions do represent different situations. But perhaps the idea behind this is that in an N-rich environment N-vacancies do not occur and that in a B-rich environment B-vacancies do not occur.

7.4.1 Methodology

The standard procedure in modelling defects in periodic structures is to construct periodic *supercells* by repeating unit cells in the periodicity directions, and this is what has been done also in the reference study. This kind of handling is a source for defect-defect interactions, that are unwanted at least if the goal is to compute the formation energies of single defects, as in this case. But the cure is to make the supercells large enough so that the defect-defect interactions die off. The very large 100-atom supercell used by Kuzubov et al. is surely large enough to achieve this. Actually 2D structures of such size are so large, that optimizing them with BFGS is quite heavy even with DFTB. Thus to find a sufficiently large supercell I computed in a test case the convergence of the formation energy as a function of supercell size In this test case the minimal unit cell was repeated $N_{\mathrm{uc}} \times N_{\mathrm{uc}} \times 1$ times along each direction. This way the largest possible minimum distance between periodic defect images for constant defect density was obtained—but for the peculiar supercell used in the reference study this is not the case due to its rectangular shape with unequal side lengths. Thus in my case convergence should occur for smaller supercell size (for smaller N_{uc}).

I chose to study this convergence for V_{BN} because it is the most severely defected vacancy studied, and hence its $E_{\mathrm{form}}(N_{\mathrm{uc}})$ probably converges more slowly than those of V_{B} and V_{N}. Actually I studied only $\Delta E(\mathrm{V}_{\mathrm{BN}}) = E_0 - E(\mathrm{V}_{\mathrm{BN}})$, i.e., I left the chemical potential $\mu(\mathrm{V}_{\mathrm{BN}})$ out (it is not relevant for the convergence). I also made a big simplification by *not* optimizing either of the structures with BFGS. This means that E_0 is energy of $N_{\mathrm{uc}} \times N_{\mathrm{uc}} \times 1$ repeated minimal, symmetric, unstrained unit cell (see Fig. 23a) and $E_{\mathrm{form}}(\mathrm{V_{BN}})$ is energy of a structure simply with adjacent B and N atoms deleted (see Fig. 23d). This simplification was to reduce the computational effort significantly, as the BFGS optimization requires $\sim 10-50$ optimization steps (in other words separate computations of potential energy). But this should not have much effect on the convergence of $\Delta E(\mathrm{V_{BN}})$.

Table 9: Convergence tests for $\Delta E(\mathrm{V_{BN}}) = E_0 - E(\mathrm{V_{BN}})$ as a function of supercell size when for simplicity neither of the structures has been optimized with BFGS. The supercell has been obtained by repeating the minimal unit cell $N_{\mathrm{uc}} \times N_{\mathrm{uc}} \times 1$ and therefore it consists of $N = 2N_{\mathrm{uc}}^2$ atoms. The Monkhorst-Pack k-point sampling is $n_k \times n_k \times 1$. For the value of n_k I chose the smallest number for which $n_k N_{\mathrm{uc}} \geq 20$ to make sure that my k-point sampling was at least as dense as the one used in the reference study.

N_{uc}	N	n_k	ΔE (eV)
4	32	5	34.761
5	50	4	34.755
6	72	4	34.752
7	98	3	34.749
8	128	3	34.746

The results of the convergence test are shown in table 9. It is clear that the convergence occurs already for small N_{uc} and the decrease in ΔE is just 0.015 eV when N_{uc} is increased from 4 to 8 while computational effort is increased dramatically. Thus I chose to use in the final computations the smallest tested N_{uc}—that is $N_{\mathrm{uc}} = 4$. In the final computations I also employed $5 \times 5 \times 1$ k-points in each direction as in test calculations for $N_{\mathrm{uc}} = 4$.

In the final calculations I optimized the structures until all the atomic forces were smaller than 0.01 eV/Å. I tried to make the defected and undefected structures as similar as possible due to the issues discussed in the previous section related to the difference in E_{DFTB} of structures of different type. So I used as big supercell for both structures and BFGS-optimized also the undefected BN layer. Now when the energies of clean and defected structures are compared, there should be the same systematical error related to these issues, and hence it should cancel out. Both of these treatments for the undefected supercell turned out be a necessity to take into account because without them the obtained results were quite odd and very far from the reference results.

As the lattice parameter I employed the previously obtained value of $a_0 = 2.508\,\text{Å}$ (see Sec. 7.2). This means that I did not use exactly the same a_0 as Kuzubov et al., but since a_0 is supposed to yield the stressless situation for the clean structures, with my parametrization usage of my own a_0 is appropriate.

I did not relax the stresses induced to the supercell through introduction of the defects, i.e., did not seek for the supercell dimensions yielding the energy minimum. In this case it can be justified in several ways: firstly, apparently Kuzubov et al. have not done it either and my goal is to replicate their computations. Secondly, also in reality the stresses caused by a single defect in a layer that is large or fixed from its edges can not change the dimensions of the layer. Thirdly, as it will be seen, the stresses caused by the vacancies are very small since the atoms surrounding the vacancies are hardly affected by the vacancy formation.

Also when applying the strains, I did not relax the strains induced in the transverse direction as I did in the case of clean BN layer, but apparently this has not been done in the reference study either.

As for the "most stable boron phase", whose energy is needed for $\mu(\mathrm{N})$, its exact definition is vague. Thus I have used a randomized boron structure which I have attempted to optimize with global minimization methods. The end result is shown in Fig. 22 and I obtained $E(\mathrm{B}_{12}) = -79.496\,\mathrm{eV}$. For $E(\mathrm{N}_2)$ I computed a value of $-14.535\,\mathrm{eV}$ and as $E(\mathrm{BN}_{\mathrm{cell}})$ I employed $E_0/16$, where E_0 is the 4×4 repeated BFGS-optimized clean unit cell with lattice parameter a_0.

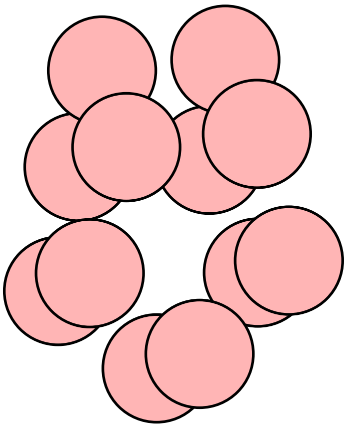

Figure 22: The B_{12} cluster I have used in Eq. (7.23). I started with a cluster with randomized initial positions and then optimized the structure with BasinHoppin global energy minimization algorithm implemented in ASE. I repeated this procedure several dozen times and then chose the final cluster with the lowest energy. That particular cluster is shown in this image and I obtained for its energy $-79.496\,\mathrm{eV}$.

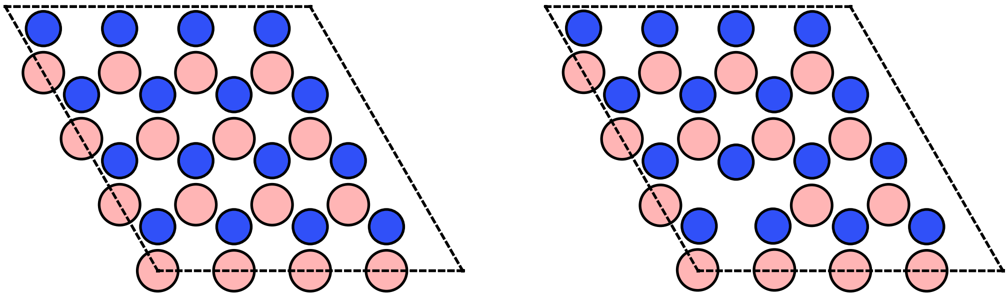

(a) The chosen final supercell.

(b) The boron vacancy ($\mathrm{V_B}$) unit cell.

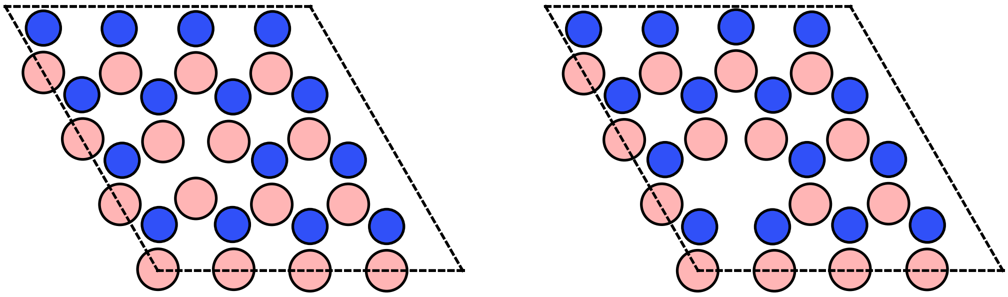

(c) The nitrogen vacancy ($\mathrm{V_N}$) unit cell.

(d) The double vacancy ($\mathrm{V_{BN}}$) unit cell. Here in the $\mathrm{V_{BN;\parallel}}$-situation the strain is applied in the $\hat{\mathbf{x}}$-direction and in the $\mathrm{V_{BN;\perp}}$-situation the strain is applied in the $\hat{\mathbf{y}}$-direction.

Figure 23: The final h-BN layer vacancy unit cells that were used in this study. All these structures have been BFGS-optimized.

7.4.2 Obtained results

As examples of used optimized structures, I have presented in Fig. 23 the unstrained optimized unit cells of the studied vacancies, as well as the original 4×4 supercell. As it can be seen, the atoms surrounding the vacancies nearly completely stay put instead of moving to fill the empty space. This is in accordance with previous vacancy studies for h-BN [42]. The reason for this is that once the atom(s) are removed and the bonds are cut, the atoms surrounding the vacancies do not manage to form any new bonds with other atoms and the cut bonds are left dangling in the space unsatisfied.

In Fig. 24 I have presented the results for vacancy formation energies versus strain for each studied vacancy type and, for comparison, also the ref-

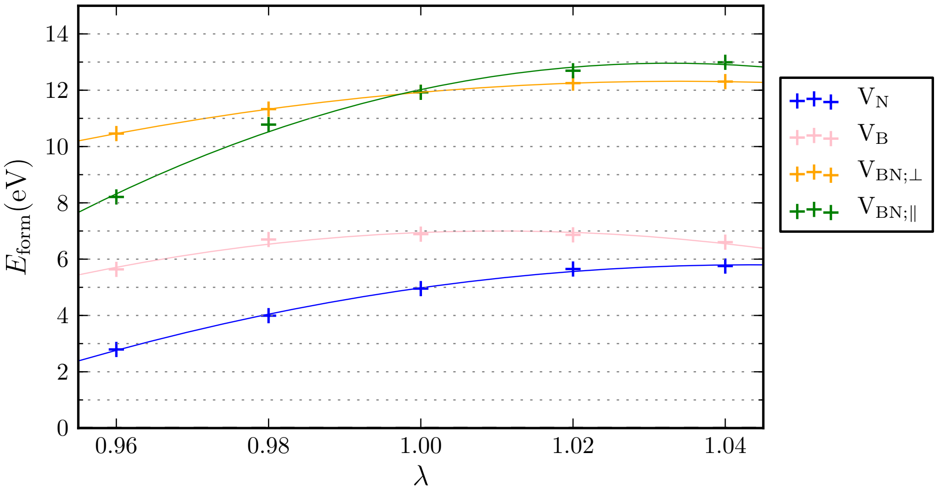

(a) DFTB vacancy formation energies versus stretch ratio λ for the h-BN monolayer.

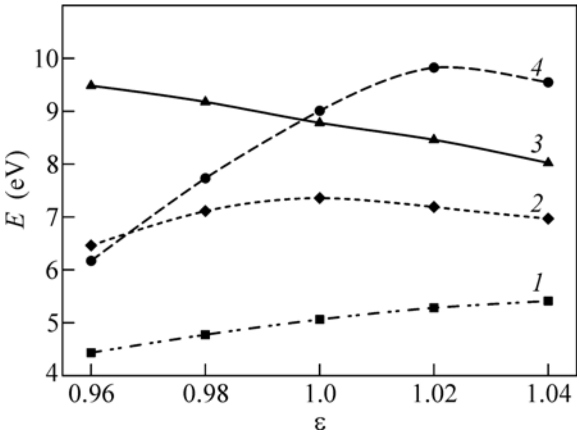

(b) Kuzubov et al. [41]: DFT vacancy formation energies versus strain with (1) V_N, (2) V_B, (3) $V_{BN;\perp}$, and (4) $V_{BN;\parallel}$-defect.

Figure 24: Comparison of DFTB (a) and reference DFT (b) vacancy formation energies. h-BN monolayer vacancy formation energies under strain both for DFTB (a) and DFT (b). For $\lambda = 1$ naturally $V_{BN;\perp} = V_{BN;\parallel}$, but in the reference paper this seems to be not the case for some odd reason. In the fittings for $E(\lambda)$ there were a lot of spread of the fitting points particularly for V_B and $V_{BN;\parallel}$. This can be seen from (a) as well. This probably indicates that for some values of strain convergence for slightly wrong density has occurred.

erence results by Kuzubov et al. These graphs do have relatively much in common, which means that my DFTB parametrization more or less has managed to capture the essential behavior of the vacancy formation energies under strain. More explicitly, particularly for $E_{\text{form}}(\mathrm{V}_\mathrm{B})$ there is excellent agreement with the DFTB and reference results. For each strain value the difference is within $1\,\mathrm{eV}$. Also the DFTB formation energy curve for the another monovacancy (i.e., V_N) obeys the DFT reference curve well. It seems that for compression the DFTB values are a bit too small (at largest $\sim 2\,\mathrm{eV}$) but for stretching they are quite equal. But the divacancy formation energies contradict strongly with the reference energies; $E_{\text{form}}(\mathrm{V}_{\mathrm{BN};\perp})$ has completely reverse behavior under strain and the difference is over $4\,\mathrm{eV}$ at its largest (for $\epsilon = 1.04$). But the $E_{\text{form}}(\mathrm{V}_{\mathrm{BN};\|})$ curve at least generally resembles the DFT curve—but is $\sim$2 eV too high in energy.

Lastly, since I already had the energies of these defected structures for various strain values, I as well computed their (reduced) Young's moduli. I fitted parabolic fits for the energies with respect to strain and then employed Eq. (7.14). But it must be stressed that in this case the *transverse stresses have not been relaxed* since I did not relax them in the E_{form}-computations either. Thus the obtained values actually are some kind of pseudo-Y_s instead of the true Y_s. Now, for example for the clean structures I obtained $451.2\,\mathrm{TPa\,nm}$ (from ϵ_x) and $450.5\,\mathrm{TPa\,nm}$ (from ϵ_y). These values are in correspondence with the previous results (in Sec. 7.2) for h-BN even though there I obtained $Y_\mathrm{s} = 315\,\mathrm{TPa\,nm}$ in the BFGS-optimized case, which is about $30\,\%$ lower value. Namely, based on the data I had for Sec. 7.2 I calculated that if the transverse strains are not relaxed, $Y_\mathrm{s} = 444.8\,\mathrm{TPa\,nm}$ (from ϵ_x) and $447.7\,\mathrm{TPa\,nm}$ (from ϵ_y).

Table 10: The pseudo-Y_s of vacancy defected h-BNs. Note that the transverse stresses are not relaxed, so these values are higher than for the real Y_s and the reductions are more relevant. But also those numbers apply only for the studied vacancy density.

Vacancy	Strain direction	Y_s(TPa nm)	Reduction (%)
V_B	$\hat{\mathbf{x}}$	263.7	-41.6
V_N	$\hat{\mathbf{x}}$	289.8	-35.8
$\mathrm{V}_{\mathrm{BN};\|}$	$\hat{\mathbf{x}}$	128.0	-71.6
$\mathrm{V}_{\mathrm{BN};\perp}$	$\hat{\mathbf{y}}$	325.7	-27.7
Perfect h-BN	$\hat{\mathbf{x}}$	451.2	
Perfect h-BN	$\hat{\mathbf{y}}$	450.5	

Since there is quite much error in the absolute value of Y_s, in this case I rather considered the *relative reduction* of the Y_s resulted from introduction of the defect. However, also with those numbers it must be noted that they depend on the size of the supercell—larger supercell means lower defect density and therefore less weakened structure. And as in this case the supercells are based on a 4×4 times repeated minimal unit cell, the obtained results correspond to very high defect densities. Nevertheless, they have been gathered to Tab. 10. Interestingly, in the case of $\mathrm{V}_{\mathrm{BN};\perp}$ the reduction is very low even when compared to the monovacancies, but reduction for $\mathrm{V}_{\mathrm{BN};||}$ is very large.

7.5 Stone-Wales defects on nanotubes

Stone-Wales (SW) defects are typical crystallographic defects that are characteristic to hexagonal (e.g. BN and carbon) structures. Unlike the vacancy defects, they are structural rearrangements, so the amount of atoms has not been changed in them. For example the so-called $5|7|7|5$ SW defects are obtained through rotating a BN atom pair by $90°$ with respect to the midpoint of the bond. This transforms four hexagons into two pentagons and two heptagons. Fig. 25 illustrates $5|7|7|5$ SW defects on zigzag nanotubes. Since there are two different kinds of B–N bonds in zigzag BNNTs[9] for which the SW-transformation can be applied, there do also exist two different kinds of $5|7|7|5$ SW defects labeled as *SW-I* and *SW-II* (the exact definitions are in the referred figure). Fig. 25 also shows that introducing the SW defect leads to formation of energetically unfavorable homoelemental bonds. So far the BN nanostructures studied do have quite similar structural and elastic properties with their carbon analogs. However, the B–B and N–N bonds cause the formation energies and elastic properties of the SW-defected tubi to significantly differ from their carbon analogs (for formation energies see for example [43]).

These homoelemental bonds also are particularly important in the context of this thesis since they employ the V_rep-functions constructed for the B–B and N–N interactions and therefore measure their quality, which has not been done in this thesis up to this point. The $5|7|7|5$ defects are particularly demanding for the quality of the used parametrization also because they put the transferability of the BN-V_rep function to more thorough test than before. Namely, the SW defects contain both a lot shorter and longer B–

---

[9] This was discussed in Sec. 3.2.

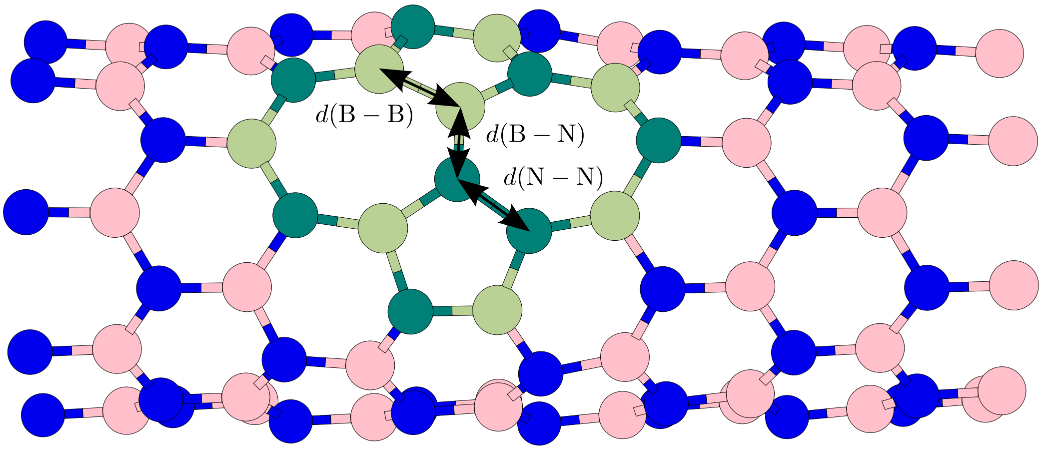

(a) The type I $5|7|7|5$ SW defect (SW-I) on a (8,0) BNNT (highlighted with green). This defect is obtained by rotating by by 90° an atom pair with that is aligned with the axis of the tube.

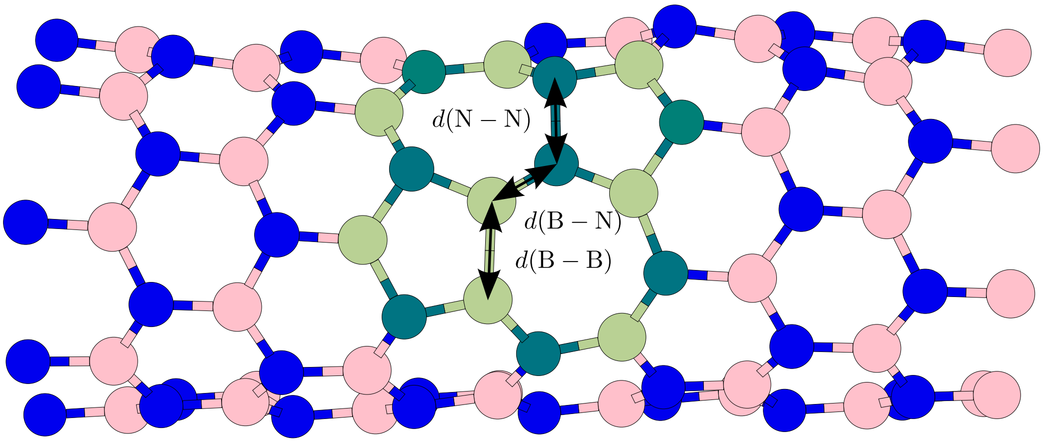

(b) The type II $5|7|7|5$ SW defect (SW-II) on a (8,0) BNNT (highlighted with green). This defect is obtained by rotating by 90° an atom pair with that is in an angle of 60° with respect to the axis of the tube.

Figure 25: The two possible orientations of the 5 | 7 | 7 | 5 Stone-Wales defect on zigzag NTs. Also definitions of the bond lengths $d(\mathrm{B}-\mathrm{B})$, $d(\mathrm{N}-\mathrm{N})$ and $d(\mathrm{B}-\mathrm{N})$ are shown. These example tubes are (8,0) BNNTs with $N_{\mathrm{uc}} = 4$ and they have been taken from my study, so they are BFGS-optimized with DFTB. To show here, I selected structures with unit cell length l closest to the equilibrium unit cell length l_0. The backsides of the NTs are not shown for clarity.

N bonds than a_0. Previously BN-$V_{\mathrm{rep}}(R)$ has been used only with quite narrow scale of R—in the process of determining the Young's moduli for different structures the used stretchings have been just a few percent and the vacancy defects in practice only broke the bonds belonging to them and did not affect rest of the bonds. This is why the $5|7|7|5$ defects also puts the quality (transferability) of the BN-V_{rep} function to more thorough test than before. Hence all in all the following computations with $5|7|7|5$ SW defects might be the most important ones so far.

Also so-called $4|8|8|4$ SW defects exist. They are similar to $5|7|7|5$ SW defects but in accordance with their name they consist of two quadrilaterals and two octagons. Therefore they only consist of B–N bonds and their formation energies are rather similar to $4|8|8|4$ SW defected carbon NTs.

In a paper by Yafei Li et al. properties of (8,0) nanotubes with $5|7|7|5$ SW defects are comprehensively investigated by means of gradient-corrected DFT simulations. The studied properties include the geometries, formation energies and electronic properties. All this is calculated for both type I and type II SW defects (SW-I and SW-II). Out of their results I have tried to reproduce with DFTB the formation energies E_{form}(SW-I) and E_{form}(SW-II) as well as the most relevant bond lengths, e.g. the most deformed bond lengths from the center of the defect. These bond lengths are the boron-boron bond $d(\mathrm{B}-\mathrm{B})$, nitrogen-nitrogen bond $d(\mathrm{N}-\mathrm{N})$ and the boron-nitrogen bond $d(\mathrm{B}-\mathrm{N})$ that was initially rotated with $90°$. Also these definitions are pictured in Fig. 25.

Also, in [44] the authors have used as initial unit cell a supercell constructed out of 4 minimal unit cells ($N_{\mathrm{uc}} = 4$), totalling to a $4 \times 4 \times 8 = 128$-atom supercell. They have stated that it is large enough to eliminate the defect-defect interactions, but I have wanted to verify this claim. Namely, since the full DFT calculations are expensive, the authors might not have had resources to verify it themselves. But since DFTB is so light, it allows such tests relatively easily compared to full DFT. Therefore I repeated my calculations also for $N_{\mathrm{uc}} = 3, 4, 5$ and 6 in the case of SW-I defect.

It is noteworthy that in reality the defected nanotubes are usually bent. But such structures can not be modelled with periodic one-dimensional k-point calculations, and thus the standard way is to perform computations for unbent tubes. Thus the appropriate periodic defect structure would be a BNNT ring constructed from bent supercells. These kinds of computations can be done quasi-one-dimensionally by revisiting the standard

Bloch theorem as discussed in Sec. 3.2. Another possibility to avoid this is to study NTs with defects symmetrically on both sides of the BNNT so that the tube is naturally unbent.

7.5.1 Methodology

I proceeded similarly to before. I first created the initial guesses for the structures with different supercell sizes, and then I optimized them with BFGS. These supercells were 3-, 4-, 5-, and 6-fold minimal unit cells, for which I used 7, 5, 4 and 4 k-points for sampling the one-dimensional Brillouin zone, respectively. This k-point density is in accordance with Li et al., who used as supercell 4 times repeated minimal unit cell and 5 k-points.

As in Sec. 7.3, after the optimization I performed parabolic fit $E(l)$ to find the equilibrium energy (E_0) and length (l_0) of each structure (both defected and clean tubes). Also for the defected structures I created linear fits for $d(\mathrm{B}-\mathrm{B})$, $d(\mathrm{B}-\mathrm{N})$ and $d(\mathrm{N}-\mathrm{N})$ with respect to l to find their values at l_0. As l_0 I used the optimal l of the defected tube, not that of the clean one. In other words after introducing the SW defects to optimized strainless clean tubes I also relaxed the induced strains from the defected tube. Also I am fairly sure that this was done also in Ref. [44] even though it was not mentioned. Besides, I checked the properties for l_0 of clean tubes, and the difference was $3\,\%$ for E_{form}(SW-I) and less for geometries as well as E_{form}(SW-II). Therefore it does not effectively matter if I did this differently from the reference study.

Also, as previously, in the comparison between defected and clean BNNTs these structures had unit cells of the same size, they were both optimized with BFGS and in the optimization the amount of used k-points as well as all the other settings were equal. Hence I did not use the properties for the minimal unit cell of the clean $(8,0)$ BNNT computed in Sec. 7.3, and rather recomputed them.

7.5.2 Obtained results

As already mentioned, Fig. 25 presents the final optimized structures. It is seen that the general geometry of the tube does not remain smooth at the SW-defected areas—the tubes have very strong local surface buckling instead. This buckling behavior is universal for SW defects, and it occurs even in flat BN and graphene sheets, as has also been experimentally observed [45]. This behavior is more strong for BN than carbon structures, though. It is a promising sign that also with my parametrization qualitatively similar parametrization shows up. Quite similar-looking buckling can also be seen in the DFT study of the Ref. [46].

I have gathered a set of different properties of the SW-I-defected $(8,0)$ BNNT for different supercell sizes to Tab. 11 to test the convergence of these properties as a function of supercell size. From these results it is obvious that for the 4-fold supercell these properties have not completely converged. Most notably the formation energy decreases with $0.12\,\mathrm{eV}$ when the size of the structures is brought up from 4-fold minimal clean unit cell to 6-fold. This difference is relatively significant, and it is expected, that the similar correction to 4-fold minimal clean unit cell DFT calculations is in the same order of magnitude. Thus the results of Yafei Li et al. for E_{form} could probably be relatively notably improved by enlarging the used unit cells. The degree of convergence is much greater for geometrical properties in my convergence tests, though.

Table 12 presents my DFTB results for both SW-I and SW-II defects compared against the reference DFT results. Firstly it is seen that my DFTB BN parametrization clearly overestimates the formation energies in both cases. The geometries are in much better agreement, though. Particularly interestingly the DFTB results for $d(\mathrm{B}-\mathrm{B})$ and $d(\mathrm{N}-\mathrm{N})$ were good. This is a sign of good quality of my V_{rep}-parametrizations for B–B and N–N interactions.

Moreover, from the DFTB data it is seen that introduction of the type I SW defect shrinks the tube with $0.14\,\mathrm{Å}$ after all the forces have been relaxed, whereas type II enlarges it with $0.04\,\mathrm{Å}$. Thus based on this, we might expect to observe type I SW defects under compression of the tube and type II SW defects under stretching.

Also I studied the Young's moduli. In the case of four times repeated minimal unit cell as the supercell, I found that introduction of SW-I defect reduces Y_{s} with $0.6\,\%$ from 283.3 TPa nm to 281.7 TPa nm, which is surprisingly small reduction. For SW-II the reduction is much more significant—$9.67\,\%$ from 283.28 TPa nm to 255.88 TPa nm. This seconds the impression of SW-II being more severely defected than SW-I. But it must again be remembered that these reductions apply for studied defect densities only.

Table 11: Effect of the supercell size for various $5|7|7|5$ SW-I defect properties on a $(8,0)$ BNNT. Both the formation energy E_{form} and several geometric properties are considered. The 3-, 4-, 5-, and 6-fold unit cells consist of 96, 128, 160 and 192 atoms, respectively, as the unit cell of a $(8,0)$ nanotube has 32 atoms.

N_{uc}	$E_{\mathrm{form}}(\mathrm{eV})$	$\Delta L(\text{Å})$	$d(\mathrm{B-B})(\text{Å})$	$d(\mathrm{B-N})(\text{Å})$	$d(\mathrm{N-N})(\text{Å})$
3	6.86	-0.141	1.683	1.478	1.443
4	6.72	-0.141	1.679	1.466	1.443
5	6.65	-0.143	1.678	1.462	1.443
6	6.60	-0.144	1.677	1.459	1.444

Table 12: Comparison of DFTB and reference bond lengths and E_{form} of both type I and II SW defects in $(8,0)$ NTs. More explicitly, the three studied bonds are the monoatomic B–B and N–N bonds introduced by the defect and the most severely defected B–N bond (see Fig. 25 for clarification). Both studies have employed 128-atom supercells.

	$d(\mathrm{B-B})(\text{Å})$			$d(\mathrm{N-N})(\text{Å})$		
	DFTB	DFT [44]	Err. (%)	DFTB	DFT [44]	Err. (%)
(8,0)-I	1.679	1.724	-2.6	1.466	1.485	-1.3
(8,0)-II	1.653	1.666	-0.8	1.449	1.442	0.5
	$d(\mathrm{B-N})(\text{Å})$			$E_{\mathrm{form}}(\mathrm{eV})$		
	DFTB	DFT [44]	Err. (%)	DFTB	DFT [44]	Err. (%)
(8,0)-I	1.443	1.414	2.1	6.72	4.85	39
(8,0)-II	1.421	1.361	4.4	7.06	5.84	21

8 Conclusions

The band structures managed to capture the essential properties of the studied structures and I believe that their accuracy is enough for introductory studies of new systems. This applied also to the geometries of the structures—unless the structures were stretched. Namely, then the behavior of the systems in the transverse direction (characterized by Poisson's ratios) was erroneous by large margin.

8.1 Possible improvements

There is obviously much room for improvement for my parametrization since as discussed in Sec. 7.3.2, in Ref. [40] BN DFTB results clearly better than mine have been performed. Their parametrization [47] shows that they used $r_{0,\mathrm{B}} = 1.48\,\text{Å}$ and $r_{0,\mathrm{N}} = 1.38\,\text{Å}$ whereas I used (see table 2) $r_{0,\mathrm{B}} = 1.60\,\text{Å}$ and $r_{0,\mathrm{N}} = 0.75\,\text{Å}$. It is glaring how small my $r_{0,\mathrm{N}}$ is. Based on the band structures and the used dimer reference systems I still believe that I chose its value correctly, but for more complex structures it simply does not seem to be good. Moreover, in [47] the authors have employed a notably larger amount of different reference systems and situations. This inevitably leads not only to better choice of x-parameters but also the V_{rep}-functions. All in all the conclusion is that to improve upon the parametrization, simply more reference systems should be used.

8.2 Postscript

At the beginning of the this project I was quite baffled about nearly everything and did not fully understand what I was doing and why. I had taken a course on DFT so I knew about it a bit, but it took a long time until the TB aspect became clear to me. That is one reason why I wanted to derive the DFTB theory so carefully in the theory section, and it eventually transformed into my research training thesis. This surely familiarized me with the subject thoroughly. Also the improvement in my knowledge of the practical simulations in computational nanoscience was of the same order of magnitude. All in all I can say that I learnt immensely during this project and this prepared me well to my upcoming postgraduate studies.

References

[1] O. Hod, *"Graphite and Hexagonal Boron-Nitride have the Same Interlayer Distance. Why?"*, *Journal of Chemical Theory and Computation*, **2012**, *8*, 1360–1369.

[2] M. L. Cohen, *"Experimental and theoretical equation of state of cubic boron nitride"*, *Nature*, **1986**, *337*, 349–352.

[3] S. Iijima, *"Helical microtubules of graphitic carbon"*, *Nature*, **1991**, *354*, 56–58.

[4] A. Rubio, J. L. Corkill, and M. L. Cohen, *"Theory of graphitic boron nitride nanotubes"*, *Phys. Rev. B*, **1994**, *49*, 5081–5084.

[5] X. Blase et al., *"Stability and Band Gap Constancy of Boron Nitride Nanotubes"*, *EPL (Europhysics Letters)*, **1994**, *28*, 335.

[6] N. G. Chopra et al., *"Boron Nitride Nanotubes"*, **1995**, *269*, 966–967.

[7] Y. J. Chen, H. Z. Zhang, and Y. Chen, *"Pure boron nitride nanowires produced from boron triiodide"*, *Nanotechnology*, **2006**, *17*, 786.

[8] Z.-G. Chen et al., *"Novel Boron Nitride Hollow Nanoribbons"*, *ACS Nano*, **2008**, *2*, 2183–2191.

[9] Y. Qiu et al., *"Synthesis of continuous boron nitride nanofibers by solution coating electrospun template fibers"*, *Nanotechnology*, **2009**, *20*, 345603.

[10] H. Zhang et al., *"Conical Boron Nitride Nanorods Synthesized Via the Ball-Milling and Annealing Method"*, *Journal of the American Ceramic Society*, **2006**, *89*, 675–679.

[11] D. Golberg et al., *"Octahedral boron nitride fullerenes formed by electron beam irradiation"*, *Applied Physics Letters*, **1998**, *73*, 2441–2443.

[12] K. S. Novoselov et al., *"Electric Field Effect in Atomically Thin Carbon Films"*, **2004**, *306*, 666–669.

[13] K. S. Novoselov et al., *"Two-dimensional atomic crystals"*, **2005**, *102*, 10451–10453.

[14] A. Pakdel et al., *"Low-dimensional boron nitride nanomaterials"*, *Materials Today*, **2012**, *15*, 256 –265.

[15] W. M. C. Foulkes and R. Haydock, *"Tight-binding models and density-functional theory"*, *Phys. Rev. B*, **1989**, *39*, 12520–12536.

[16] M. Elstner et al., *"Self-consistent-charge density-functional tight-binding method for simulations of complex materials properties"*, *Phys. Rev. B*, **1998**, *58*, 7260–7268.

[17] P. Hohenberg and W. Kohn, *"Inhomogeneous Electron Gas"*, *Phys. Rev.*, **1964**, *136*, B864–B871.

[18] R. van Leeuwen. *Introduction to density-functional theory*. 2012.

[19] P. Koskinen and V. Mäkinen, *"Density-functional tight-binding for beginners"*, *Computational Materials Science*, **2009**, *47*, 237 –253.

[20] S. G. Louie, S. Froyen, and M. L. Cohen, *"Nonlinear ionic pseudopotentials in spin-density-functional calculations"*, *Phys. Rev. B*, **1982**, *26*, 1738–1742.

[21] G. B. Bachelet, D. R. Hamann, and M. Schlüter, *"Pseudopotentials that work: From H to Pu"*, *Phys. Rev. B*, **1982**, *26*, 4199–4228.

[22] N. Troullier and J. L. Martins, *"Efficient pseudopotentials for plane-wave calculations"*, *Phys. Rev. B*, **1991**, *43*, 1993–2006.

[23] J. C. Slater and G. F. Koster, *"Simplified LCAO Method for the Periodic Potential Problem"*, *Phys. Rev.*, **1954**, *94*, 1498–1524.

[24] D. Frenkel and B. Smit, eds., *Understanding Molecular Simulation*, Second Edition. San Diego: Academic Press, 2002.

[25] P. Koskinen and O. O. Kit, *"Efficient Approach for Simulating Distorted Materials"*, *Phys. Rev. Lett.*, **2010**, *105*, 106401.

[26] O. O. Kit, L. Pastewka, and P. Koskinen, *"Revised periodic boundary conditions: Fundamentals, electrostatics, and the tight-binding approximation"*, *Phys. Rev. B*, **2011**, *84*, 155431.

[27] R. Feynman, R. Leighton, and M. Sands, *The Feynman Lectures on Physics (Part 2)*, Addison-Wesley Publishing Company, 1963. Chap. 38: Elasticity.

[28] V. Verma, V. K. Jindal, and K. Dharamvir, *"Elastic moduli of a boron nitride nanotube"*, *Nanotechnology*, **2007**, *18*, 435711.

[29] P. Koskinen. *The HOTBIT project*. 2008. URL: `https://trac.cc.jyu.fi/projects/hotbit/`.

[30] S. R. Bahn and K. W. Jacobsen, *"An object-oriented scripting interface to a legacy electronic structure code"*, *Comput. Sci. Eng.*, **2002**, *4*, 56–66.

[31] Debichem Team. *gElemental 1.2.0*. 2007. URL: `http://packages.ubuntu.com/eo/source/lucid/gelemental`.

[32] M. Winter. *WebElements: the periodic table on the web*. 2008. URL: `http://www.webelements.com/`.

[33] T. Gray, N. Mann, and M. Whitby. *Covalent Radius of the elements.* 2014. URL: `http://www.periodictable.com/Properties/A/CovalentRadius.html`.

[34] K. Huber and G. Herzberg, *Molecular Spectra and Molecular Structure*, Van Nostrand Reinhold Co., 1979.

[35] J.-F. Jia, H.-S. Wu, and H. Jiao, *"The structure and electronic property of BN nanotube"*, *Physica B: Condensed Matter*, **2006**, *381*, 90 –95.

[36] J. J. Mortensen, L. B. Hansen, and K. W. Jacobsen, *"Real-space grid implementation of the projector augmented wave method"*, *Phys. Rev. B*, **2005**, *71*, 035109.

[37] J. Enkovaara et al., *"Electronic structure calculations with GPAW: a real-space implementation of the projector augmented-wave method"*, *Journal of Physics: Condensed Matter*, **2010**, *22*, 253202.

[38] K. N. Kudin, G. E. Scuseria, and B. I. Yakobson, *"C_2F, BN, and C nanoshell elasticity from* ab initio *computations"*, *Phys. Rev. B*, **2001**, *64*, 235406.

[39] B. Baumeier, P. Krüger, and J. Pollmann, *"Structural, elastic, and electronic properties of SiC, BN, and BeO nanotubes"*, *Phys. Rev. B*, **2007**, *76*, 085407.

[40] E. Hernández et al., *"Elastic Properties of C and $B_xC_yN_z$ Composite Nanotubes"*, *Phys. Rev. Lett.*, **1998**, *80*, 4502–4505.

[41] A. Kuzubov et al., *"Theoretical study of vacancies and adatoms in white graphene"*, *JETP Letters*, **2011**, *93*, 335–338.

[42] T. B. Ngwenya, A. M. Ukpong, and N. Chetty, *"Defect states of complexes involving a vacancy on the boron site in boronitrene"*, *Phys. Rev. B*, **2011**, *84*, 245425.

[43] H. F. Bettinger et al., *"Mechanically induced defects and strength of BN nanotubes"*, *Phys. Rev. B*, **2002**, *65*, 041406.

[44] Y. Li et al., *"Stone–Wales Defects in Single-Walled Boron Nitride Nanotubes: Formation Energies, Electronic Structures, and Reactivity"*, *The Journal of Physical Chemistry C*, **2008**, *112*, 1365–1370.

[45] Y. Miyamoto et al., *"Spectroscopic characterization of Stone-Wales defects in nanotubes"*, *Phys. Rev. B*, **2004**, *69*, 121413.

[46] H. Roohi, M. Jahantab, and M. Yakta, *"Effect of the Stone–Wales (SW) defect on the response of BNNT to axial tension and compression: a quantum chemical study"*, *Structural Chemistry*, **2014**, 1–12.

[47] J. Widany et al., *"Density-functional-based construction of transferable nonorthogonal tight-binding potentials for B, N, BN, BH, and NH"*, *Phys. Rev. B*, **1996**, *53*, 4443–4452.